Struct Bond (2006) 119: 1–87
DOI 10.1007/430_005

Published online: 2 December 2005

Structural Aspects of Layered Double Hydroxides

David G. Evans[1] (✉) · Robert C. T. Slade[2] (✉)

[1]Ministry of Education Key Laboratory of Science and Technology of Controllable Chemical Reactions, Beijing University of Chemical Technology, 100029 Beijing, P.R. China
dgevans@mail.buct.edu.cn

[2]Department of Chemistry, University of Surrey, Guildford GU2 7XH, UK
R.Slade@surrey.ac.uk

Abstract Layered double hydroxides (LDHs) have been known for a considerable time and have been widely studied. The basic features of their structure, involving positively charged brucite-like layers together with charge-balancing anions and water in interlayer galleries are well understood, but some detailed aspects of their structure have been the subject of controversy in the literature. In this article we review the wide range of experimental and theoretical studies of the structure of LDHs, highlighting areas of consensus and currently unresolved issues. We focus on the range of composition for which LDHs may be formed, possible layer stacking polytypes, arrangement of guest species in the interlayer galleries and the extent of order-disorder phenomena, both long-range and short-range, in the layers and interlayer galleries.

Keywords Layered double hydroxide · Hydrotalcite · Structure · Diffraction · Polytype · Order-disorder

Abbreviations

AEC	Anion exchange capacity
AFM	Atomic force microscopy
AQ15	Anthraquinone-1,5-disulfonate
AQ2	Anthraquinone-2-sulfonate
AQ26	Anthraquinone-2,6-disulfonate
BPC	*p*-Benzoylbenzoate
CSC	4′-chloro-4-stilbenecarboxylic acid
DSC	Differential scanning calorimetry
EDAX	Energy dispersive analysis of X-rays
EXAFS	Extended X-ray absorption fine structure
HH	Head-to-head
HT	Head-to-tail
ICP	Inductively coupled plasma emission spectrophotometry
IP	Image plate
IR	Infrared
JCPDS	Joint committee on powder diffraction standards
LB	Langmuir-Blodgett
LDH	Layered double hydroxide
MBSA	5-Benzoyl-4-hydroxy-2-methoxybenzenesulfonic acid
NEXAFS	Near edge X-ray absorption spectroscopy (synonym for XANES)
NHA	4-Nitrohippuric acid
NMR	Nuclear magnetic resonance
SAED	Selected area electron diffraction
STEM	Scanning transmission electron microscopy
STM	Scanning tunneling microscopy
UV	Ultraviolet
XAS	X-ray absorption spectroscopy
XANES	X-ray absorption near-edge spectroscopy
XRD	X-ray diffraction

1 Introduction

Layered double hydroxides (LDHs) [1–3] have been known for over 150 years since the discovery of the mineral hydrotalcite, and a large class of minerals with closely related structures are usually known to mineralogists as the sjögrenite-hydrotalcite group [4]. Although the stoichiometry of hydrotalcite, $[Mg_6Al_2(OH)_{16}]CO_3{\cdot}4H_2O$, was first correctly determined by Manasse in 1915, it was not until pioneering single crystal X-ray diffraction (XRD) studies on mineral samples were carried out by Allmann [5] and Taylor [6, 7] in the 1960s that the main structural features of LDHs were understood. Nearly 40 years later, however, many of the fine details of the structure such as the range of possible compositions and stoichiometry, the extent of ordering of metal cations within the layers, the stacking arrangement of the layers and the arrangement of anions and water molecules in the interlayer galleries are not fully understood and have been the subject of some controversy in the literature. In this article we review the wide range of experimental and theoretical studies of the structure of LDHs, highlighting areas of consensus and currently unresolved issues. In addition to due reference to key papers from the earlier literature, recent work published up to early 2005 has been covered.

2 Basic Structural Features

2.1 Brucite Layers

The basic layer structure of LDHs is based on that of brucite $[Mg(OH)_2]$ which is of the CdI_2 type, typically associated with small polarizing cations and polarizable anions. It consists of magnesium ions surrounded approximately octahedrally by hydroxide ions. These octahedral units form infinite layers by edge-sharing, with the hydroxide ions sitting perpendicular to the plane of the layers as shown in Fig. 1 [8]. The layers then stack on top of one another to form the three-dimensional structure. From the point of view of close-packing, the structure can be said to be composed of close-packed planes of hydroxyl anions that lie on a triangular lattice. The metal cations occupy the octahedral holes between alternate pairs of OH planes and thus occupy a triangular lattice identical to that occupied by the OH ions. In actual fact, both the local geometry around the metal and the close-packing of the hydroxyl anions are strongly distorted away from the idealized arrangements. The octahedra are compressed along the stacking axis, so that the local geometry at the metal is D_{3d}, rather than O_h. This has the effect of increasing the O$\cdots$O and Mg$\cdots$Mg distances parallel to the plane from 0.2973 nm (ideal

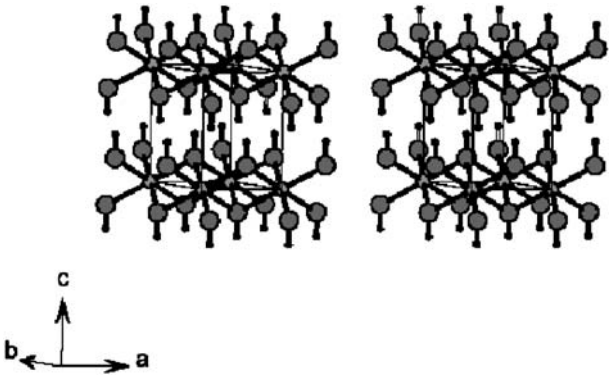

Fig. 1 Stereographic projection of brucite. Reprinted with permission from L. Eriksson, U. Palmqvist, Studsvik Neutron Research Laboratory Report 482. Copyright University of Stockholm

O_h geometry) to 0.3142 nm (experimental distance) and decreasing the thickness of the layers from 0.2427 to 0.2112 nm, with the O – M – O bond angles becoming 96.7° and 83.3° rather than a regular 90° [9]. This distortion has been discussed from a molecular orbital viewpoint [10] and an almost constant distortion has been suggested for all brucite-like hydroxides on the basis of the correlation between unit cell parameters and M – O distances [11]. The distortion of the brucite layers does not change the hexagonal symmetry ($a_o = b_o = 0.3142$ nm, $c_o = 0.4766$ nm, $\gamma = 120°$) and the space group is $P\bar{3}m1$. Note that the value of a_o is equal to the nearest neighbor Mg$\cdots$Mg distances parallel to the plane. The O – H bonds are directed along the threefold axes towards the vacant tetrahedral site in the adjacent layers. The nature of the weak forces between the layers has been the subject of considerable controversy in the literature with different importance being attached to contributions from dispersion forces and hydrogen bonding [8, 12–14].

2.2 Cation Substitution in Brucite-like Layers

2.2.1 Possible Identity of M^{II}/M^{III} Ions and Range of Values of the M^{II}/M^{III} Ratio

The basic structure of an LDH may be derived by substitution of a fraction of the divalent cations in a brucite lattice by trivalent cations such that the layers acquire a positive charge, which is balanced by intercalation of anions (and, usually, water) between the layers. It is the possibility of varying the identity and relative proportions of the di- and trivalent cations as well as the identity of the interlayer ions that gives rise to the large variety of materials having the general formula $[M^{II}_{1-x}M^{III}_{x}(OH)_2]^{x+}[A^{n-}]_{x/n}\cdot yH_2O$, which

belong to the LDH family. Many ternary LDHs involving mixtures of different M^{II} and/or M^{III} cations can also be prepared and even quaternary LDHs have been reported [15]. In fact the range of materials is even larger than suggested by this formula because materials containing monovalent lithium ions of the type $[LiAl_2(OH)_6]^+[A^{n-}]_{1/n}\cdot yH_2O$ are also known [16] and have similar structures.

A number of empirical studies have attempted to define the boundaries that indicate which metal ions can form LDHs. For example, the roles of the absolute values of ionic radii and the difference in ionic radii of M^{II} and M^{III} [3, 17–21] as well as the values of the solubility products of $M^{II}(OH)_2$ and $M^{II}CO_3$ [22] have been speculated on in the literature. In earlier publications [1, 23], it was often stated that ions such as Cu^{2+} that are subject to a Jahn-Teller distortion do not form LDHs unless diluted by other cations [24], but more recently examples of Cu^{II}-containing LDHs such as $[Cu_{0.69}Cr_{0.31}(OH)_2]Cl_{0.31}\cdot 0.61H_2O$ [25, 26] have been well characterized (see Sect. 3.2.2), although the material does show a corrugation of the sheets associated with the Jahn-Teller distortion around individual Cu^{II} centers as discussed in Sect. 3.4.

More recently a number of studies of the thermodynamic factors affecting the formation of LDHs have been reported. The enthalpies of formation from the elements of a series of $Mg/Al-CO_3$ LDHs with different Mg/Al ratios have been measured by high-temperature oxide-melt solution calorimetry [27]. Compared with a mixture of $Mg(OH)_2$, $Al(OH)_3$, $MgCO_3$ and water and it was found that the LDHs are more stable by 10–20 kJmol^{-1}, but there is no correlation with Mg/Al ratio. Similar results were obtained [28] from calorimetric measurements of the heats of formation of LDHs of the type $[Co_{0.8}Al_{0.2}(OH)_2](NO_3)_{0.2y}(CO_3)_{0.1(1-y)}\cdot(0.7-0.3y)H_2O$ and $[(Ni_yCo_{1-y})_{0.8}Al_{0.2}(OH)_2](CO_3)_{0.1}\cdot 0.7H_2O$. Based on measurements of solubility products of $[M_4Al_2(OH)_{12}]CO_3\cdot nH_2O$, it has been concluded [29, 30] that the thermodynamic stability of the LDHs is greater than that of the corresponding divalent hydroxides below pH $\approx$ 10 (M = Zn), 9 (M = Co) and 8 (M = Ni); for M = Mg, the LDH is more stable up at least pH 12. It has been proposed [31, 32] that simple thermodynamic models can be used to determine the standard molar Gibbs free energy of formation of LDHs by, for example, using the tabulated values for the corresponding divalent and trivalent metal hydroxides and the salt of the divalent cation according to the following stoichiometric equation:

$$\begin{aligned}&(1-3x/2)M^{II}(OH)_2 + xM^{III}(OH)_3 + (x/2)M^{II}(A^{n-})_{2/n}\\ &= [M^{II}{}_{1-x}M^{III}{}_x(OH)_2](A^{n-})_{x/n}\,,\end{aligned} \tag{1}$$

although water was apparently not included in these calculations. Standard Gibbs free energies of formation of several so-called green-rust type LDHs of the type $[Fe^{II}{}_{1-x}Fe^{III}{}_x(OH)_2]^{x+}(A^{n-})_{x/n}\cdot nH_2O$ have been tabulated [33]. It

has been suggested that equilibria between these species and related ternary species such as $[Fe^{II}_{1-x-y}Mg_yFe^{III}_x(OH)_2](OH)_x \cdot nH_2O$ are responsible for controlling the distribution of iron in hydromorphic soils and relevant solubility products have been determined [34–36]. Braterman and coworkers [37, 38] have analyzed the stabilities of LDHs of the type $[M^{II}_{1-x}M^{III}_x(OH)_2]Cl_x \cdot nH_2O$ relative to the corresponding metal hydroxides/hydrous oxides. The LDH stabilities were found to vary in the order Mg < Mn < Co ≈ Ni < Zn for M^{II} and Al < Fe for M^{III}. On the basis of pH titration curves for the reaction of NaOH with the mixed chloride salt solutions, it was suggested that the hydroxide or hydrous oxide is generally formed first at lower pH and subsequently reacts with the aqueous M^{II} ions at higher pH to form the LDH. The LDHs were shown to be generally thermodynamically unfavorable with respect to mixtures of metal hydroxides, but mass action effects associated with the high concentration of the anion in solution drive the system in the direction of the LDH. In contrast, for the case of M^{III} = Cr, the formation of $[M^{II}_{1-x}Cr^{III}_x(OH)_2]Cl_x \cdot nH_2O$ occurs in a single step without formation of $Cr(OH)_3$. The solubility products of the LDHs vary in the order Zn < Ni ≈ Co. For M^{II} = Mg, the corresponding LDH chloride could not be prepared although the sulfate analogue could be isolated via a two-step process.

It is often said [1, 3, 19, 21] that pure LDH phases can only be formed for stoichiometries in the range $0.20 < x < 0.33$, i.e. M^{II}/M^{III} ratios in the range 2–4. It has been argued that for $x > 0.33$, the presence of $M^{III} - O - M^{III}$ linkages would be required and these are unfavorable from the point of view of charge repulsion (the so-called cation avoidance rule) [36, 39, 40]. It has been demonstrated, however, that such $M^{III} - O - M^{III}$ linkages *can* occur in LDHs, at least in the case of M = Cr. Reaction of a perchlorate solution of the dimer $[(H_2O)_4Cr(\mu - OH)_2Cr(OH_2)_4]^{4+}$ with ZnO and subsequent anion exchange affords [41] grayish-blue $[Zn_7Cr_4(OH)_{22}]CO_3 \cdot 5H_2O$, which has a ligand field splitting less than that of blue-green $[Zn_4Cr_2(OH)_{12}]CO_3 \cdot 3H_2O$. The existence of the dimeric unit in the Zn_7Cr_4 LDH was confirmed by UV-visible spectroscopy and ion-exchange chromatography after dissolution of the LDH in perchloric acid.

In the dioctahedral gibbsite [γ-$Al(OH)_3$] lattice only two-thirds of the octahedral sites are occupied by cations. A novel variant of LDHs having the formula $[M^{II}Al_4(OH)_{12}](NO_3)_2 \cdot nH_2O$ (M^{II} = Co, Ni, Cu, Zn) have been prepared [42] by reaction of activated gibbsite with the corresponding $M^{II}(NO_3)_2$ solutions. Half of the cation vacancies have been filled with M^{II} cations, so that although the M^{II}/Al ratio is 1 : 4, there are still cation vacancies unlike in the trioctahedral brucite-like layers of conventional LDHs where all the octahedral sites are occupied. In the case of monovalent Li^+ cations, the vacancies in gibbsite can be completely occupied giving a series of LDHs containing $[LiAl_2(OH)_6]^+$ layers that have been widely studied and fully structurally characterized as noted above [16].

Theoretical calculations [43] based on first principles molecular dynamics discussed in Sect. 3.2.6 have suggested that Mg_nAl LDHs are most stable for $n = 3$ (i.e. $x = 0.25$) and indeed many minerals, including hydrotalcite itself, have this stoichiometry [4]. It has been reported that the synthesis of LDHs (with benzoate or terephthalate anions in the interlayers) from solutions containing Mg/Al = 2, leads to LDHs having the same composition when the synthesis is carried out at moderate temperatures but LDHs with Mg/Al = 3 (plus AlOOH) when the reaction is carried out under hydrothermal conditions [44]. It was proposed that the latter ratio represents the thermodynamically most favorable product. A similar observation has been reported [45] for solutions with $Ni^{II}/Fe^{III} = 2$, where hydrothermal preparation led to segregation of an LDH with $Ni^{II}/Fe^{III} = 3$ and $Ni^{II}Fe^{III}{}_2O_4$. An attempt to synthesize a $Co^{II}{}_5Al$ LDH resulted in partial oxidation of the Co^{II} and formation of a $Co^{II}{}_{0.7}Co^{III}{}_{0.3}$ LDH with complete migration of Al^{3+} from the layers to generate interlayer aluminum oxy-species [46].

There have been many claims that LDHs can be formed with stoichiometries outside the range $0.20 < x < 0.33$ [17, 21], with reported values of x down to as low as 0.07 for $Mg/Ga-CO_3$ LDHs [47] and as high as 0.41–0.48 for $M^{II}/M^{III}-CO_3$ LDHs (M^{II} = Mg, Ni, Co, Cu; M^{III} = Al, V) [48–52] and 0.5 for Fe^{II}/Fe^{III} LDHs [53]. It has been suggested [54] that ion-exchange reactions at relatively low pH favor leaching of M^{II} ions from the layers and thus gives rise to high values of x. There are, however, many difficulties in determining the exact value of x in LDHs. Elemental analysis of the metal content of a solid phase will give erroneous values if the LDH is mixed with $M^{II}(OH)_2$, $M^{II}(OH)_3/M^{III}OOH$ or other phases that might be expected to segregate [36] when the synthesis mixture contains either very high or very low M^{II}/M^{III} ratios. Whilst such phases can sometimes be observed by XRD [44, 55–58], more often than not they are likely to be amorphous and remain undetected by XRD [59]. It has been noted that preferred orientation of LDH samples tends to make it difficult to observe weak reflections from small amounts of such impurities [60]. Other methods sometimes provide evidence of impurity phases. Small quantities of Co_3O_4 admixed with $Mg/Co^{II}/Co^{III}$ LDHs have been identified by FTIR [61]. The presence of significant quantities of amorphous iron(III) oxides such as ferrihydrite $Fe_5HO_8\cdot 4H_2O$ mixed with Mg/Fe^{III} LDHs has been detected [62, 63] by Mössbauer spectroscopy at 4.2 K, since ferrihydrite and related species are magnetically ordered at this temperature and give a sextet in the Mössbauer spectrum whereas the Fe^{III} ions in the LDH are not and give a doublet. It has also been suggested, however, that the presence of $Fe^{III}-O-Fe^{III}$ moieties in the LDH itself can be inferred from Mössbauer spectroscopy and it has been speculated [64] that the acidic nature of the $MgFe_2OH$ units favors deprotonation so that the anion exchange capacity of the materials remains constant when $x > 0.33$, i.e. the structure can be written as $[Mg_{1-x}Fe_x(OH)_{2-y}O_y](CO_3)_{(x-y)/2}\cdot nH_2O$.

It has been proposed that, if no change in Mg/Al ratio is observed after washing an $Mg/Al-CO_3$ LDH with hot NaOH, this can be taken to indicate the absence of amorphous aluminum oxy-species [51]. It has also been suggested [65] that consistent values of the metal content of the bulk phase (e.g. as determined by ICP) and that of the surface (as determined by EDAX) is good evidence for the formation of a single LDH phase. It has been proposed that use of a high resolution scanning transmission electron microscope (STEM) coupled with EDAX allows the composition of LDH platelets to be determined in the presence of non-LDH impurities, which have particles with clearly different morphology [49]. Since carbonate-containing LDHs are characterized by the formula $[M^{II}_{1-x}M^{III}_{x}(OH)_2](CO_3)_{x/2}\cdot yH_2O$, it is sometimes suggested that analysis of the carbon content gives a more reliable guide to the value of x than metal analysis [57]. Other studies have, however, indicated [66, 67] that LDHs can adsorb significant amounts of CO_2 or carbonate anions on external non-gallery surfaces, affecting the carbon content and so suggesting that this may not be a reliable indication of the value of x.

On balance, it seems, therefore, that the range of stoichiometries for which LDH phases can be prepared is relatively narrow and that many of the materials reported in the literature with unusually high or low values of x are probably not pure single phases.

Structural studies of LDHs discussed in Sects. 3.3 and 3.4 indicate that the metal-oxygen octahedra in LDHs are compressed along the c axis exactly as for brucite with the O – M – O bond angles being distorted considerably (typically by 7–8°) from an ideal octahedral arrangement. It has been suggested that the observed broadening of the d–d transitions of Cr^{III} ions in LDHs is associated with this distortion from O_h to D_{3d} symmetry [41, 68]. As noted in Sect. 2.1, the value of the unit cell parameter a_o of brucite (0.3142 nm) is equivalent to the mean distance between adjacent cation centers in the close-packed sheets and the value of the corresponding parameter for LDHs can be correlated with the average radii of the metal cations in the layers. To a first approximation, the value of a_o may be calculated [56, 69] assuming Vegard's law and an ideal atomic arrangement for the cations; in that case $a_o = \sqrt{2d(M-O)}$, where the metal-oxygen bond length $d(M-O)$ is related to the ionic radii by the equation

$$d(\text{M-O}) = (1-x)r(M^{II}) + xr(M^{III}) .$$

From this it follows that

$$\delta a_o/\delta x = -\sqrt{2}[r(M^{II}) - r(M^{III})] .$$

The values of a_o for $Mg_{1-x}Al_x$ LDHs ($\approx$ 0.302–0.307 nm) are smaller than the value for brucite and decrease with x, since the Shannon crystal radius of Al^{3+} is smaller than that of Mg^{2+} (0.0675 vs. 0.0860 nm) [70]. Some typical data are shown in Fig. 2 for $Mg/Al-CO_3$ and $Zn/Al-CO_3$ LDHs [19] (the Shannon crystal radius of Zn^{2+} is 0.088 nm) and there are

many other examples in the literature for a wide variety of LDHs [20, 39, 46, 55, 71–77]. *Ab initio* molecular orbital calculations on dimers of the type $[(H_2O)_2(OH)_2Mg(\mu\text{-}OH)_2Mg(OH)_2(OH_2)]^{2-}$ and $[(H_2O)_2(OH)_2Mg(\mu\text{-}OH)_2Al(OH)_2(OH_2)]^{-}$ have reproduced the experimental values of the M···M distances in brucite and LDHs [78].

Where there is no correlation between the value of a_o and the apparent composition of the LDH, this may indicate that other non-LDH phases are also present [58]. It has often been observed in the case of Mg/Al LDHs with interlayer carbonate [51] or nitrate [55] anions that the value of a_o remains essentially constant (≈ 0.304 nm) for values of $x \geq 0.33$. In some cases the presence of an impurity such as gibbsite has been observed by XRD [55], sug-

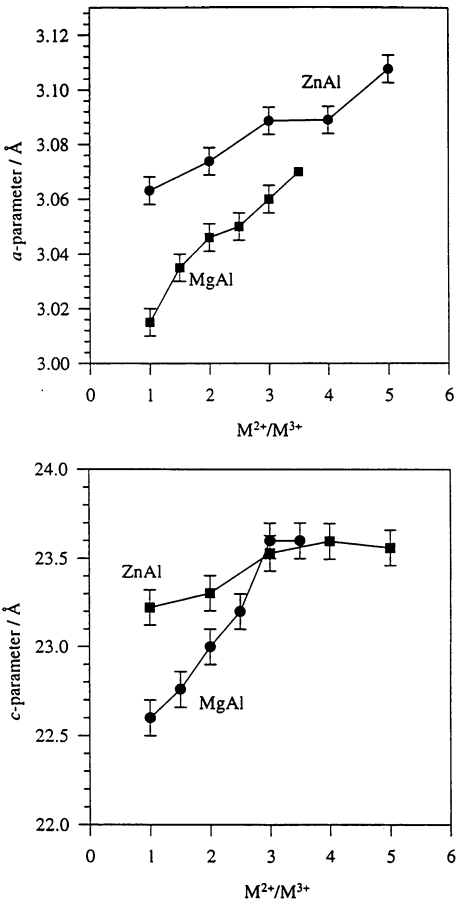

Fig. 2 Variation of the hexagonal unit cell parameters of $Mg/Al-CO_3$ and $Zn/Al-CO_3$ LDHs with the M^{II}/M^{III} ratio used in their preparation. Reprinted with permission from [19]. Copyright Cambridge University Press

gesting that the LDH phase has $x \approx 0.33$ with the excess Al^{3+} incorporated in the impurity. It has been argued, however, [51] that a value of (≈ 0.304 nm) represents the closest possible approach of Mg^{2+} and Al^{3+} cations and pure LDH phases with $x > 0.33$ also have $a_o \approx 0.304$ nm. With $[Fe(CN)_6]^{3-}$ as the guest anion in Mg/Al LDHs, a linear variation in the value of a_o against x in the range 0.10–0.48 has been reported, however, [76] with a value of $x = 0.48$ being associated with $a_o = 0.302$ nm. A correlation of the value of a_o with values of x up to 0.44 has also been reported for $Zn/Al - CO_3$ LDHs [49]. Although in principle, the value of a_o provides a useful way of estimating the value of x (at least up to $x \approx 0.33$), as discussed in Sect. 3.1, the experimental value of a_o is determined from the position of the (110) reflection in the powder XRD pattern. This reflection is often weak and may be broadened and overlap with the adjacent (113) reflection so that its position may be difficult to determine sufficiently accurately to give a meaningful measure of x. In some cases, deconvolution of the overlapping (110) and (113) reflections has been reported [55, 79] in an attempt to overcome this problem.

The basal spacing of an LDH (the distance from the center of one layer to that in the adjacent layer) is obviously much greater than that in brucite ($c_o = 0.4766$ nm) because of the absence of any interlayer anions and water in the latter. The LDH basal spacing shows some correlation with composition of the layers, although clearly the size of the anion and the extent of hydration will also have a major influence [1, 17, 19]. For $Mg_nAl - CO_3$ LDHs it has been reported that the basal spacing decreases from 0.7928 nm for $n = 5$ to 0.7591 nm for $n = 24$. [N.B. As discussed below, the crystallinity of LDH materials reported in the literature varies over a very wide range. Structural data are therefore given to varying numbers of significant figures in the literature, (hopefully!) taking into account the degree of crystallinity of the sample; the quoted values are reproduced in this review without any attempt at harmonization]. There is a small contraction in the layer thickness from 0.2001 nm ($n = 5$) to 0.1959 nm ($n = 2$) (as compared with 0.2101 nm in brucite [8, 13]), which parallels the decrease in a_o. Almost all of the change in basal spacing, however, can be attributed to the decrease in the thickness of the interlayer galleries [39]. The charge density of the layers increases with decreasing n leading to stronger electrostatic bonding with interlayer anions and stronger hydrogen bonding with interlayer water molecules. In the case of $[Ni_{6-x}Mg_xFe_2(OH)_{16}]CO_3 \cdot 4H_2O$, the basal spacing was reported to show a monotonic increase from 0.778 nm ($x = 0$) to 0.791 ($x = 6$) although the overall cationic charge on the layers does not change [80]. This was interpreted as indicating that OH groups bonded to Ni^{2+} are more strongly polarized than those bonded to Mg^{2+} and hence form stronger hydrogen bonds with interlayer carbonate anions. A similar increase in basal spacing in LDHs of the type $[Co_2Fe_yAl_{1-y}(OH)_2]Cl \cdot nH_2O$ from 0.7637 nm ($y = 0$) to 0.7893 nm ($y = 1$) was ascribed to a variation in the thickness of the layers, however [72].

2.2.2 LDHs with M^{IV} Ions?

Although it has long been established that many combinations and permutations of divalent and trivalent cations can form LDHs and that one monovalent cation (Li^+) is also able to form LDHs based on $[LiAl_2(OH)_6]^+$ layers, the question of possible incorporation of tetravalent ions into the LDH layers has been more controversial. A number of recent papers have reported the possibility of synthesizing LDHs containing M^{IV} ions including $Mg/Al/Zr^{IV} - CO_3$ [81–84], $Mg/Al/Sn^{IV} - CO_3$ [85], $M^{II}/Al/Sn^{IV} - CO_3$ (M^{II} = Co, Ni) [86], $M^{II}/Al/Sn^{IV} - CO_3$ (M^{II} = Mg, Ni, Zn) [87], $Mg/Al/Ti^{IV} - CO_3$ [88], $Mg/Al/Si^{IV} - CO_3$ [89] and even a $Zn/Ti^{IV} - CO_3$ LDH containing no trivalent cations [90].

Recently, however, considerable doubt has been cast on these conclusions. In the case of the putative $Mg/Al/Sn^{IV} - CO_3$, $Mg/Al/Zr^{IV} - CO_3$ and $Co/Al/Sn^{IV} - CO_3$ materials it has been unambiguously shown by X-ray absorption spectroscopy (XAS) and Mössbauer spectroscopy that the tetravalent cations are segregated from the LDH structure and form amorphous M^{IV} oxide-like particles [69]. It was further demonstrated that the increased values of a_o previously attributed to the introduction of the large M^{IV} cations could equally well be explained by the changes in Mg/Al ratio in an LDH phase with no incorporation of M^{IV}. A similar analysis of a material described as a $Co/Al/Ti^{IV} - CO_3$ LDH has also clearly shown that the Ti^{IV} cations are not incorporated in the LDH sheets [91]. These results highlight the dangers of postulating the composition of an LDH based solely on analytical data and the value of unit cell parameters, as discussed in Sect. 2.2.1 for M^{II}/M^{III} LDHs.

2.3 LDH Interlayers

The interlayer galleries of LDHs contain both interlayer anions and water molecules and there is a complex network of hydrogen bonds between layer hydroxyl groups, anions and water molecules. The interlayers are substantially disordered and hydrogen bonds are in a continuous state of flux so that the precise nature of the interlayer is extremely complex [3]. The bonding between octahedral layers and interlayers involves a combination of electrostatic effects and hydrogen bonding. Hydroxyl groups, particularly those bonded to trivalent cations are strongly polarized and interact with the interlayer anions. Every anion has to satisfy excess positive charges on both of the sandwiching octahedral layers, which are electrically balanced by two neighboring interlayers; it has been suggested that charge compensation in LDHs has many of the characteristics of resonance effects [92].

The structure of the interlayer galleries is discussed in detail in Sect. 3.2.

2.4
Layer Rigidity

The rigidity of the layers in a two-dimensional solid has a significant effect on its properties [93]. An interlayer rigidity parameter $p \approx 5$ was determined for LDHs by fitting the basal spacing of $[Zn_{0.61}Al_{0.39}(OH)_2](CO_3)_{0.195(1-y)}Cl_{0.39y}\cdot n H_2O$ as a function of composition y to the standard version of the discrete finite layer rigidity model [94, 95]. This value indicates LDH layers are much more rigid than those in graphite ($p \approx 2$) and much less rigid than those of 2 : 1 phyllosilicate clays such as vermiculite ($p \approx 7$) and are more comparable to, although somewhat more rigid than, metal dichalcogenides ($p \approx 3.5$) [93]. These values are consistent with the number of planes of atoms from which the layers are composed (one for graphite, three for LDHs and metal dichalcogenides and seven for 2 : 1 clays).

As a result of the relatively rigid layers, strong forces are exerted on the interlayer guests in LDHs. From the magnitude of the red shift in the photoluminescence observed on intercalation of $[SmW_{10}O_{36}]^{9-}$ in LDHs, it has been estimated that the layers exert a uniaxial stress of about 14 GPa on the guest anion [96, 97].

3
Detailed Structural Characterization of LDHs

3.1
Stacking Sequences in LDH Polytypes

The brucite-like layers in LDHs may be stacked in different ways, which gives rise to a variety of possible polytype structures. All sites in the (110) plane of the close packed hydroxide layers may be represented as **A**, **B** or **C** related by lattice translations of (1/3, 2/3, 0) or (2/3, 1/3, 0), and the location of octahedral holes occupied by metal cations can be described analogously as **a**, **b** or **c**. Thus a single brucite layer can be represented as **AbC** (since, if close packed hydroxyls occupy **A** and **C** sites, the cations must, of necessity, occupy **b** sites the abbreviation is sometimes simplified to **AC**, but we retain the full description here). **AbC** layers may be stacked in various ways giving rise to a large number of possible polytypes. At the most basic level, these polytypes may be classified in terms of the number of sheets stacked along the *c* axis of the unit cell, but such an approach overlooks some interesting detailed structural features associated with the stacking of the sheets. If the opposing OH groups of adjacent layers lie vertically above one another (say both in **C** sites), a trigonal prismatic arrangement (denoted by =) results; if the hydroxyls are offset (say one layer in **C** sites and those of an adjacent layer in either **A** or **B** sites) then the six OH groups form an octahedral arrangement denoted by ∼. Thus

brucite itself can be denoted as **...AbC∼AbC...** or **1H**, where the "**1**" denotes a one-layer polytype and the "**H**" denotes a stacking sequence with hexagonal symmetry. Bookin and Drits [98–100] have systematically derived all of the possible polytypes for other stacking sequences. There are three possible two-layer polytypes, each of which has hexagonal stacking of the layers, which can be denoted as follows:

...AbC=CbA=AbC... $\mathbf{2H_1}$
...AbC∼AcB∼AbC... $\mathbf{2H_2}$
...AbC∼BcA=AbC... $\mathbf{2H_3}$

Note that in the case of the $\mathbf{2H_1}$ polytype, the cations all occupy **b** positions, i.e. are aligned on a normal to the layers (this is also the case for the **1H** polytype), whereas for the other two polytypes the cations alternate between **b** and **c** sites. Note also that the interlayers in the $\mathbf{2H_1}$ polytype are all prismatic and those in the $\mathbf{2H_2}$ polytype are all octahedral, whilst in the $\mathbf{2H_3}$ polytype both types of interlayers are present.

There are nine possible three-layer polytypes. Two of these have rhombohedral symmetry (**3R**):

...AbC=CaB=BcA=AbC... $\mathbf{3R_1}$
...AbC∼BcA∼CaB∼AbC... $\mathbf{3R_2}$

whilst the remaining seven have hexagonal symmetry:

...AbC∼AcB∼AcB∼AbC... $\mathbf{3H_1}$
...AbC∼AcB∼CaB∼AbC... $\mathbf{3H_2}$
...AbC∼AcB=BcA∼AbC... $\mathbf{3H_3}$
...AbC∼AbC=CbA=AbC... $\mathbf{3H_4}$
...AbC∼AcB=BaC∼AbC... $\mathbf{3H_5}$
...AbC∼AcB∼CbA=AbC... $\mathbf{3H_6}$
...AbC∼AbA∼BcA=AbC... $\mathbf{3H_7}$

Note that the cations are homogenously distributed over **a**, **b** and **c** sites in the case of the $\mathbf{3R_1}$, $\mathbf{3R_2}$ and $\mathbf{3H_2}$ polytypes. For the $\mathbf{3R_1}$ polytype, the interlayers are all prismatic and in the case of $\mathbf{3R_2}$, $\mathbf{3H_1}$ and $\mathbf{3H_2}$ they are all octahedral; other polytypes involve both types of interlayers.

Bookin and Drits [98–100] have also described the large number of possible six-layer polytypes, some of which have rhombohedral symmetry (**6R**) and the remainder hexagonal symmetry (**6H**).

The identity of the polytype present in a given LDH sample may, in principle at least, be determined from the powder XRD pattern, although as we shall see for many LDHs this is not possible, as the amount of useful information therein is limited. By convention, the indexing of powder patterns for rhombohedral polytypes is based on a triple hexagonal unit cell (see Fig. 3).

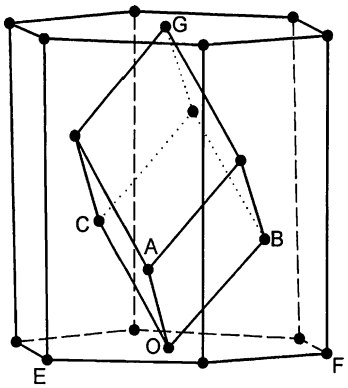

Fig. 3 Relationship between the triple hexagonal cell with axes **OE**, **OF**, **OG** to the primitive rhombohedral cell with axes **OA**, **OB**, **OC**

Although such a cell is not primitive, it is easier to visualize and facilitates direct comparison with hexagonal structures.

The reflections in the XRD pattern of an LDH fall into three groups:

(1) A series of strong basal (00*l*) reflections at low angles allow direct determination of the basal spacing normal to the (00*l*) plane (c_o), which equals the thickness of one brucite-like layer plus one interlayer. For an *n*-layer polytype, the unit cell parameter $c = nc_o$, and the lowest angle reflection is indexed as (00*n*) although its spacing always corresponds to c_o. Higher order (00*l*) reflections generally have spacings corresponding to $c_o/2$, $c_o/3$, ... However, this relationship will break down if there is imperfect stacking along the *c* axis. This can arise if there is interstratification (interlayers have varying anions and/or water composition) [101, 102] or varying extents of disorder in the interlayers [100, 103]. In addition, if the LDH is composed of very thin platelets, the small coherent scattering domains in the *c* direction lead to the basal reflection being shifted to a slightly lower angle, giving an apparent spacing that is greater than the true value of c_o calculated from the higher order basal reflections [100].

Where basal and non-basal reflections overlap, useful information can sometimes be obtained by comparing the intensities of XRD patterns of preferentially ordered samples with those of randomly oriented samples. The former may be prepared by drying suspensions of finely ground LDHs in water on glass slides [104] or by thorough pressing and sliding of the finely ground sample [105]. The latter may be obtained by means of the McMurdie [106] or Petrov [105] methods. The intensities of reflections from planes oriented approximately parallel to the sample holder (i.e. (00*l*) and other planes closely inclined to the basal plane) are enhanced relative to those of other planes for preferentially ordered samples. If the two XRD patterns are subtracted from one another (after preliminary normalization of the inten-

sity of a reflection from a plane inclined at approximately 45° to the basal plane), overlapping basal and non-basal reflections can be resolved [105]. For example, using this method Stanimirova [105] has concluded that a hydrotalcite mineral sample from Snarum in Norway contains a mixture of three polytypes.

(2) The position of the (110) reflection at high angle (near 60° 2θ for Cu K_α radiation) allows the value of the lattice parameter a_o to be determined, since $a_o = 2d(110)$. The value of a_o corresponds to the distance between two metal cations and its value should therefore reflect the radii of the cations, as discussed in Sect. 2.2.1.

(3) Finally, the positions of the (01l) and/or (10l) reflections at intermediate angles can be used to determine the stacking pattern of the layers. Using the values of a_o and c_o determined as above, the number of layers stacked along the c axis of the unit cell can be determined by calculating the values of $d(hkl)$ for each possible value of c (c_o, $2c_o$, $3c_o$...) using the relationship

$$1/d^2(hkl) = 4(h^2 + hk + k^2)/3a_o^2 + l^2/c^2 .$$

The true c value gives coincident calculated and experimental values for the positions of the (01l) and/or (10l) reflections within experimental error.

Furthermore, rhombohedral and hexagonal structures can be distinguished by systematic absences: for rhombohedral structures, reflections are systematically absent unless $-h + k + l = 3n$, where n is an integer and h, k and l are the (hexagonal) Miller indices, whilst the presence of strong reflections with $-h + k + l \neq 3n$ indicates hexagonal symmetry [44]. The diffraction pattern in Fig. 4a is that of a synthetic hydrotalcite $[Mg_6Al_2(OH)_{16}](CO_3)\cdot 4H_2O$ [107]. The observed reflections can be indexed in a three-layer **3R** polytype with rhombohedral symmetry (space group $R\bar{3}m$) with unit cell values of $a_o = 0.306$ nm and $c = 2.34$ nm. In this case, the basal repeat distance, c_o, is $c/3$. The pattern in Fig. 4b [107] is that of the mineral manasseite (JCPDS 14–525) which has the same formula as hydrotalcite and the reflections can be indexed in a two layer **2H** polytype with hexagonal symmetry (space group $P6_3/mmc$) with unit cell values of $a_o = 0.306$ nm and $c = 1.56$ nm. The basal spacing c_o corresponds to $c/2$ and is numerically identical to that in hydrotalcite.

In order to distinguish between different polytypes with closely related stacking sequences it is essential to analyze the *intensities* of the non-basal reflections. Bookin and Drits [98–100] have simulated the diffraction patterns of many different polytypes. Although only qualitative results were obtained because the calculations neglect scattering of anions and water molecules in the interlayers, a set of criteria were derived that can be used to distinguish between different polytypes. For example, for the $\mathbf{3R}_1$ polytype, intensities of (01(l+1)) reflections are stronger than (10l) ($l = 3n + 1$, n = integer) whereas the reverse is true for the $\mathbf{3R}_2$ polytype. The presence of (012), (015) and (018) reflections in Fig. 4a indicates that hydrotalcite has the $\mathbf{3R}_1$ structure

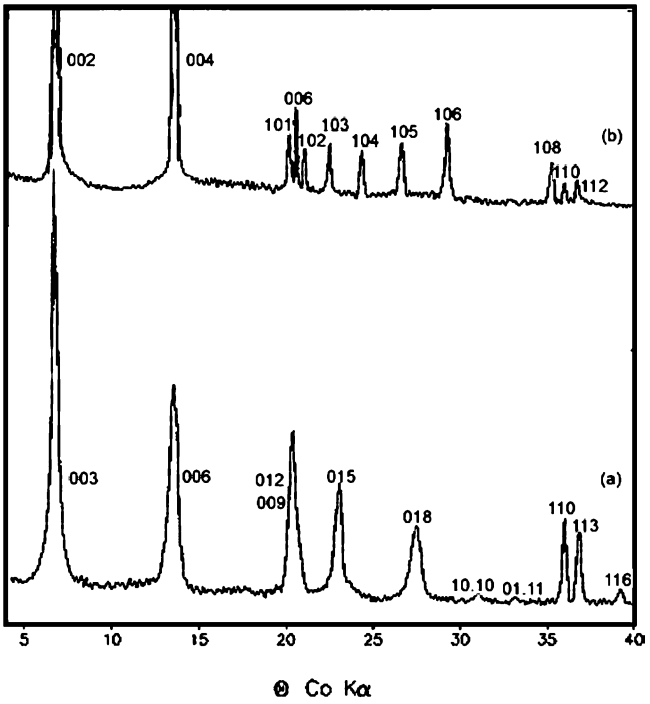

Fig. 4 Diffraction patterns of **a** a synthetic hydrotalcite $[Mg_6Al_2(OH)_{16}](CO_3)\cdot 4H_2O$ which has a **3R** polytype and **b** the mineral manasseite which has the same formula as hydrotalcite but a **2H** polytype. Reprinted with permission from [107]. Copyright Kluwer Academic Publishers

and it is generally believed that most carbonate-containing LDHs have this structure [7, 100] since, the prismatic arrangement of hydroxyl groups allows those in both upper and lower layers to form hydrogen bonds with the oxygen atoms of the carbonate anions (see Sect. 3.2). Jones et al. [108] have reported the synthesis of the $\mathbf{3R}_2$ polytype of an LDH by hydrothermal treatment of a mixture of a flash calcined gibbsite and magnesium oxide, characterized by strong reflections that can be indexed as (101), (104) and (107) (Fig. 5). It was suggested that the majority of the interlayer anions are hydroxide, rather than carbonate, consistent with the observation that carbonate ions generally occupy prismatic interlayers. In this case there would be a cubic close packing sequence formed by hydroxyl groups of neighboring layers and the interlayer hydroxide ions. Based on an analysis of the intensities of the (01*l*) reflections, Moggridge et al. [44] have shown that Mg/Al LDHs containing interlayer benzoate or terephthalate anions both have the $\mathbf{3R}_1$ structure.

Distinguishing between different polytypes with hexagonal symmetry is more difficult, since the intensities of reflections are sensitive to the identity of the interlayer anion. Simulated XRD patterns suggest that manas-

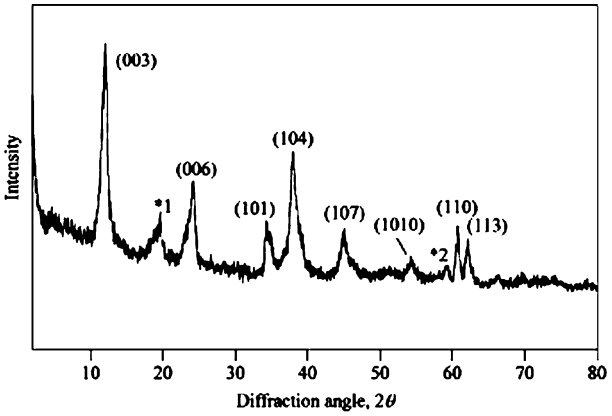

Fig. 5 Diffraction pattern of a $\mathbf{3R}_2$ polytype of an $Mg/Al-CO_3$ LDH (peaks *1 and *2 are probably due to brucite). Reprinted with permission from [108]. Copyright Royal Society of Chemistry

seite and sjögrenite (one polytype of $[Mg_6Fe_2(OH)_{16}]CO_3{\cdot}4.5H_2O$) have the $\mathbf{2H}_1$ structure, which was confirmed by single crystal X-ray diffraction on the latter mineral [7]. Whereas carbonate favors prismatic interlayers (as found in $\mathbf{3R}_1$ and $\mathbf{2H}_1$ polytypes), hydrotalcite-like minerals containing interlayer sulfate ions have been found [99] to exist in polytypes with both prismatic ($\mathbf{3R}_1$) and octahedral ($\mathbf{3R}_2$, $\mathbf{3H}_2$) interlayers with the latter being more common.

In mineral samples, different polytypes are often found intergrown. For example, hydrotalcite and manasseite often occur together with the latter on the inside and the former on the outside of the grains [71]. This has been interpreted as indicating that the latter is favored by high temperature since the inside of the grains cools more slowly than the outside. Pons et al. [71] have suggested that the $\mathbf{3R}_1$ polytype can be constructed from a stack of identical brucite **AbC** layers by translations of $(2a/3 + b/3)$ between consecutive layers whilst formation of the $2H_1$ polytype requires a translation of $(2a/3 + b/3)$ followed by a 60° rotation. Thus formation of the latter requires higher temperatures. An alternative explanation was suggested by Hofmeister and von Platen [92], who noted that although the interlayers are prismatic in each case so that the layer-interlayer interactions are the same, they differ in that the cations in adjacent layers are directly superimposed on lattice rows parallel to the c axis in the case of $\mathbf{2H}_1$ but are shifted by $(2a/3, b/3)$ between adjacent layers in the case of the $\mathbf{3R}_1$ polytype. This indicates that long-range interactions between cations in adjacent layers may influence the stacking of the layers. Thus hexagonal stacking of the layers to give the $\mathbf{2H}_1$ polytype with eclipsed cations requires higher energy than rhombohedral stacking to give the $\mathbf{3R}_1$ polytype where the cations are stag-

gered. Among the large number of synthetic LDH carbonates, no examples of the **2H**$_1$ polytype have been directly prepared [100]. Interestingly, however, it has also recently been claimed [109] that under pressure a synthetic hydrotalcite transforms irreversibly to a manasseite-like phase at about 1.5 GPa. Further compression leads to formation of an amorphous phase at pressures of 4.0–4.5 GPa. Thus the occurrence of manasseite inside hydrotalcite in mineral grains may reflect the pressure exerted on the core of the grains as the surface cools.

In some cases, the stacking sequence in synthetic samples changes as a function of temperature. For example [95], the XRD pattern of a Zn/Al – Cl LDH shows that it exists as the **3R**$_1$ polytype at ambient temperature, whilst heating at 150 °C results in partial dehydration accompanied by a transformation to the **2H**$_1$ polytype. A $Ni^{II}/Co^{III} - CO_3$ LDH having the **3R**$_1$ structure was converted to a **1H** polytype with a reduced basal spacing on heating at 200 °C; the **3R**$_1$ polytype was regenerated by rehydration [110]. It was suggested that the carbonate anions are monografted to the slabs in the **1H** polytype. Pausch et al. [51] reported the synthesis of LDHs with interlayer hydroxide anions. At lower reaction temperatures, the **3R**$_1$ polytype was formed. At higher temperatures (e.g. 150 °C, 100 MPa for Mg_3Al) a second polytype was formed, for which a disordered layer stacking was proposed. Bookin and Drits [100] subsequently suggested, however, that the XRD pattern of the latter phase could be indexed as the **3R**$_2$ polytype with a cubic close packing of layer hydroxyl groups and interlayer hydroxide ions. As noted above, the same polytype was observed for an Mg/Al LDH with interlayers containing predominantly hydroxyl anions [108]. In the case of the Friedel's salt halide series $[Ca_2Al(OH)_6]^+[X]^-\cdot 2H_2O$, the materials exist as rhombohedral polytypes [**6R** (X = Cl), both **6R** and **3R** (X = Br) and **3R** (X = I)] at high temperature and undergo a phase transition to a monoclinic polytype on cooling [111, 112]. A sample of the mineral stichtite with the formula $[(Mg_{5.94}Ca_{0.01})_{5.95}(Cr_{1.29}Al_{0.51}Fe^{III}_{0.25})_{2.05}(OH)_{15.1}](CO_3)_{1.47}\cdot 3.7H_2O$ exists as pink grains that have the **3R**$_1$ structure with a basal spacing c_o of 0.776 nm [113]. On irradiation with visible light or X-rays, a green species is formed which has the **1H** polytype stacking with a reduced basal spacing of 0.737 nm.

In the case of Li/Al LDHs, it has been shown that $[LiAl_2(OH)_6]Cl\cdot nH_2O$ can exist in both rhombohedral (when $n = 2$) [114] and hexagonal (when $n = 1$) [16] polytypes, although in this case the materials are prepared from different $Al(OH)_3$ precursors rather than being interconverted by heating. Interestingly, the two polymorphs show some differences in their intercalation behavior [114]. The related compound $[LiAl_2(OH)_6]OH\cdot nH_2O$ has a random stacking of layers that can be modeled with a 54 layer structure and has pseudohexagonal symmetry [115].

Unfortunately, for many of the synthetic LDHs that have been reported in the literature the XRD patterns are less informative than those in Figs. 4

and 5. Methods of synthesis that give highly crystalline samples have been reviewed by He et al. in Chapter 2 of this volume, and in these cases materials often do have diffraction patterns that allow the polytype to be determined unambiguously. Experimental and simulated diffraction patterns for a $Co^{II}_{2.19}Fe^{III} - CO_3$ LDH produced [116] by aerial oxidation of mixed Co^{II}/Fe^{II} solutions are shown in Fig. 6 and indicate a $\mathbf{3R_1}$ polytype with a_o = 0.312 nm and c = 2.278 nm. When an $Mg_{2.01}Mn^{III} - CO_3$ LDH is formed [117] by aerial oxidation of $Mg(NO_3)_2/MnCO_3$ mixtures at constant pH a highly crystalline material with a $\mathbf{3R_1}$ polytype is formed as shown by the diffraction pattern in Fig. 7a, but when an analogous material is prepared by traditional coprecipitation methods a much less crystalline material is obtained (Fig. 7b).

Many synthetic LDHs give diffraction patterns even less well defined than that in Fig. 7b (typical examples [118] are shown in Fig. 8) and in such cases it may only be possible to determine the basal spacing from the positions of the (00l) reflections. The lines can then be indexed as a one-layer polytype since there is no need or justification for using a larger unit cell [118]. In fact, however, in the literature many similar patterns are still indexed using the **3R** stacking sequence. If the (110) reflection is resolved, then the unit cell parameter a_o can be calculated, but if this reflection is broadened and overlaps with other reflections at higher angle, even this may not be possible with any degree of certainty as discussed in Sect. 2.2.1.

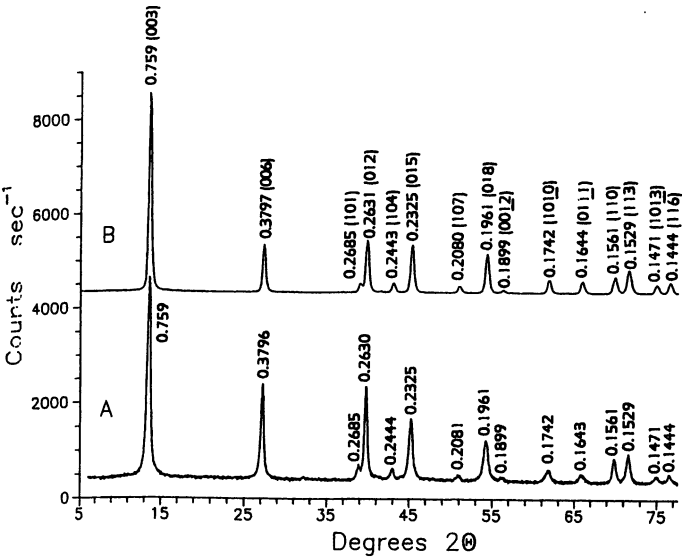

Fig. 6 Experimental **A** and simulated **B** diffraction patterns for a $Co^{II}/Fe^{III} - CO_3$ LDH produced by aerial oxidation of mixed Co^{II}/Fe^{II} solutions which indicate a $\mathbf{3R_1}$ polytype. Reprinted with permission from [116]. Copyright Academic Press

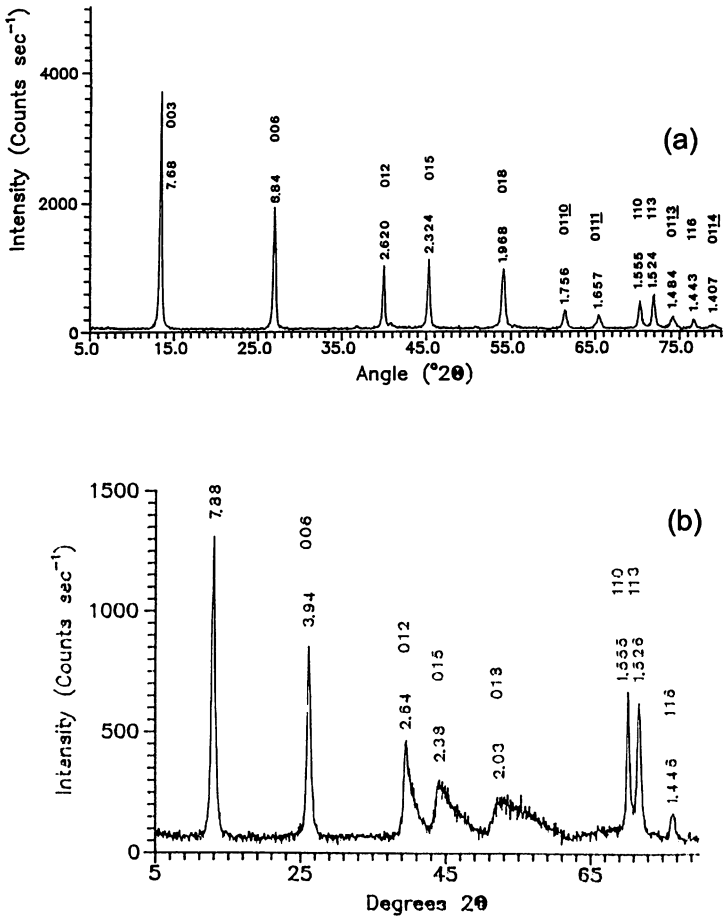

Fig. 7 XRD patterns of **a** an $Mg/Mn^{III}-CO_3$ LDH formed by aerial oxidation of $Mg(NO_3)_2/MnCO_3$ mixtures at constant pH and **b** an analogous material prepared by traditional coprecipitation methods. Reprinted with permission from [117]. Copyright The Mineralogical Society

There are a number of reasons why the XRD peaks of LDH samples are often rather broad. The relatively small domain size, particularly in the (00*l*) direction, leads to line broadening. The Scherrer equation may be used to estimate the domain size in the *a* and *c* directions from the width of the (110) and (00*l*) reflections, respectively [119, 120], although the inherent approximations in this method should always be borne in mind [121, 122].

If the broadening of peaks is non-uniform and characteristic of certain families of planes, or is so excessive as to give unrealistically small crystallite sizes, factors other than crystallite size must also be considered [123]. Various kinds of disorder may be incorporated during the crystallization process

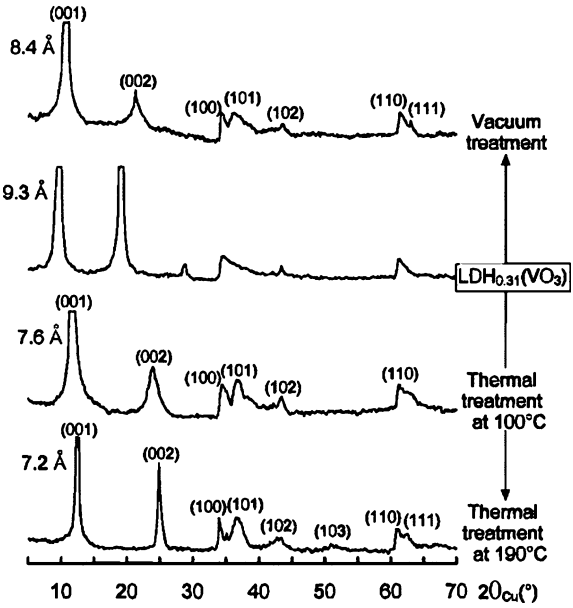

Fig. 8 Examples of diffraction patterns of poorly crystalline LDHs that can best be indexed as one layer polytypes. Reprinted with permission from [118]. Copyright American Chemical Society

leading to a loss of "crystallinity" (see [124] for recommendations regarding use of the term "crystallinity"). Several authors have investigated the different types of disorder present in divalent metal hydroxides having the brucite structure [125–128]. The XRD patterns may be simulated with the DIFFaX program [39], which utilizes a statistical recursive approach in order to model extended planar faults. The various types of slabs present in the material are constructed from the ideal atomic positions and the unit-cell parameters. These slabs are then packed along the *c* direction using the stacking vectors (1/3, 2/3, 1) and (2/3, 1/3, 1) along with (0, 0, 1). The use of the former two stacking vectors at low (< 0.15) probabilities simulates the effect of stacking faults by introduction of cubic close packed ABC motifs in the normal hexagonal close packed ABAB packing and leads to selective broadening of the (*h*0*l*) (101 and 102) reflections [103, 126, 128]. The use of all three stacking vectors with equal (0.3333) or almost equal probabilities affords a more random packing of layers, corresponding to turbostratic disorder. In these cases, in addition to an increased broadening of the (*h*0*l*) reflections, the (*hk*0) (100 and 110) reflections become essentially two-dimensional *hk* in nature and acquire a "saw tooth" or "shark's fin" line shape, rising sharply and displaying an asymmetry on the high angle side [20, 128].

Similar simulations can be carried out for LDHs and also show that if the positions of cations in adjacent layers are not correlated along the *c* axis,

i.e. there are stacking faults, then significant diminution in intensities of certain reflections are expected. For example, for the case of the $\mathbf{3R}_1$ polytype, if a small number of such faults are present, the position, intensities and narrow linewidths of the (11*l*) reflections are unchanged whereas the intensity of the set of (10*l*) reflections is reduced and the lines are broadened, and they are shifted to lower angle than that expected on the basis of the cell defined by the (11*l*) reflections [100, 103]. If the number of faults is so large that the cations are completely uncorrelated along the *c* direction, the (10*l*) reflections have the "shark's fin" peak shape associated with turbostratic structures [20, 100, 129, 130].

In synthetic samples, stacking faults often arise from an intergrowth of rhombohedral and hexagonal polytypes that gives rise to broad asymmetric (01*l*)/(10*l*) reflections in the XRD patterns as shown in Fig. 7b. Rebours et al. [39] have proposed that the occurrence of faults can be quantified in terms of a "fault probability" (FP), where FP = 1.0 describes a pure rhombohedral polytype $\mathbf{3R}_1$ and FP = 0.0 a pure hexagonal polytype $\mathbf{2H}_1$, whilst a completely random stacking has FP = 0.5. They estimated that FP$\cong$ 0.6 for a number of Mg/Ga and Ni/Al LDHs whilst an $Mg_{1.8}Al$ LDH had an essentially pure rhombohedral structure, as shown by the sharpness and symmetry of the (01*l*) reflections. This was rationalized by noting that, as described above, the arrangement of cations is different for the two polytypes and that although the local symmetry of the interlayer is the same for both polymorphs, charge compensating anions will not interact with the layers in the same way [92]. In the case of the $\mathbf{2H}_1$ polytype, the compensating forces are perpendicular to the layers, but in the case of the $\mathbf{3R}_1$ polytype they are directed more diagonally through the interlayer to the next octahedral layer. When the cations have a high average charge density (e.g. Mg_2Al), leading to extensive polarization of the hydroxyl groups, the staggered arrangement of cations in the $\mathbf{3R}_1$ polytype may be favored over the eclipsed arrangement in the $\mathbf{2H}_1$ polytype. When the cations have lower average charge density (e.g. Mg_3Al or Mg_2Ga), the difference between the two polytypes may be less marked, leading to a greater prevalence of stacking faults. Kamath et al. [103], however, have suggested that the XRD pattern of another Mg/Al LDH with very similar composition can best be simulated using the same approach by assuming a random intergrowth of $\mathbf{3R}_1$ (60%) and $\mathbf{3R}_2$ (40%) polytypes (see the simulated and calculated patterns in Fig. 9). They chose the $\mathbf{3R}_2$ polytype on the grounds that a synthetic example has been reported [108] as discussed above, but it should be noted that this is believed to contain mostly hydroxide, rather than carbonate, anions in the interlayers. This indicates that the nature and degree of stacking faults observed may vary according to method of preparation as well as sample composition. It should also be noted that, as in any empirical fit, there may not be a unique solution and several solutions involving different stacking sequences may exist.

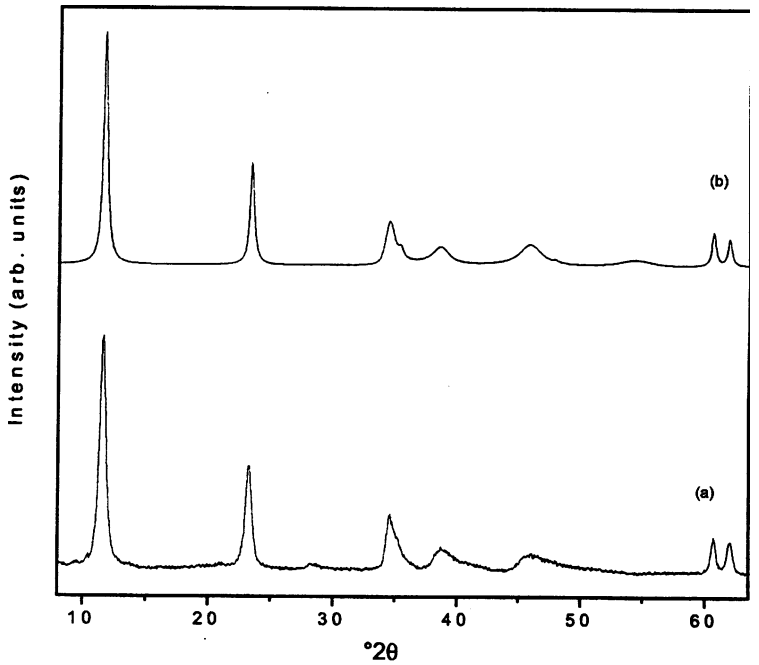

Fig. 9 **a** Experimental diffraction pattern of an $Mg/Al-CO_3$ LDH and **b** the simulated pattern assuming a random intergrowth of $\mathbf{3R}_1$ (60%) and $\mathbf{3R}_2$ (40%) polytypes. Reprinted with permission from [103]. Copyright The Clay Minerals Society

Stacking faults and turbostratic distortion have been associated [101] with a mismatch in the geometries of layers and interlayer anions, which prevents an ideal packing of the slabs of the type that is often observed with interlayer carbonate anions. Delmas et al. [131, 132] have suggested, however, that an alternative explanation, local distortions within slabs due to microstrains arising from the distribution of electrostatic charges, is more likely. They based this conclusion on the fact that a γ-oxyhydride with the formula $H_{0.20}Na_{0.12}K_{0.21}(H_2O)_{0.47}Ni_{0.70}Co_{0.30}O_2$ can be converted to a vanadate-intercalated LDH by reduction with hydrogen peroxide in the presence of ammonium metavanadate (a so-called *chimie douce* method of synthesis) and then subsequently regenerated by oxidation [131]. The XRD pattern of the γ-oxyhydride precursor exhibits sharp (01*l*) (strong) and (10*l*) (weak) reflections characteristic of a regular rhombohedral stacking (space group $R\bar{3}m$, $\mathbf{3R}_1$ polytype in the notation used above, *P*3 type in the notation used for layered metal oxides), and thus extensive rotation of the slabs would be required if the reduction-oxidation processes were to be accompanied by a switch between rhombohedral and turbostratic stacking. It was suggested that this is unlikely under the mild conditions employed.

3.2 Arrangement of Anions and Water in Interlayer Galleries

3.2.1 Evidence from X-ray Diffraction

A considerable amount of information can be obtained about the location and bonding of the interlayer anions by XRD, although the detailed structure of the highly disordered hydrogen bonding network in the interlayer galleries is not amenable to study by this method.

When the intercalated anions do not contain atoms with large scattering power, intensities of the basal (00*l*) reflections are mainly governed by the X-ray intensity scattered by metal cations in the host layers as discussed in Sect. 3.1 and the intensities generally decrease as *l* increases, although some anomalous intensities can be observed even with organic guests containing only light atoms [20, 44, 133]. Care should be taken where the positions of the (006) reflections of the intercalated species are close to those of the (003) reflections of possible impurities such as LDH-Cl/NO_3 precursors or LDH-CO_3 derived by uptake of atmospheric carbon dioxide [104]. The positions of the basal reflections of Ni^{II}/Fe^{III} and Ni^{II}/Co^{III} LDHs containing interlayer carbonate anions show no change on heating up to 160 °C, but the intensity of the (006) reflection (I(006)) decreases relative to I(003). Simple simulations suggest a reduction in interlamellar electron density associated with loss of water is responsible [110]. If the interlayer contains a metal complex anion as the guest, the second basal reflection is generally although not always [134] more intense than the first, which has been attributed to an increased electron density at the midpoint of the interlayers, where the metal is presumed to be located [54, 135–138]. A similar inversion of intensity has been observed for sulfonated 9,10-anthraquinones [139, 140]. Many examples of polyoxometallate anions intercalated in LDHs have been reported and inversion of intensities of basal reflections is sometimes, but not always, observed [60, 141, 142]. (In these cases, an additional broad peak is often observed between the first and second basal reflections, which is usually attributed to a partially hydrolyzed salt of the polyoxometallate [141]). More detailed studies can indicate the orientation of the guest anion in the interlayer galleries since the resultant distribution of electron density as a function of fractional coordinate along the *c* axis is reflected in the intensities of the basal reflections. Intercalation of paramolybdate ($[Mo_7O_{24}]^{6-}$) in Mg/Al LDHs gave a material showing no (003) reflection [143]. The intensities of the (00*l*) reflections were calculated from structure factors and Lorentz polarization factors for two model structures (having the same basal spacing) with different orientations of the paramolybdate anion (Fig. 10). The calculated intensities for model A [0.1 ($l = 3$), 100.0 ($l = 6$), 45.8 ($l = 9$), 0.2 ($l = 12$) and 12.4 ($l = 15$)] were very close to the observed intensities.

Simulation with the DIFFaX program of the XRD patterns of simple model structures involving MO_2 (M = Mo, W) slabs inserted to varying extents between slabs of NiO_2 were shown [101] to be remarkably effective in reproducing the XRD patterns of materials composed of $[M_2O_7]^{2-}$ anions intercalated in Ni^{II}/Co^{III} LDHs, where I(003) < I(006) and the ratio of the intensities varies with the amount of interlayer guest. Intercalation of $[Cr_2O_7]^{2-}$ anions in Ni^{II}/Al LDHs [144] gives a material with similar interlayer spacing but with I(003) > I(006), presumably associated with the presence of first row transition metals in both layers and interlayers. Intercalation of the same anion in Mg/Al LDHs [145] gives a material with I(003) < I(006). A significant broadening of the (006) reflection was observed in the XRD patterns of $[M_2O_7]^{4-}$ (M = V, P) intercalated in the latter host, which was attributed to a disorder in the periodicity of the (00*l*) planes, possibly related to the formation of polymeric chains in the interlayer galleries [146]. In the case of 9,10-anthaquinone-2,6-disulfonate, two intercalated phases with basal spacings of 1.9 and 1.2 nm could be prepared [140]. It was proposed that these involve almost vertical and tilted guest anions, respectively. Interestingly the (00*l*) peak intensities show very different patterns, which presumably reflect the different locations of the sulfur atoms along the *c* axis. Ferrocenecarboxylate and 1,1′-ferrocenedicarboxylate anions have been intercalated in Zn/Al LDHs giving materials [120] with basal spacings of 2.00 and 1.55 nm. These were interpreted in terms of a bilayer and monolayer of guest species, respectively, as discussed in Sect. 3.2.4. The (00*l*) peak intensities also show very different patterns, again presumably reflecting the different locations of the one or two iron atoms along the *c* axis. When the intensities of several (5 or more) (00*l*) reflections are well-defined, a one-dimensional electron density distribution along the *c* axis may be calculated. In this method, which

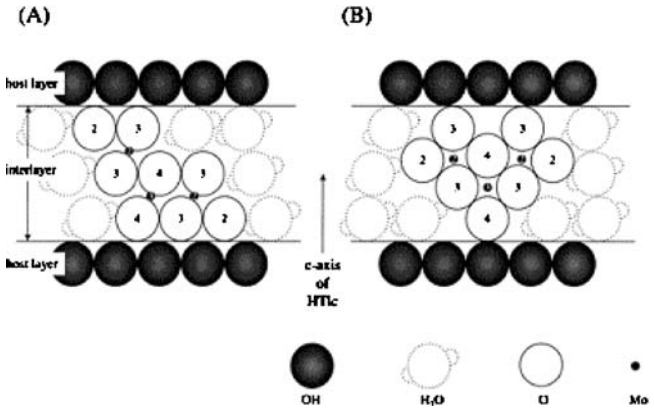

Fig. 10 Two possible orientations of paramolybdate ($[Mo_7O_{24}]^{6-}$) in the interlayer of LDHs. Reprinted with permission from [143]. Copyright American Chemical Society

has been widely used for other layered solids [147–149], peak intensities are obtained from integrated peak areas and, after correction for Lorentz polarization effects, used to generate structure factors and then finally electron density maps can be generated for $z = 0$–1. To date, there have been only a few reports of such calculations for LDHs. In the case of a tetrasulfonated perylene dye intercalated in an Mg/Al LDH, the electron density distribution plot obtained is shown in Fig. 11. The high electron densities at the edges ($z = 0$ and $z = c_o$) are associated with the close packed metal hydroxide layers, whereas the two maxima in electron density in the interlayer gallery are attributed to the sulfur atoms, since these have the highest scattering power. The two minima in electron density can be associated with the C – N single bonds, which are the site of minimum electron density in the molecule. On this basis, the structural model shown in Fig. 11 was proposed [150].

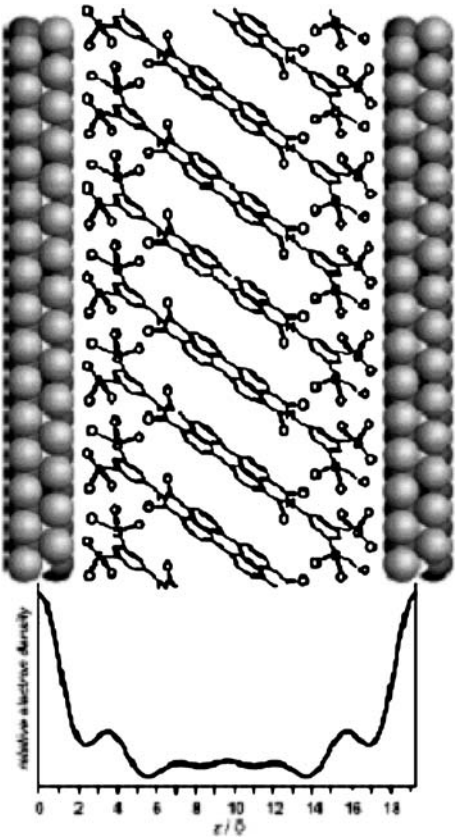

Fig. 11 One-dimensional electron density projection along the *c*-axis for a perylene dye intercalated in an Mg/Al LDH and a structural model based on this data. Reprinted with permission from [150]. Copyright Wiley

In the case of stearate ions intercalated in Mg/Al LDHs, the electron density shows a pronounced minimum in the center of the interlayer region, which is consistent with the presence of a bilayer of guest molecules [151, 152]. The electron density distribution for an anionic azobenzene derivative intercalated in an Mg/Al LDH has also been reported [153].

3.2.2 Rietveld Refinement of Interlayer Structure

When sufficiently large, defect-free single crystals of a material are available, its structure can be precisely determined by X-ray diffraction. Unfortunately, most LDHs are only available in the form of fine crystallites, and this is generally not possible.

When suitable crystals are not available, the Rietveld technique can be used to refine structural details (atomic coordinates and site occupancies) for LDHs, if their idealized structure is known. If there is disorder present, such as stacking faults or interstratification, which as discussed in Sect. 3.1 are common for layered species such as LDHs, then a Rietveld refinement will not be possible [39]. Care must be taken to avoid preferential orientation of the platelets [105, 106, 123, 154]. A Rietveld analysis for an LDH with the formula $[Zn_4Al_2(OH)_{12}]Cl_2{\cdot}nH_2O$ has been reported [106]. The layers stack in the $\mathbf{3R}_1$ polytype ($R\bar{3}m$ space group). Several possible locations for interlayer chloride ions and water molecules were considered: the 3(b) sites (site symmetry $\bar{3}m$) at the midpoint of the O$\cdots$O vector between oxygen atoms of adjacent layers, and adjoining sets of sites distributed in groups of six around the three-fold O$\cdots$O axis – 18(g) positions (site symmetry .2) (Fig. 12) or 18(h) positions (site symmetry .m).

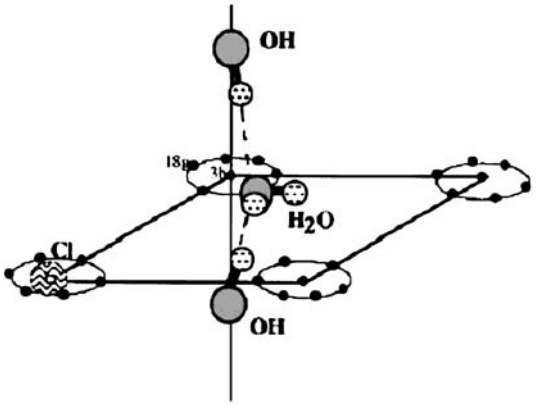

Fig. 12 Possible location of interlayer species in $[Zn_4Al_2(OH)_{12}]Cl_2{\cdot}nH_2O$. Reprinted with permission from [106]. Copyright Academic Press

Geometrical considerations suggest that for chloride ions, OH· · ·Cl· · ·HO hydrogen bonding will be maximized if the anions occupy 3(*b*) sites, whereas OH· · ·O· · ·HO hydrogen bonding is optimized if the water molecules occupy 18(*g*) or 18(*h*) sites. For the fully hydrated ambient temperature material ($n = 4$), the results indicate that the water molecules do indeed occupy the 18(*g*) or 18(*h*) sites and the chloride ions exhibit strong oscillations around the equilibrium position 3(*b*) associated with their hydrogen bonding interaction with water molecules. Experimental, calculated and difference powder XRD patterns are shown in Fig. 13 [106]. At higher temperatures as water is progressively removed, the chloride ions become increasingly localized in 3(*b*) positions. This is reflected in an increase of the intensity of (110) reflection relative to that of the (113) reflection observed in both experimental and simulated XRD patterns.

Rietveld refinement of analogous $[M_4Cr_2(OH)_{12}]Cl_2{\cdot}4H_2O$ (M = Zn, Cu) materials suggest that the chloride ions also occupy 18(*g*) sites with the water molecules disordered over 18(*g*) (M = Zn) or 36(*i*) (M = Cu) sites [25]. It was suggested that the layer oxygen-chloride distances (O· · ·Cl = 0.2827 nm for M = Zn and 0.2916 nm for M = Cu) are consistent with the presence of OH· · ·Cl hydrogen bonding since they are similar to the O· · ·O distances between hydroxyl groups and water molecules (0.2827 nm for M = Zn and 0.3151 nm for M = Cu), for which hydrogen bonding can be demon-

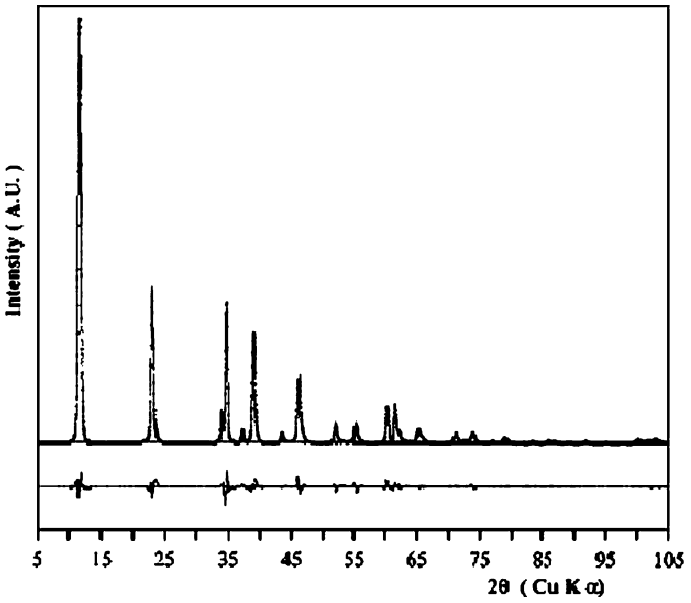

Fig. 13 Experimental, calculated and difference powder XRD patterns for $[Zn_4Al_2(OH)_{12}]Cl_2{\cdot}nH_2O$ at ambient temperature. Reprinted with permission from [106]. Copyright Academic Press

strated by IR spectroscopy. Refinement of the structure of the related green rust material with approximate stoichiometry $[Fe^{II}_4Fe^{III}_2(OH)_{12}]Cl_2{\cdot}4H_2O$ at ambient temperature suggested that chloride and water both occupy sites off the three-fold O···O axes, with the water slightly closer to the axis than the chloride (0.032 nm vs. 0.080 nm) [155]. This was ascribed to the larger radius of Cl^-. A single crystal study of the mineral iowaite, $[(Mg_{5.9}Fe^{II}_{0.1})Fe^{III}_2(OH)_{16}]Cl_{1.4}(OH)_{0.48}(CO_3)_{0.06}{\cdot}4H_2O$ (space group $R\bar{3}m$) suggested that disordered interlayer $Cl^-/OH^-/H_2O$ species were located off the three-fold O···O axes [156].

A Rietveld refinement of a second green rust with approximate stoichiometry $[Fe^{II}_4Fe^{III}_2(OH)_{12}]SO_4{\cdot}ca.\ 8H_2O$ revealed a different packing sequence and interlayer structure [157]. The material has the single layer **1H** polytype and the interlayer consists of a double layer of sulfate anions and water molecules (Fig. 14), as discussed in more detail in Sects. 3.5 and 4.3. The layer hydroxyl groups and interlayer oxygen atoms have an almost ideal hexagonal close packed arrangement and the stacking sequence may be described as **AbC(∼*A*)(∼*C*)AbC**, (where **(∼*A*)** represents an interlayer species located in, or close to, an A site). On geometrical grounds, it can be seen that sulfate is unable to form the $\mathbf{3R}_1$ polytype with a single layer of anions as described above for either planar (e.g. carbonate) or spherical (e.g. chloride) anions, where the stacking sequence can be denoted **AbC(∼*C*)CaB(∼*B*)BcA(∼*A*)AbC.**

Rietveld refinements of the structures of Mg_nAl-CO_3 LDHs ($n = 2.0, 5.0$) have been reported [39]. The oxygen atoms of both carbonate ions and water molecules were found to occupy a single set of 18(*h*) sites distributed around the three-fold O···O axis with a $\mathbf{3R}_1$ polytype stacking (space group $R\bar{3}m$).

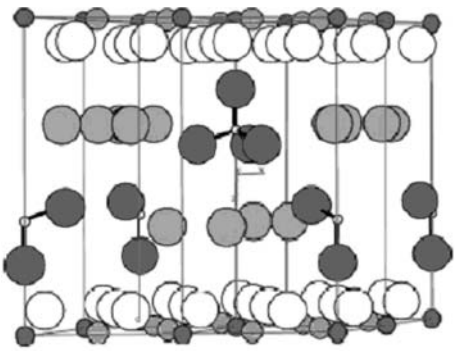

Fig. 14 View of the ordered interlayer structure of the green rust with stoichiometry $[Fe^{II}_4Fe^{III}_2(OH)_{12}]SO_4{\cdot}\ ca.\ 8H_2O$. Reprinted with permission from [157]. Copyright Elsevier SAS

3.2.3 Spectroscopic Measurements

The coordination environment around the metal in complex anions intercalated in LDHs has been studied by XAS. Extended X-ray absorption fine structure (EXAFS) studies of noble metal chloro-complexes such as $[IrCl_6]^{2-}$ [137] and $[PtCl_6]^{2-}$ [138] indicate that intercalation in LDHs is accompanied by partial hydrolysis of the M – Cl bonds. Molybdenum K-edge EXAFS measurements suggested that reaction of a Zn/Al LDH containing intercalated 2,2′-bipyridine-5,5′-dicarboxylate anions with $MoO_2Cl_2(THF)_2$ afforded a material containing a hydrolyzed species based on $[O_2Mo – O – MoO_2]$ units rather than the anticipated bipyridyl complex, since there was no evidence of Mo – Cl or Mo – N coordination shells [50]. In the case of the oxalato-complexes $[M^{II}(C_2O_4)_2]^{2-}$ (M^{II} = Cu, Co) and $[M^{III}(C_2O_4)_3]^{3-}$ (M^{III} = Ga, Mn), intercalated in Mg_2Al and Zn_2Al LDHs, EXAFS studies indicated only minor changes in coordination environment compared with that in salts of the complexes, with the perturbations induced by Mg_2Al layers being slightly more significant [135]. Comparison of the third coordination shell of $[M(C_2O_4)_3]^{3-}$ (M = Ga, Mn) indicated that the ions were oriented differently in the interlayer galleries, with the former having two short and four long Ga···O distances and the latter having three short and three long Mn···O distances, corresponding to the arrangements shown in Fig. 15.

EXAFS studies of $[M_2O_7]^{2-}$ (M = Mo, W) intercalated in Ni^{II}/Co^{III} LDHs indicated that the geometry of the intercalated anions was very similar to that in their salts [101] with one long M – O bond (involving a bridging M – O – M unit) and three shorter M – O bonds making up a distorted tetrahedral coordination shell around the metal. A second coordination shell containing two oxygen atoms was ascribed to water molecules pointing towards triangular faces of MO_4 tetrahedra. A similar conclusion was drawn in the case of $[CrO_4]^{2-}$ and $[Cr_2O_7]^{2-}$ intercalated in Ni/Al LDHs [144]. Since the degree of oligomerization in polyoxometallates is very sensitive to pH, changes in the structure of the anion may be observed on intercalation in LDHs. Comparison of EXAFS data for intercalated species with those of reference compounds often provide a useful insight into the structure of the guest [158]. For example, X-ray absorption near-edge spectroscopy (XANES) and EXAFS data at the V K-edge of a material produced by ion-exchange of a Zn/Al – Cl LDH with ammonium metavanadate are essentially identical to that of a decavanadate salt, suggesting that $[V_{10}O_{28}]^{6-}$ anions are present in the interlayer galleries of the material [159]. When the intercalation reactions were carried out at higher pH, the EXAFS data suggest that the interlayers contain polymeric anions based on VO_4 tetrahedra.

EXAFS cannot be used to distinguish between $[Fe(CN)_6]^{4-}$ and $[Fe(CN)_6]^{3-}$ because the difference in Fe – C and Fe···N distances is within experimental error. Simulation of the Fe K-edge XANES absorption edge indicates, how-

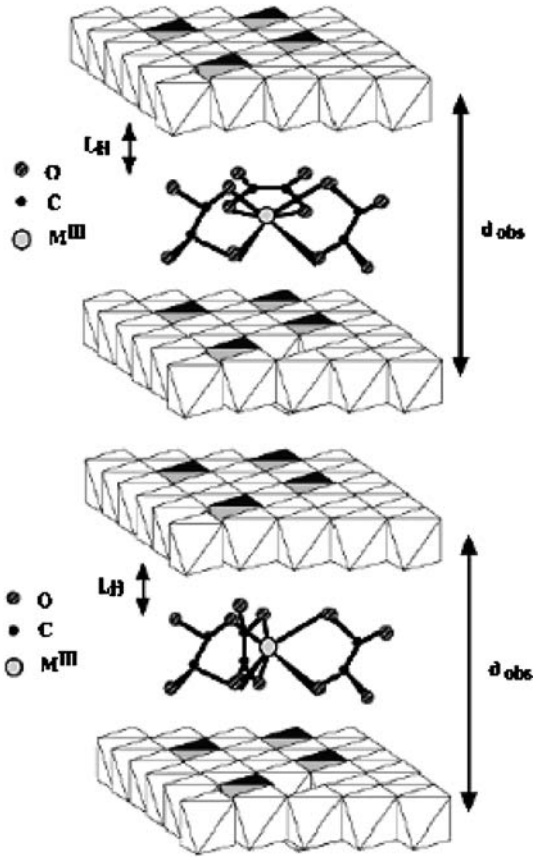

Fig. 15 Different arrangements of $[M^{III}(C_2O_4)_3]^{3-}$ in LDH intergalleries: M = Mn (*top*) and M = Ga (*bottom*). Reprinted with permission from [135]. Copyright American Chemical Society

ever, that intercalation of either $[Fe(CN)_6]^{4-}$ or $[Fe(CN)_6]^{3-}$ in LDHs leads to a partial redox reaction and a mixture of both species being present in the interlayers [160].

Vibrational spectroscopy has been widely applied in the study of LDHs [161, 162] but a somewhat confusing variety of spectral data and interpretations have appeared in the literature. In this section, we focus on the information that can be obtained regarding the structure of the interlayer anions. The unperturbed carbonate ion has point symmetry D_{3h}. Group theoretical analysis predicts four normal modes: the ν_1 symmetric stretch of A_1' symmetry at 1063 cm^{-1}, the ν_2 out of plane bend of A_2'' symmetry at 880 cm^{-1}, the ν_3 asymmetric stretch of E′ symmetry at 1415 cm^{-1}, and the ν_4 in plane bend of E′ symmetry at 680 cm^{-1} [22]. The ν_2 mode is IR active only, the ν_1 mode is Raman active only, whilst the two E′ modes are both IR and Ra-

man active. Although many publications merely report a broad band in the C-O stretching region of the IR spectrum, band component analysis suggests that the ν_3 band is split into two bands separated by some 30–60 cm^{-1} [163]. This can be interpreted in terms of a lowering of the symmetry to C_{2v} or C_s. In such cases the ν_1 stretch should become allowed and indeed a weak band can often be seen [161] at about 1060 cm^{-1}. It has been suggested [161] that lowering of symmetry is associated with hydrogen bonding of the carbonate anion to layer hydroxyl groups and/or interlayer water molecules. A number of studies by Frost, Kloprogge and co-workers [163–166] on LDHs containing a variety of cations have indicated that the position of the two peaks arising from the ν_3 band depend on the nature of the divalent cation, suggesting that the variation in polarizing power of the cation affects the hydrogen bonding between the hydroxyl groups bound to it and the carbonate anion. A similar suggestion has been advanced for a series of LDHs with varying trivalent cations [73].

Some authors have suggested that the ν_3 band of the nitrate ion in LDHs shows a similar splitting, although others have reported a single band indicative of no loss of symmetry, with additional bands being assigned to carbonate impurities [22, 161]. The arrangement of nitrate ions in the interlayer galleries of LDHs has been the subject of some controversy in the literature. Xu and Zeng [55, 79] have reported that there is an abrupt increase in basal spacing in LDHs of the type $[Mg_{1-x}Al_x(OH)_2](NO_3)_x \cdot nH_2O$ when x exceeds 0.26, although Marcelin et al. [167] reported that the difference was much smaller if the preparation was carried out under hydrothermal conditions (This may indicate that the actual Mg/Al ratio in the layers tends towards 3 under hydrothermal conditions as discussed in Sect. 2.2.1). It was suggested [55, 79] that when $x < 0.26$, the nitrate anions lie in the center of the interlayer galleries with their planes parallel to the layers analogous to the position adopted by carbonate anions, with their oxygen atoms located either between hydroxyl groups on adjacent layers where there are prismatic layers or hydrogen bonded more directly to just one layer if there are octahedral interlayers [168]. When $x > 0.26$, it was proposed that alternate nitrate ions are shifted up and down the c axis with their planes remaining parallel to the layers so that they are strongly hydrogen bonded to one layer and do not interact significantly with the other (the so-called "stick-lying" model) [55, 79]. It was suggested that this structure is not observed for carbonate-containing LDHs since for a given value of x the number of divalent carbonate anions incorporated is half that of the monovalent nitrate ions, and there is still space for the former to be accommodated in the center of the interlayer galleries even at high layer charge densities. It was proposed that the "stick-lying" model is more plausible than the alternative model involving tilting of the nitrate anions in the interlayer galleries on several grounds: the nitrate ion shows no evidence of distortion from D_{3h} symmetry in the IR spectrum whilst the ν_{OH} stretching band shows two components sepa-

rated by $\approx 100\,cm^{-1}$, which was taken to indicate that some layer hydroxyl groups are hydrogen bonded to nitrate whilst others are not; ^{15}N NMR measurements [169] between – 100 °C and + 80 °C on LDHs with Mg/Al ≈ 3 are consistent with either the nitrate being rigidly held or undergoing a rapid rotation about the three-fold axis, but it should be noted that no data have been reported for LDHs with the higher interlayer spacing associated with Mg/Al ≈ 2. The "stick-lying" model been supported by Gonçalves et al. [50] who noted that on replacing nitrate by 2,2′-bipyridine-5,5′-dicarboxylate anions, which pack almost vertically with their longest dimension nearly parallel to the layers, two components were no longer observed in the ν_{OH} stretching band (although the band is very broad), suggesting that there are no longer two types of layer hydroxyl groups.

On heating LDHs of the type $[Mg_{1-x}Al_x(OH)_2](NO_3)_x{\cdot}nH_2O$ at 400 °C it was suggested [170] on the basis of IR spectroscopy and XRD, that most nitrate ions are retained in the interlayer space, some with D_{3h} symmetry and the remainder arranged vertically, directly attached to one partially hydroxylated sheet (corresponding to C_{2v} symmetry). Raman studies on a single crystal of a related compound $[Ca_4Al_2(OH)_{12}](NO_3)_2{\cdot}nH_2O$ ($n = 4, 2, 1$) indicated [171] that as water is progressively removed, the symmetric stretching mode ν_1 with A_1' symmetry shifts from 1059 ($n = 4$) to 1070 ($n = 2$) to 1055 cm^{-1} ($n = 1$) whilst the ν_4 in plane bend with E′ symmetry, which is split slightly when $n = 4$, is split more clearly into two components for $n = 2$ and gives a single peak when $n = 1$. These results were interpreted in terms of a mondentate nitrate ion bonded to one sheet, a bidentate nitrate bridging two sheets and a nitrate ion parallel to the layers, respectively. These suggestions were confirmed [171] by single crystal XRD for $n = 4$ and $n = 2$. In these materials, as described in Sect. 4.1, the calcium ion is seven coordinate with the six hydroxyl groups being augmented by oxygen atoms of either water or nitrate ions perpendicular to the layers (50% probability of each) when $n = 4$ or nitrate ions when $n = 2$ [171, 172]. The nitrate ions in the former compound are highly disordered, showing essentially free rotation about an axis perpendicular to the layers. Partial dehydration and change in coordination mode of the nitrate ion is accompanied by a contraction in basal spacing from 0.862 to 0.805 nm. A combined heating stage Raman microscopy and IR emission spectroscopy study of an Mg/Al LDH containing a mixture of carbonate and nitrate in the interlayers suggested [173] that nitrate ions are present in the centers of interlayers at room temperature but become grafted to the layers in a unidentate fashion at 150–170 °C. Grafting is commonly observed if LDHs are heated, as discussed in Sect. 4.1.

A variety of anionic transition metal cyano-complexes have been intercalated in LDHs and their structure investigated by vibrational spectroscopy [161]. There is general agreement that octahedral complexes such as $[Fe(CN)_6]^{4-}$ and $[Fe(CN)_6]^{3-}$ intercalated in LDHs align themselves with their three-fold axis perpendicular to the sheets, but the spectra are gen-

erally complicated by the presence of a number of peaks apart from those associated with the anion that was initially intercalated. These have been variously ascribed to the results of redox processes, hydrolysis, or the presence of salts [134, 174–176]. Ignoring these complications, for the case of intercalated $[Fe(CN)_6]^{4-}$ for example, the expected one IR active band (T_{1u} in O_h symmetry) is split into two bands, which can be attributed to a decrease in symmetry to D_{3d} (in which case the bands can be assigned as A_{2u} and E_u) [174, 175, 177]. The E_u band is (x, y) polarized whilst the A_{2u} band is z-polarized. Braterman et al. [134, 174, 177] have compared IR spectra of conventional (non-oriented) materials with those of an oriented sample prepared by allowing an aqueous suspension to evaporate on a barium fluoride disk. In the case of the oriented sample, the molecular three-fold z-axis, the crystallographic c axis and the direction of propagation of the light all coincide [177]. In this case, the material is probed with light polarized in the (x, y) direction for which the A_{2u} mode is forbidden. Thus whilst the conventional spectrum shows two bands, in the spectrum of the oriented sample the lower frequency E_{2u} component is suppressed [174, 177]. This method could potentially be applied to investigate the orientation of other guest anions, although care must be taken to avoid artifacts caused by uneven coverage [177].

Solid state ^{13}C MAS NMR studies of some organic guests have been reported [178, 179]. This method also allows the presence of co-intercalated carbonate and/or bicarbonate anions to be detected [179]. It was found that the UV absorbing agent 5-benzoyl-4-hydroxy-2-methoxybenzenesulfonic acid (MBSA), having both a strongly acidic sulfonic acid group and a weakly acidic phenolic group, could be intercalated as either a monovalent or divalent anion depending on the pH [180]. The sulfonate groups were proposed to be hydrogen bonded to triads of hydroxyl groups, since the IR spectral features in the 1000–1300 cm^{-1} region were nearly identical to those observed for the guanidinium salt of $MBSA^{1-}$, which has been shown by single crystal XRD to have the sulfonate group in a site of C_{3v} symmetry, hydrogen bonded to guanidinium protons [181].

A ^2H solid state NMR investigation of terephthalate dynamics and orientation in LDHs of the type $[Mg_{1-x}Al_x(OH)_2]\{(p\text{-}C_6D_4(COO)_2)_y(CO_3)_{1-y}\}_{x/2} \cdot nH_2O$ has been reported [182]. When $x = 0.37$ and $y = 0.9$, the observed interlayer spacing was 1.42 nm, corresponding to a vertical arrangement of terephthalate anions [183], and the variable temperature ^2H spectra in the range 245 to 355 K were simulated using a model involving free rotation about the C – COO axis, rather than discrete 180° flips. It was suggested that the mobility of the terephthalate anions is inhibited as the carbonate content of the interlayer gallery is increased. When $x = 0.29$ and $y = 0.51$, the interlayer spacing was 0.76 nm, corresponding to a horizontal orientation of interlayer terephthalate anions [183]. A fraction of the terephthalate anions were found to be undergoing a similar rotation, but since this seems unlikely in the constrained environment of the contracted interlayers, it was

suggested this might be due to rotation of surface adsorbed terephthalate anions.

A ^{35}Cl NMR study of the structure and dynamical behavior of ClO_4^- intercalated into Mg/Al and Li/Al LDHs has shown that the anion is rigidly held at low relative humidities and temperatures, but undergoes rapid isotropic reorientation at high relative humidities and temperatures [184]. In contrast, ^{77}Se NMR measurements by the same authors on LDHs containing interlayer SeO_4^{2-} indicate that the anion does not undergo isotropic reorientation at any relative humidity. This was ascribed to the greater ionic charge of the selenate ion compared with the perchlorate [185].

A ^{35}Cl NMR study of chloride ions intercalated in an Mg_3Al-Cl LDH and the related LDH-like hydrocalumite $[Ca_4Al_2(OH)_{12}]Cl_2{\cdot}4H_2O$ has been reported [186]. In the case of the Mg_3Al-Cl LDH, the ^{35}Cl NMR data show a poorly resolved signal indicating a range of Cl^- environments in a disordered interlayer. There is a change from triaxial to uniaxial or nearly uniaxial symmetry over a broad temperature interval below – 40 °C, suggesting a phase transition, which can also be observed by differential scanning calorimetry (DSC). In contrast, in the Ca/Al system where water molecules are coordinated to calcium ions in a seventh coordination site as discussed in Sect. 4.1, the interlayer water and chloride ions are well ordered. This may be associated with the known ordered distribution of Ca^{2+} and Al^{3+} cations in the layers (Sect. 3.3). NMR and DSC data suggest that there is a well-defined, essentially first order phase transition near 6 °C, at which the symmetry of the Cl^- site changes from triaxial in the low temperature phase to uniaxial or nearly so in the high temperature phase. The latter is a result of dynamic averaging of the hydrogen bonding interactions associated with highly mobile water and chloride ions [186]. ^1H NMR studies on $[LiAl_2(OH)_6]Cl{\cdot}xH_2O$ have also demonstrated the presence of dynamically disordered water molecules [187]. An early ^1H NMR study [167] claimed that the C_2 axis of the water molecules in an Mg/Al LDH containing interlayer nitrate ions was perpendicular to the crystallographic *c* axis, but it was later argued this was incorrect [188]. This latter study indicated that both the C_3 axis of carbonate ions and the C_2 axis of water molecules are parallel to the *c* axis and that the water possesses rotational freedom about its C_2 axis.

Mössbauer spectroscopy has been used to investigate the oxidation state of iron in complexes such as $[Fe(CN)_6]^{3-/4-}$ intercalated in LDHs [176]. By means of Mössbauer spectroscopy, it has also been demonstrated that ferrocene sulfonates intercalated in LDHs decompose on attempted ion-exchange with sodium carbonate solutions and that the liberated Fe^{3+} ions become incorporated in the layers [189].

XANES (also known as near edge X-ray absorption spectroscopy, NEXAFS) at the carbon edge provides a means of determining the orientation of organic molecules relative to a planar surface and has traditionally been used to investigate organic adsorbates on single crystal surfaces. Moggridge and

co-workers proposed [104, 190] that XANES might be a potential way of determining the orientation of organic guests in the interlayer galleries of LDHs, using benzoate as an example. At room temperature, the plane of the benzoate ion in an Mg_2Al LDH was found to be tilted $35 \pm 10°$ to the layers, whereas after heating at 50–100 °C, the benzoate lies parallel to the layers. It was later shown [44] that the first figure is an underestimate because partial dehydration and reorientation of the benzoate anions occurs under the vacuum used during the XANES experiment, and the observed result must therefore be the average of the figure for flat and almost vertical benzoate anions. This correlates well with the observed [44] decrease in basal spacing from 1.54 to 0.90 nm. In the case of Mg_3Al LDHs, the lower benzoate loading required results in the anions adopting an essentially flat orientation even at room temperature and no evidence for an expanded structure was obtained, although it has been reported [191] in non-dried samples. The area occupied by a flat lying benzoate ion, excluding van der Waals radii, is ≈ 0.21 nm^2, whereas the area available per unit charge in Mg_2Al and Mg_3Al LDHs is ≈ 0.24 and ≈ 0.36 nm^2. Thus a flat orientation of benzoate anions results in considerable steric crowding in the former, but not in the latter, case [44].

The photophysical and photochemical properties of intercalated chromophores is of interest because of the potential application of these materials in photophysical devices and in nonlinear optics; furthermore the photophysical and photochemical response of the chromophore can provide information about the interlayer organization. In the case of fluorescein, the absorption and emission spectra of intercalated and surface adsorbed dye are markedly different, with the former being similar to the crystalline disodium salt and the latter being similar to that of the dye in solution. It was concluded that the intercalated anions are arranged in an ordered form resembling that in the crystal with π–π interactions between the chromophores [192]. The fluorescence of methyl orange-intercalated LDHs is similar that of the microcrystalline dye but is shifted to slightly higher energy in the case of the hydrated species, whilst dehydration leads to a shift to lower energy. This was interpreted in terms of the packing of the anions in the dehydrated form being closer to that in the dye itself [193]. The absorption spectrum of 9-anthracenecarboxylate intercalated in LDHs shows an unexpected band around 490 nm that was attributed to an aggregate of the guest anions. Excitation around 500 nm generates an emission attributed to the same type of aggregate [133]. UV spectroscopic evidence for aggregates of salicylate anions intercalated in LDHs has also been reported [194]. It has been suggested that conventional and space-resolved fluorescence spectra obtained by confocal fluorescence spectroscopy can give valuable information about the distribution of fluorescent dyes in the interlayer galleries of LDHs [195]. Reaction of 4-nitrohippuric acid ($O_2NC_6H_4CONHCH_2COOH$) (NHA) with $[LiAl_2(OH)_6]Cl$ leads to intercalation of the neutral organic molecule with-

out loss of chloride ion. The resulting material exhibits frequency-doubling characteristics, indicating an ordered array of guest molecules within the interlayer galleries [196]. Interestingly, crystals of pure NHA do not exhibit any nonlinear optical properties as a result of the centrosymmetric packing in the crystal.

The alignment of 4′-chloro-4-stilbenecarboxylic acid (CSC) intercalated in Mg/Al LDHs has been investigated [197] by electric linear dichroism, which indicated that the guest anions were intercalated as a double layer, with the tilt of the molecular plane being $\approx 40°$.

3.2.4 Molecular Modeling

It is generally accepted that the interlayer arrangement in LDHs depends strongly on the area available to each anion. Since the distance between adjacent metal ions in the layers is equal to the unit cell parameter a_o, the area occupied by one $M(OH)_2$ unit (shown by the rhomb highlighted in Fig. 16) is $a_o^2 \sin 60°$ [193]. For an LDH with layers of the type $[M^{II}{}_{1-x}M^{III}{}_x(OH)_2]^{x+}$, the area per unit charge is therefore $(1/x)a_o^2 \sin 60°$.

When a monovalent anion balances the positive charge on one side of the sheet, the same charge is not "available" for another anion approaching the sheet on the other side. This means a monolayer of intercalated monovalent anions can be formed if their cross-sectional area is $\leq (1/x)a_o^2 \sin 60°$, regardless of whether the anions "see" the positive charges of the layer on only one side or on both sides of the sheet.

The gallery height in LDHs is normally estimated [1] by subtracting the thickness of the brucite-like layers (assumed [198] to be 0.48 nm) from the

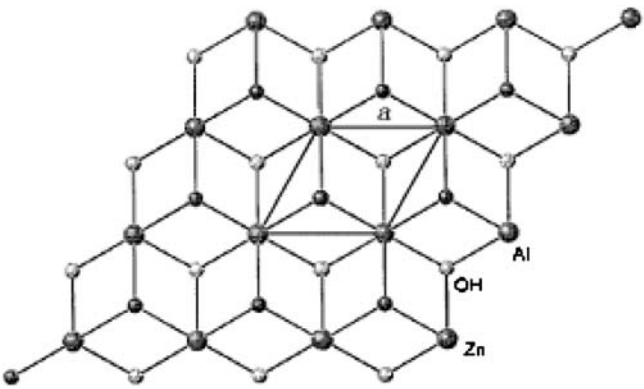

Fig. 16 Top view of brucite-like layer, where the area occupied by one $M(OH)_2$ unit is shown by the highlighted rhomb. Reprinted with permission from [193]. Copyright American Chemical Society

basal spacing determined by XRD, i.e. $d_{basal} = 0.48 + l_{anion}$ (nm), where l_{anion} includes the van der Waals radii of appropriate external atoms of the anion. Alternatively it has been suggested [130, 189, 199] that the basal spacing in intercalated carboxylate or sulfonate species can be estimated by the equation $d_{basal} = l_{layer} + 2l_{O-H-O} + l'_{anion}$, where the layer thickness (l_{layer}) is 0.21 nm (the intralayer O···O distance perpendicular to the layers in brucite [13]), l_{O-H-O} corresponds to the length of a strongly hydrogen bonded O – H··O unit (0.27 nm) and l'_{anion} is the length of the anion. Thus $d_{basal} = 0.75 + l'_{anion}$ (nm).

A theoretical model for estimating the textural properties of LDHs by combining geometrical models of the layers and the intercalated anions has recently been proposed [200]. The model allows the estimation of interpillar distances, interlamellar and external areas, the interlamellar free volume, fraction of external anions and the apparent and true density of the LDH. For well-crystallized LDH samples, good agreement between calculated and experimental results was found, whereas for poorly crystalline samples, a correlation between the degree of crystallite agglomeration and experimental values was proposed. For example, the very high surface area of an $Mg_{3.3}Al - [Fe(CN)_6]^{3-}$ LDH was satisfactorily rationalized [200] and the model has also been used to aid in the discussion of the orientation of $[H_4Co_2Mo_{10}O_{38}]^{6-}$ anions in Mg/Al LDHs [201].

Calculations based on simple molecular models and the charge density of the layers suggest that sulfopropylated-β-cyclodextrin and carboxyethylated-β-cyclodextrin are arranged in the interlayer galleries with their conical axis parallel to the layers with a packing structure which is similar to that in crystalline cyclodextrin complexes, where the molecules are arranged in a brickwork pattern [202].

The molecular dimensions of the (4-phenylazophenyl)acetate anion have been calculated [153] based on the molecular structure determined by the MM2 semiempirical molecular dynamics method together with appropriate van der Waals radii (Fig. 17). The area per unit negative charge on the layers can be calculated from the crystallographic structure. At low anion loadings, it was found that the guest anions lie parallel to the layers for LDHs with Mg/Al ratios of either 2 or 3. At higher loadings, a vertical orientation is observed. In the case of Mg/Al = 3, the cross-sectional area of the guest is smaller than the area per unit charge on the layers so that the molecules are arranged in an antiparallel fashion with little interaction between them. For Mg/Al = 2, the cross-sectional area of the guest is larger than the area per unit charge, so the molecules are slightly staggered in order to reduce the lateral interactions, leading to an increase in interlayer distance (Fig. 18).

The most probable arrangement of fluorescein anions in LDHs has been investigated [192] using Hyperchem, a molecular visualization and simulation program and the predicted arrangement was consistent with both the

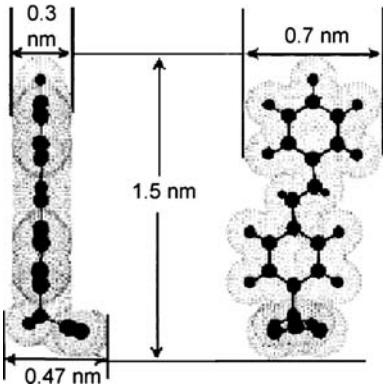

Fig. 17 Calculated molecular dimensions of the (4-phenylazophenyl)acetate anion. Reprinted with permission from [153]. Copyright American Chemical Society

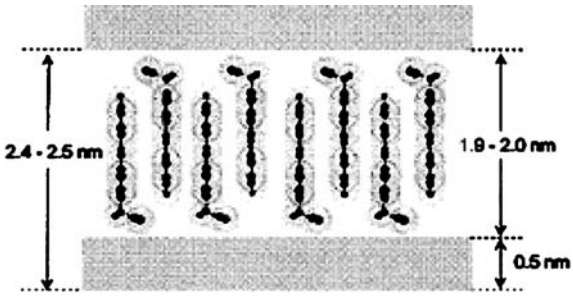

Fig. 18 Staggered arrangement of the (4-phenylazophenyl)acetate anion in LDH galleries. Reprinted with permission from [153]. Copyright American Chemical Society

observed basal spacing and the fluorescence behavior of the intercalate discussed in Sect. 3.2.3.

The approximate van der Waals dimensions of the methyl orange molecule have been calculated using the Hyperchem program and are shown in Fig. 19 [193]. It was calculated that the cross-sectional area is $\approx 0.22\,nm^2$ at the $-SO_3^-$ group (although other workers [203] have estimated the area to be as large as $0.27\,nm^2$) and $\approx 0.29\,nm^2$ at the $-N(CH_3)_2$ group. When intercalated in a Zn_2Al host, for which the unit layer charge area is $\approx 0.25\,nm^2$, the fact that the cross-sectional area of the $-N(CH_3)_2$ moiety is larger than the area available suggests that the molecules will pack in an antiparallel fashion, as shown by the computer model in Fig. 20a. It was suggested that in the hydrated state, water molecules may occupy the space between $-N(CH_3)_2$ groups and the layers, whereas when the structure is dehydrated the methyl orange anions can further interpenetrate as shown in Fig. 20b. Interestingly, the difference in basal spacing between hydrated and dehydrated forms, 0.27 nm, is very close to the diameter of a water molecule [193].

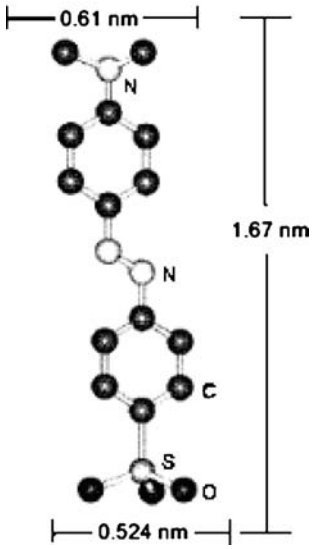

Fig. 19 Approximate van der Waals dimensions of the methyl orange molecule calculated using the Hyperchem program. Reprinted with permission from [193]. Copyright American Chemical Society

The intercalation of dodecyl sulfate, for which the calculated cross-sectional area is $\approx 0.28\,nm^2$, in Zn_nCr^{III} LDHs with $n = 2, 3$ and 6 has been reported [204]. The observed basal spacing was similar in each case and characteristic of a monolayer of surfactant. The estimated area per unit charge in the LDHs is 23, 30 and 54 nm^2, respectively. It was suggested in the case of Zn_3Cr, the similarity between the cross-sectional area of the surfactant and the available area per unit charge leads to the formation of a closely packed monolayer of surfactant anions. In the case of Zn_6Cr, intercalation of just sufficient anions to balance the layer charge would lead to them being too widely spaced to allow significant hydrophobic interactions between the alkyl chains. Therefore additional surfactant anions along with sodium cations are incorporated to give a closely packed monolayer of surfactant species. The presence of significant amounts of sodium was confirmed by elemental analysis. In contrast, for Zn_2Cr, there is insufficient space in a monolayer to accommodate the necessary amount of surfactant anions to balance the high layer charge and as a result, co-intercalation of nitrate ions, confirmed by elemental analysis, is observed. In the case of Mg_nAl LDHs ($n = 2$–5) intercalated with dodecyl sulfate, it was shown that the affinity for chlorinated organic solvents reached a maximum for $n = 3$, which was interpreted in terms of the arrangement of surfactant being optimized for inclusion of hydrophobic guest molecules [205].

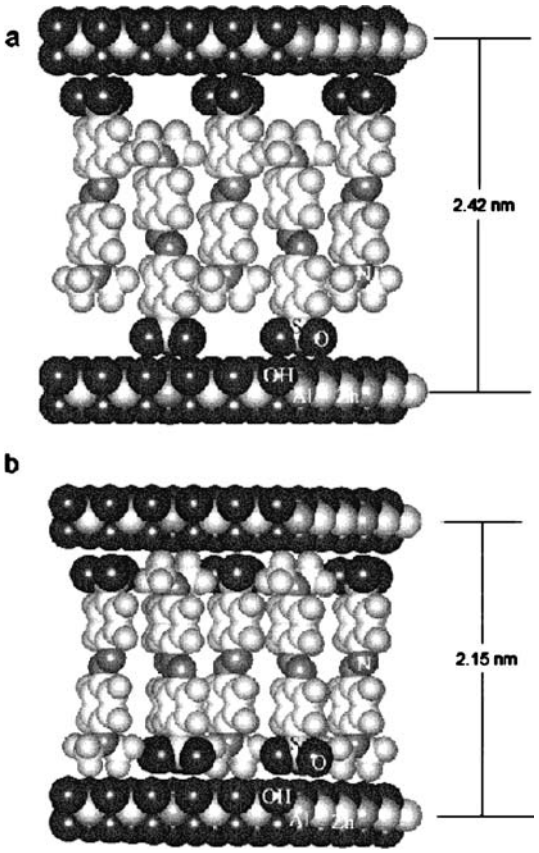

Fig. 20 Models showing arrangement of methyl orange anions in **a** hydrated and **b** dehydrated LDHs. Reprinted with permission from [193]. Copyright American Chemical Society

The molecular dimensions of the non-steroidal anti-inflammatory drugs salicylate and naproxen have been determined using the CS Chem 3D Pro program. Comparison of the dimensions of the anions (taking into account the van der Waals radii of the external atoms) with the observed basal spacings suggested that both anions form a tilted bilayer of anti-parallel molecules with carboxylate groups pointing towards the layers and the hydrophobic parts of the molecule oriented towards the center of the interlayer galleries [179].

An analogous anti-parallel packing with interpenetrating chains was proposed for dodecylbenzene sulfonate intercalated in an Mg_2Al LDH [203]. It was suggested that there are strong hydrophobic interactions between the alkyl chains because the calculated accessible area of a methylene group in the galleries (0.22 nm^2) is similar to that in a close-packed monolayer (0.20 nm^2),

and that this contributes to the high affinity of the surfactant for the host layers (as shown by the observation that it partly displaces carbonate anions from the interlayer galleries). In the case of reactions of ethanolic solutions of myristic acid, $CH_3(CH_2)_{12}COOH$, with an Mg_3Al-Cl LDH, it was found that the acid was intercalated as neutral molecules in a bilayer and chloride anions were retained as charge-balancing anions in the interlayers [206].

A model for the arrangement of a bis(2-mercapto-2,2-diphenylethanoate) dioxomolybdate(VI) complex, $\{MoO_2[OOCC(S)(C_6H_5)_2]_2\}^{2-}$, in an LDH has been proposed on the basis of the crystal structure of the ammonium salt of the anion precursor [207]. Models of the arrangement of ferrocenecarboxylate and 1,1′-ferrocenedicarboxylate in LDHs have been suggested, using the conformation and dimensions of the guest molecules obtained from single crystal XRD studies on their heterobimetallic complexes, together with the van der Waals radius of oxygen [120]. The area occupied by a 1,1′-ferrocenedicarboxylate dianion having its longest dimension perpendicular to the layers was estimated to be $\approx 0.40\,nm^2$, which is smaller than the calculated maximum area available and a monolayer arrangement of the dianions was proposed; for the ferrocenecarboxylate, a monolayer is not possible on packing grounds and a bilayer of monoanions was proposed. This is consistent with the observed interlayer spacings of 1.55 and 2.00 nm respectively. On dehydration, the dianion reorientates so that its longest dimension is almost parallel to the layers and a reduced layer spacing of 1.23 nm is observed. Napthalene-2,6-disulfonate was reported to intercalate into a Ca_2Al layered double hydroxide-like host material as a tilted monolayer, whereas naphthalene-2-sulfonate was intercalated as a perpendicular bilayer [208]. Similarly when intercalated in Zn_2Al LDHs, anthraquinone-1,5-disulfonate (AQ15) and anthraquinone-2,6-disulfonate (AQ26) are arranged in a monolayer, whereas anthraquinone-2-sulfonate (AQ2) is arranged in a bilayer with interdigitated antiparallel guest anions [209]. Interestingly, competitive intercalation experiments showed that the affinity of the LDH for the three ions varies in the order AQ2 > AQ26 $\gg$ AQ15, which was taken to indicate that the hydrophobic interactions between the anions in the bilayer structure contribute significantly to the stability of the intercalated monovalent species. This type of molecular recognition capability has also been demonstrated for other LDHs by means of the selective uptake of fumarate from fumarate/maleate mixtures, of one isomer from a mixture of naphthalene disulfonates, and of terephthalate from mixtures of all three benzenedicarboxylate isomers by Li/Al LDHs [210, 211]. The extent of separation was found to be both temperature and solvent dependent. The latter suggests that differences in solvation architecture around the anion in the bulk solvent and in the interlayer galleries play an important role in the affinity of LDHs for a particular anion [19]. The relative disposition of the negative charges in the dianions also presumably has a significant effect [19].

Experimental measurements and computer simulations have demonstrated that the orientation of terephthalate anions in the interlayer galleries of LDHs is strongly dependent on both the charge density of the layers and the interlayer water content [183]. LDHs with high layer charge density (e.g. Mg_2Al) and high water content give materials with a basal spacing of 1.40 nm, suggesting a vertical orientation of the anion with respect to the layers is favored. For lower layer charge density (e.g. Mg_3Al) and low water content, a basal spacing of 0.84 nm is observed, consistent with a horizontal orientation of the anion. The two phases may be interconverted by cycles of dehydration-rehydration.

It has been suggested [212] that under true coprecipitation conditions near pH $\approx$ 10 (at lower pH, precipitation of the trivalent metal hydroxide occurs first, followed by reaction with M^{2+} cations in solution), that Mg/Al and Mg/Ga LDHs with interlayer terephthalate ions only form when the $Mg^{2+} : Al^{3+}(Ga^{3+})$ ratio is 2 : 1 and that chloride intercalates are formed at higher ratios. At lower pH, it was suggested that mixtures of an LDH having $Mg^{2+} : Al^{3+}(Ga^{3+})$ = 2 : 1 with α-FeOOH or GaOOH were formed when the $Mg^{2+} : Al^{3+}(Ga^{3+})$ ratio in the reaction mixture exceeded 2 : 1. This was interpreted in terms of a high layer charge density being necessary for the incorporation of hydrophobic anions such as terephthalate in LDH interlayers in order to create a continuous hydrophobic layer between the sheets.

Many workers have shown [3, 19] that the gallery height in LDHs containing long chain aliphatic carboxylate, dicarboxylate, sulfonate or sulfate guests increases as the chain length increases. For the case of α,ω-dicarboxylate anions $^{-}OOC(CH_2)_nCOO^{-}$, the basal spacing shows a mean increase of $\approx$ 0.127 nm/CH_2 from n = 3 to 12 as shown in Fig. 21 [213] for Mg/Al LDH

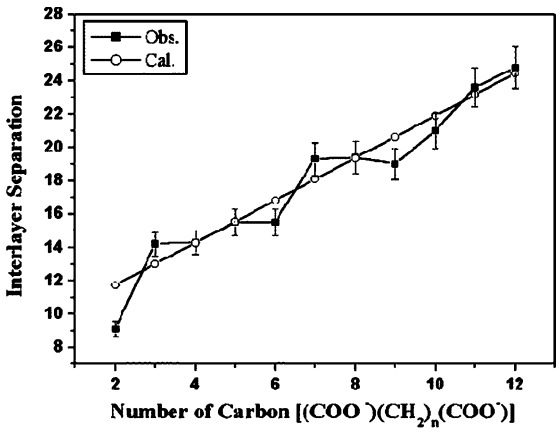

Fig. 21 Variation in basal spacing of α,ω-dicarboxylate anions $^{-}OOC(CH_2)_nCOO^{-}$, intercalated in Mg/Al LDH nanocrystals supported on silicon substrates. Reprinted with permission from [213]. Copyright American Chemical Society

nanocrystals supported on silicon substrates. Since this is approximately equal to the projection of the C – C bond length on the chain axis [214], it implies a monolayer of anions oriented vertically in the interlayer galleries. A bilayer of anions would imply an increase of twice this value if the molecules are vertical, or less than twice if the molecules are oriented at an angle to the layer [1, 215].

Most examples of alkyl carboxylates (as well as other long-chain monofunctional surfactant anions such as alkyl sulfates and alkyl sulfonates) intercalated in LDHs have their hydrocarbon chains closely packed in a monolayer, as an interdigitated structure or in a bilayer tilted at an angle of about 55° with respect to the layers [19, 204]. This is similar to the tilting habit of saturated fatty acids in their crystals and allows both carboxylate oxygen atoms to form hydrogen bonds equally to the hydroxide layers [216]. It has been reported that formation of monolayer/interdigitated structures is favored by high temperature [152]. It was shown that reaction of Mg_nAl LDHs ($n = 2, 3$ or 4) with sodium stearate led to the uptake of C_{18} guest species of up to 230% of the anion exchange capacity (AEC), giving interlayer arrangements very similar to the Langmuir-Blodgett (LB) bilayer structure [151]. Two-dimensional XRD measurements on cast films of the intercalates were carried out using an image plate (IP) detector. The IP image (Fig. 22) shows a series of basal reflections in the vertical direction and additional peaks in the lateral direction (Fig. 23), which is consistent with a regularly aligned disposition of the C_{18} guests in a distorted hexagonal structure in the LDH interlayers (Fig. 24).

This arrangement is also similar to that adopted by the headgroups of long chain aliphatic acids in LB films. Intercalation at over 100% AEC was shown to be a result of co-intercalation of sodium cations or neutral stearic acid molecules. In the case of *trans*-$CH_3(CH_2)_7CH=CH(CH_2)_7COOH$ (elaidic acid), two different intercalated LDHs with a monolayer of elaidate anions

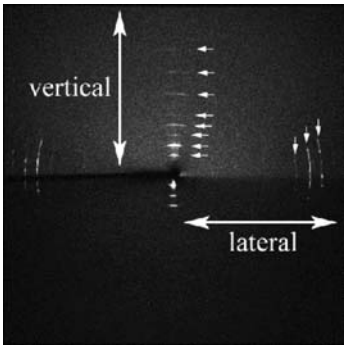

Fig. 22 Image plate study of a stearate/LDH cast film. Reprinted with permission from [151]. Copyright American Chemical Society

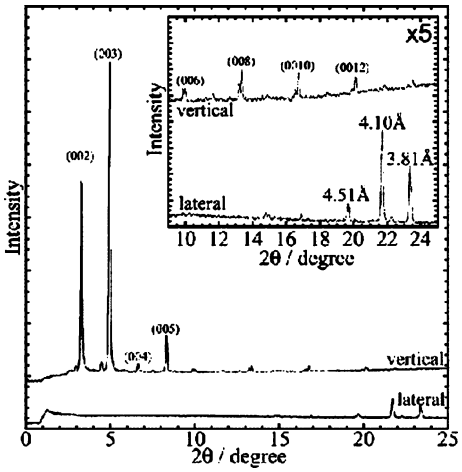

Fig. 23 XRD diffraction patterns in the lateral and vertical directions in the image plate study of a stearate/LDH cast film. Reprinted with permission from [151]. Copyright American Chemical Society

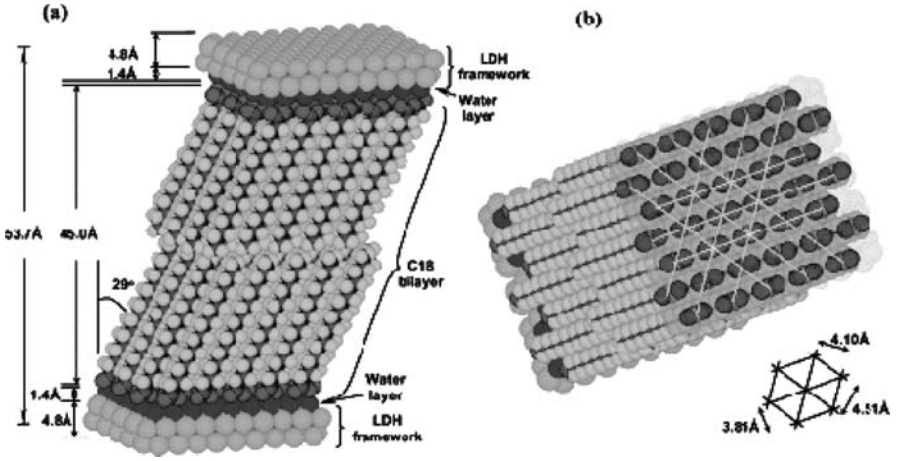

Fig. 24 Structural model of a stearate/LDH composite showing **a** tilted C_{18} bilayer and **b** regular packing of C_{18} in the interlayer galleries. Reprinted with permission from [151]. Copyright American Chemical Society

(basal spacing of 3.08 nm) and a mixed bilayer of elaidate anions and neutral elaidic acid molecules (basal spacing of 4.88 nm) have been prepared (Fig. 25). In the case of the corresponding *cis*-isomer (oleic acid), however, the kink in the chain imposed by the double bond allows the chains to overlap only in the region below the double bond, sticking the chains together like Velcro (Fig. 25), resulting in a basal spacing of 3.56 nm. The geometry of the oleate anions is similar to that adopted by oleic acid itself [216].

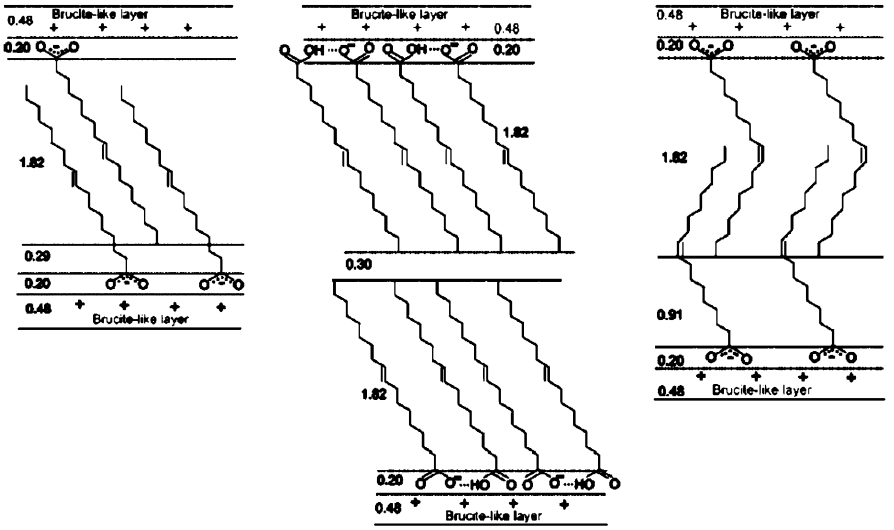

Fig. 25 Proposed packing arrangements in LDHs intercalated with a monolayer of elaidate anions (*on the left*), a mixed bilayer of elaidate anions and neutral elaidic acid molecules (*center*) and oleate anions (*on the right*). Reprinted with permission from [216]. Copyright American Chemical Society

3.2.5 Guest-guest Interactions

The photo-induced [2 + 2] dimerization of crystalline *trans*-cinnamic acid has been shown to require both close contacts of approximately 0.4 nm and a specific orientation of the unsaturated bonds, and can therefore be used to explore the arrangement of cinnamate ions in the interlayer galleries of LDHs [19, 217]. It was suggested that the packing of *o*-chlorocinnamate and *p*-chlorocinnamate as bilayers between LDH layers is qualitatively similar to the packing of the same ions between the cations in their hydrated sodium salts [218]. Head-to-head (HH) cyclodimers were formed selectively on irradiation of LDHs containing interlayer cinnamate ions, indicating that the arrangement of anions in the interlayer galleries is such as to preclude the formation of the head to tail (HT) dimer. The ratio of *anti*-HH to *syn*-HH increases markedly as the Mg/Al ratio in the layers increases; it was argued that longer guest-guest distances give an appropriate geometry for formation of the *anti*-HH isomer [219]. This system has also been studied [217] using molecular mechanics computer simulations of the type discussed in Sect. 3.2.6. In agreement with experiment, it was found that for Mg/Al ratios of 2 and 3, the arrangement of monomer pairs was unfavorable for HT dimerization and the selectivity to *anti*-HH dimer increased with increasing Mg/Al ratio. A model with Mg/Al of 6 and 20 wt % water content was observed to

have a very disordered interlayer arrangement with a preference for *syn*-HT dimer formation, whilst increasing the water content to 30 wt % led to *cis-trans* isomerization rather than dimerization being favored since the guest species are relatively far apart. This highlights the role of both layer charge density and water content on reactivity of guest species. In all cases, the water molecules were found to have a tendency to migrate towards the faces of the hydroxyl sheets. The packing model discussed earlier for 4′-chloro-4-stilbenecarboxylic acid (CSC) intercalated in Mg/Al LDHs was found to be consistent with the observed stereochemistry of the photodimerization of CSC in the interlayer galleries [197].

Intercalation of (*Z*, *Z*)-2,4-hexadienedioic acid (muconic acid) in an $LiAl_2$ LDH has been reported. On photoirradiation of an aqueous suspension of the material, the guest molecules underwent polymerization. It was proposed that a vertical arrangement of guest molecules in the interlayer galleries results in the 1,3-diene moieties being arranged in a face-to-face manner, with a suitable orientation and distance for the propagation of radicals induced by photoirradiation [220].

Aromatic ketocarboxylate anions $p\text{-}CH_3C_6H_4CO(CH_2)_nCO_2^-$ with varying chain lengths (n = 4–10) have been intercalated in Mg/Al LDHs [221]. The observed gallery heights show a much smaller increase with n (2.2 nm for n = 4 to 2.5 nm for n = 10) than that in the anion itself (1.36 nm for n = 4 and 2.12 nm for n = 10), suggesting that the chains become increasingly interdigitated as their length increases. Norrish type II photochemical reactions of the intercalates have been studied [221], since these reactions have been widely used as a probe for investigating ordered anisotropic systems. Either elimination (E) products (*p*-methylacetophenone and alkenecarboxylates) or cyclization (C) products (cyclobutanols) can be obtained. In solution, the ratio of C/E products was found to be independent of n for the above anions, whereas the intercalated anions with longer chain lengths (n = 6–10) gave negligible amounts of C products. Formation of C products proceeds via a cisoid diradical, whereas E products are derived from a transoid diradical and it was proposed that formation of the more bulky cisoid diradical was inhibited in interlayer galleries containing the anions with longer more interpenetrating chains [221]. Photochemical hydrogen abstraction reactions from aliphatic carboxylate anions by *p*-benzoylbenzoate (BPC) co-intercalated in LDHs have been reported. Compared with reactions in solution, the co-intercalated species showed a high selectivity for hydrogen abstraction from methylene groups close to the methyl terminus of the alkyl chain [18]. This was interpreted in terms of an antiparallel packing of BPC and carboxylate anions.

The enthalpy changes associated with exchange of chloride ions in a $Zn_{2.2}Al$ LDH by a variety of dicarboxylate anions (oxalate, succinate, adipate and tartrate) have been measured by microcalorimetry [222]. With the exception of tartrate, the exchange processes are endothermic and the enthalpies

of exchange vary linearly with the number of carbon atoms, consistent with the intercalated dicarboxylate anions being perpendicular to the layers. The energetic parameters are consistent with the presence of hydrophobic interactions between the CH_2 groups of succinate and adipate anions and hydrogen bonding between the OH groups of the tartrate anions. Since the calculated distance between uniformly spaced tartrate anions is too high to allow hydrogen bonding of this type, it was proposed that pairs or domains of closely spaced tartrate anions were present.

3.2.6 Molecular Dynamics Simulations

Far IR spectroscopy is a useful technique to study the structural environment and dynamics of water molecules and ions in the interlayer galleries of LDHs, since it directly probes the intermolecular and hydrogen bonding interactions [223]. Spectra, which can be recorded by pressing small amounts of powder onto one side of a piece of Scotch tape, are often difficult to interpret because of the complex network of intermolecular interactions present and molecular dynamics simulations have been employed in order to assist in the interpretation [223].

The principal limitation of the molecular dynamics technique is the accuracy of the forcefield employed, and several methods have been proposed for calculations involving LDHs [223, 224]. It was found that the forcefield used in early work was unsatisfactory since it predicted an unreasonable contraction in the *ab* plane and a modified forcefield was subsequently employed [224, 225]. Calculations using the latter forcefield have suggested that carbonate anions lie midway between, and generally coplanar with, the hydroxide layers [224]. Calculations using the same forcefield suggested that in the case of (*S*)-phenylalanine intercalated in Mg/Al LDH, the guest molecules adopted an interdigitated bilayer arrangement with their long axis approximately perpendicular to the layers [225]. The phenyl rings form a hydrophobic region in the middle of the interlayer with an edge to face orientation being preferred, possibly indicative of weak but directional $C-H\cdots\pi$ bonding (Fig. 26). The oxygen atoms of water molecules together with those of the carboxylate groups form an oxygen monolayer on the surface of the hydroxide layers, giving hydrogen bonding interactions with an $H\cdots O$ distance of ≈ 0.22 nm and variable $O\text{-}H\cdots O$ angle (Fig. 27).

In LDHs, the layer hydroxyl groups can act as hydrogen bond donors to both the interlayer anions and the oxygen atoms of interlayer water molecules. The interlayer water molecules can also form hydrogen bonds between themselves and can act as hydrogen bond donors to the interlayer anions. A molecular dynamics study of an Mg_3Al-Cl LDH has been reported by Wang et al. [223], and indicated that the interlayer species are distributed between two sublayers such that none of them is able to form direct hydrogen

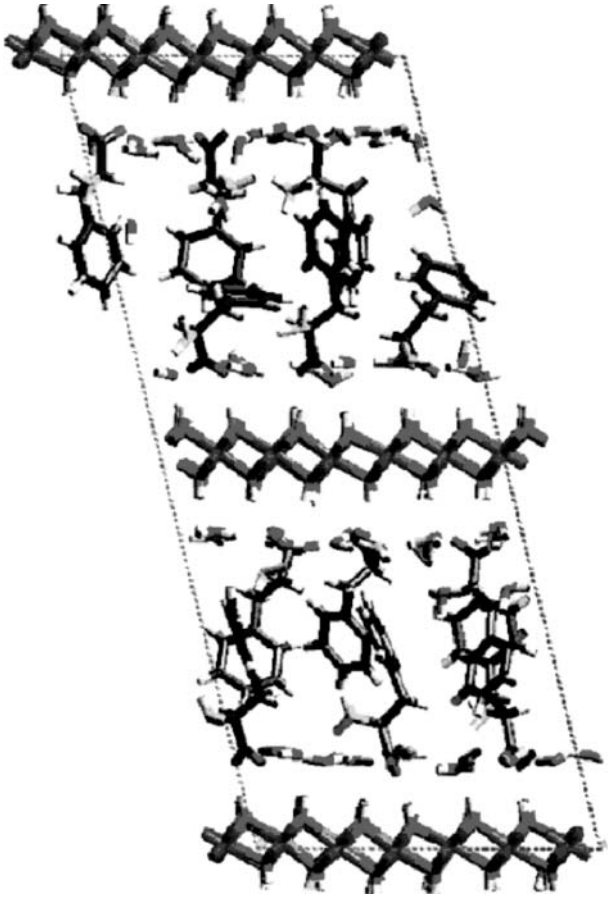

Fig. 26 Molecular dynamics simulation cell of (*S*)-phenylalanine intercalated in an Mg/Al LDH. Reprinted with permission from [225]. Copyright American Chemical Society

bonds to both neighboring octahedral sheets simultaneously (Fig. 28). Each Cl^- ion accepts ≈ 2.5 hydrogen bonds from layer hydroxyl groups but ≈ 4 hydrogen bonds from neighboring water molecules. The average structural environment of the Cl^- anions was said to be strikingly similar to that of the ion in bulk aqueous solution. The average local structural environment of the interlayer water molecules involves ≈ 3.8 hydrogen bonds to layer hydroxyl groups, Cl^- and other water molecules, which is quite different from that in bulk liquid water and more similar to that in ice (which have ≈ 3.2 and 4 hydrogen bonds per molecule, respectively). A good agreement was observed between simulated far IR spectra using the above structural model and the experimental spectra [223].

For $[LiAl_2(OH)_6]Cl{\cdot}H_2O$, molecular dynamics simulations suggest that the both interlayer water molecules and chloride anions are located in the middle

Fig. 27 Possible hydrogen bonding interactions for (*S*)-phenylalanine intercalated in an Mg/Al LDH. Reprinted with permission from [225]. Copyright American Chemical Society

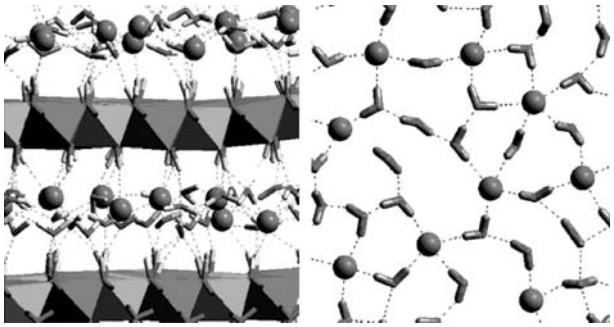

Fig. 28 Results of a molecular dynamics study of an $Mg_3Al - Cl$ LDH: the structure viewed along the (010) direction is shown on the *left* and the arrangement of interlayer Cl^- and H_2O molecules viewed along the (001) direction is shown on the *right*. *Dashed lines* represent hydrogen bonding. Reprinted with permission from [223]. Copyright Mineralogical Society of America

of the interlayer [226]. The oxygen atoms of water molecules act as hydrogen bond acceptors with one hydroxyl group from the layer above and one from the layer below. The plane of the water molecules is parallel to the layers, such that its hydrogen atoms can form hydrogen bonds to separate chloride anions, giving a distorted tetrahedral environment about the oxygen atom. A minority of the chloride ions are in one of two types of trigonal prismatic sites coordinated to three hydroxyl groups from the layer above and three from the layer below (one type is directly above lithium cations, the other between vacant tetrahedral sites in the layers), whilst the majority are in distorted octahedral sites, forming six hydrogen bonds to two hydroxyl groups from the upper layer, two from

the lower layer and two hydrogen atoms of different water molecules. Separate signals can be observed in the ^{35}Cl NMR spectrum at room temperature, which become nearly fully averaged at 70 °C. In the anhydrous material, the chloride anions all occupy prismatic sites along three-fold Cl···$(OH)_3$····Li···$(OH)_3$ axes, consistent with the observed crystal structure [16].

Molecular dynamics simulations of the structure of hydrocalumite, $[Ca_2Al(OH)_6]Cl{\cdot}2H_2O$, have been reported [227, 228]. In this material, unlike other LDHs, the calcium ions do not occupy sites in the center of the layers but half are shifted up along the *c* direction and half down. The calcium ions are seven-coordinate, being bonded to a water molecule in the interlayer towards which they are shifted in addition to the usual six hydroxyl groups. Thus the water molecules form two sublayers on either side of the center of the interlayer along the *c* axis. The simulations suggest the presence of a 10 coordinate chloride ion, with the water molecules undergoing rapid librations (hindered hopping rotations) about the Ca – O bond perpendicular to the layers (note that in this case, as a result of coordination to the calcium ion, the C_2 axis of the water molecules is neither parallel to, or perpendicular to the layers but at an angle of $\approx 50°$). Each water molecule is hydrogen bonded to three pairs of chloride ions for 2/3 of the time, so at any instant is bonded to four chloride ions. With respect to the chloride ion, at any instant there are four hydrogen bonds to neighboring water molecules, but averaged over time there are six hydrogen bonds with 2/3 occupancy. Structural studies involving single crystal XRD [111] and synchrotron [112] and conventional [229] powder XRD are essentially in agreement with this model. Above ≈ 308 K, the structure adopts a rhombohedral **6R** polytype (space group $R\bar{3}c$) where the chloride is surrounded by a distorted trigonal prism of hydroxyl groups from two adjacent layers and six additional water molecules giving a slightly distorted icosahedral coordination shell [111]. The water molecules have orientational disorder with partial occupancy of 2/3, giving a net total of four hydrogen bonds to water molecules in addition to the six to layer hydroxyl groups [112]. On cooling, the compound transforms to a monoclinic two layer polytype (space group $C2/c$) with a shift of chloride anions along $(010)_h$ and water molecules along $(210)_h$ of the hexagonal cell as indicated by the arrows in Fig. 29. This results in an ordering of the hydrogen bonding, with each chloride forming four strong hydrogen bonds to water molecules rather than six weaker bonds as in the high temperature polytype. The phase transition has also been studied by variable temperature ^{27}Al MAS NMR spectroscopy [230].

It was suggested that the changes in ^{27}Al quadrupole coupling parameters confirm the key role played by hydrogen bonding in the structural changes which occur during the phase transition. A similar phase transition is observed in the case of the corresponding bromide and iodide analogues [111]. The transition temperature between high and low temperature polytypes decreases from 309 K (X = Cl) to 123 K (X = I) from which it was concluded that

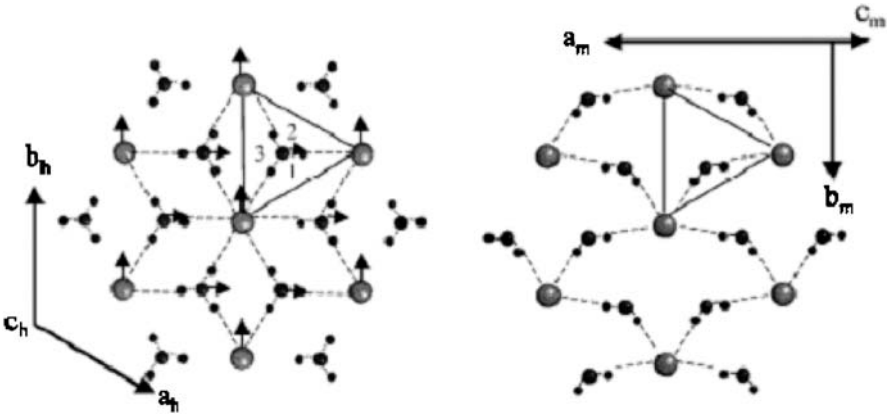

Fig. 29 Interlayer structure of $[Ca_2Al(OH)_6]Cl{\cdot}2H_2O$: the high-temperature rhombohedral form (represented by a projection along the c_h axis is shown on the *left* and the low-temperature monoclinic form (represented by a projection on the (a_m, b_m) plane is shown on the *right*. Reprinted with permission from [112]. Copyright Elsevier Science Ltd

the smaller chloride ion favored the low temperature polytype (four strong hydrogen bonds) over the high temperature polytype (six weaker hydrogen bonds) because of its stronger hydrogen bonding capability [111].

Similar phenomena have also been reported in the literature for related materials. For example, two different modifications of $[Ca_4Al_2(OH)_{12}]CO_3 \cdot 5H_2O$ have been prepared at different temperatures and both have been characterized by single crystal XRD [231, 232]. In the high temperature form [231], which crystallizes in the non-centrosymmetric space group $P1$, 3/4 of the calcium ions in each layer are coordinated to water molecules and the remaining 1/4 to carbonate anions (in addition to six layer hydroxyl groups). In the low temperature form [232], which crystallizes with pseudohexagonal symmetry (centrosymmetric space group $P\bar{1}$), the calcium ions in alternate sheets are all coordinated to water molecules, whereas those in the remaining sheets are coordinated to carbonate or water molecules with 50% probability. This system has not yet been studied by molecular mechanics, however.

Molecular dynamics simulations have been carried out on $[Mg_2Al(OH)]Cl \cdot n\ H_2O$ [233, 234]. The results suggest that the material has a similar structure to hydrocalumite with each magnesium being displaced along the c axis from the center of the layers and coordinated to a water molecule or chloride anion, in addition to six hydroxyl groups. The studies indicate that a minimum in the hydration energy is observed for $n = 2$, in which a well-developed, although disordered, hydrogen bonding network similar to that in hydrocalumite is formed with each available site in the O-type interlayer being occupied by either an anion or water molecule. In contrast, structural studies of magnesium-containing LDHs have always suggested that the Mg^{2+} ion is six-coordinate, however.

The structure of anhydrous intercalates of the type $[LiAl_2(OH)_6]X$ (X = Cl, Br, NO_3) has been investigated using energy minimization methods [235]. In the case of the halide ions, the optimized structures were found to adopt a hexagonal $\mathbf{2H}_1$ polytype with eclipsed (*P* type) metal hydroxide layers with the halide anions forming Li···X···Li···X chains through the lattice perpendicular to the layers. In the case of X = NO_3, the nitrogen atom was found to occupy the same site as the halide ions with the oxygen atoms disordered over six sites, leading to two nitrate ions related by a 180° rotation in the *ab* plane existing in a disordered structure. The calculations are in good agreement with the experimental structures determined by synchrotron X-ray and neutron powder diffraction [16].

First principles molecular dynamics calculations have also been used to investigate the structure of Mg/Al LDHs. It was concluded that the $\mathbf{2H}_1$ polytype with *P* type interlayers is more stable than the **1H** polytype with O type interlayers and that the aluminum and chloride ions are aligned vertically along the *c* axis [43]. In this case, computing limitations precluded calculations on a three-layer polytype (e.g. $\mathbf{3R}_1$ with *P* type interlayers and a staggered arrangement of cations along the *c* axis) or the introduction of any interlayer water molecules. The conclusions from these calculations are not consistent with the results from Rietveld analyses of Zn/Al or $Fe^{II}{}_2Fe^{III}$ LDHs with interlayer chloride anions [25, 106, 155] in which the chloride and water molecules occupy *P* type interlayers and are located in sets of sites distributed in groups of six around the three-fold O···O axis or exhibit strong oscillations around an equilibrium position along the O···O axis (see Sect. 3.2.2). It should be noted, however, that as discussed above, the structure of the interlayer in $[LiAl_2(OH)_6]Cl{\cdot}nH_2O$ is different for the anhydrous material ($n = 0$) and the hydrated material ($n = 1$), so any simulations which exclude water may lead to significant differences between experimental and optimized calculated structures.

There has been an attempt [236] to optimize the arrangement of IO_3^- ions intercalated in an Mg_3Al LDHs using the CASTEP (Cambridge serial total energy package) code, which is allows density functional theory calculations for crystal structures. The calculations suggested that the oxygen atoms of the IO_3^- anion were preferentially hydrogen bonded to $Mg_2Al(OH)$ groups rather than $Mg_3(OH)$ groups. The calculations were carried out on anhydrous systems, however, whereas the experimental systems are hydrated [237] and only a very limited section of the lattice was included in the calculations.

3.2.7 Interlayer Galleries and Hydration

As we have seen, the interlayer galleries in LDHs can be considered to be made up of hexagonal close-packed sites parallel to the close-packed layers of hydroxyl groups and metal cations, with one crystallographic site per metal [17, 238]. The maximum amount of water which can be accommo-

dated in the interlayer galleries of an LDH with $[M^{II}_{1-x}M^{III}_{x}(OH)_2]^{x+}$ layers is therefore given by $(1 - Nx/n)$ where N is the number of sites occupied by an anion of charge n [143]. The three oxygen atoms of a carbonate group occupy three sites and the remainder can be occupied by water or left vacant. The general formula for an LDH-carbonate can be expressed as

$$[M^{II}_{1-x}M^{III}_{x}(OH)_2](CO_3)_{x/2} \cdot (H_2O)_{1-3x/2-\Delta}$$

where Δ represents the number of vacant interlayer sites [7]. Thus in the mineral hydrotalcite, there is one vacant layer site per $[Mg_6Al_2(OH)_{16}]CO_3{\cdot}4H_2O$ formula unit. In synthetic LDHs, the experimentally determined amount of water can exceed $(1 - Nx/n)$ in which case it is assumed that there is both interlayer or *intrinsic* water [95] and *extrinsic* water adsorbed on external non-gallery surfaces [239]. The maximum amount of intrinsic water that can be co-intercalated with other, larger, anions can be estimated in an analogous manner. As discussed in Sect. 3.2.1, the intensities of the (00l) reflections of a paramolybdate-intercalated LDH can be simulated using a model [143] involving three close-packed layers of interlayer oxygen atoms from the polyoxometallate and water molecules.

A comprehensive study by Hou et al. [240] has shown that LDHs exhibit a diverse range of swelling and water sorption behavior, and can be divided into three categories. Type 1 have significantly expandable basal spacings (0.15–0.30 nm); Type 2 are slightly expandable (< 0.05 nm) and have significant interlayer water exchange; Type 3 are essentially non-expandable with little interlayer water exchange. For Type 1 (e.g. $Mg_3Al - SO_4$), the fully expanded phases have a two-water layer structure, and the phase transition from one layer to two layers as determined by XRD correlates with both a significant step in the water sorption isotherm and changes in the interlayer structure and dynamics as observed by NMR. Type 2 (e.g. $Mg_3Al - ClO_4$) only form one-water layer structures and the interlayer anion may undergo dynamical disordering at high relative humidities. For Type 3 phases (e.g. $Mg_3Al - Cl$) there is little interlayer water sorption because their interlayers are essentially closed, due to the small size or planar shape of the anions.

The arrangement of anions in green rust materials of the type $[Fe^{II}_{1-x}Fe^{III}_{x}(OH)_2]Cl_x{\cdot}yH_2O$ has been explored in detail [241]. According to a Rietveld refinement, the layers adopt the $\mathbf{3R}_1$ polytype and the stacking sequence can be written in the form **AbC(*C*)CaB(*B*)BcA(*A*)AbC**, where the letters in italics denote the interlayer species. Within a single layer, the O···O distance in the hexagonal pavement is equal to the unit cell parameter a_o (0.32 nm), whereas the diameter of a chloride anion is 0.36 nm. Thus in the hexagonal pavement of the interlayer, the six nearest-neighbor sites to a chloride ion cannot be occupied by another chloride anion (although they can be filled at random by water molecules). If this exclusion criterion is met, the maximum value of x is 1/3, with each chloride having six nearest neighbors at $a_o\sqrt{3}$. For $x \leq 1/3$ some of these next nearest neighbor

sites are vacant or may be filled by water molecules. The amount of water is $y \leq 1 - x$. A random array of chloride anions that respects the exclusion rule is shown in Fig. 30a. There exists a correlation between the distribution of anions from one interlayer to the next (see Fig. 30b and c). Each anion shares its charge with one Fe^{III} of the layer underneath and one of the layer above. As shown by the stacking sequence **AbC(*C*)CaB(*B*)BcA**, for the chloride in position ***B***, the adjacent Fe^{III} ions in the layer above occupy one of three **a** positions whilst the interlayer chloride ions in the interlayer above occupy one of six ***C*** positions. Three of these involve *cis*-arrangements of O – H···Cl about the metal and other three have *trans*-O – H···Cl with the former being more favorable [241]. Mössbauer spectroscopy confirms that only one type of Fe^{III} site is present. There are two types of Fe^{II} site, however, as shown in Fig. 30d: one type denoted $Fe^{II}(Cl)$ is coordinated to the two O – H···Cl units in an analogous manner to Fe^{III}, whilst the other, denoted $Fe^{II}(H_2O)$ is coordinated to an O – H···OH_2 or O – H···[vacancy] moiety in one interlayer. The $Fe^{III} : Fe^{II}(Cl) : Fe^{II}(H_2O)$ ratio is $x : x : 1 - 2x$, consistent with the results from Mössbauer spectroscopy [241]. A similar an-

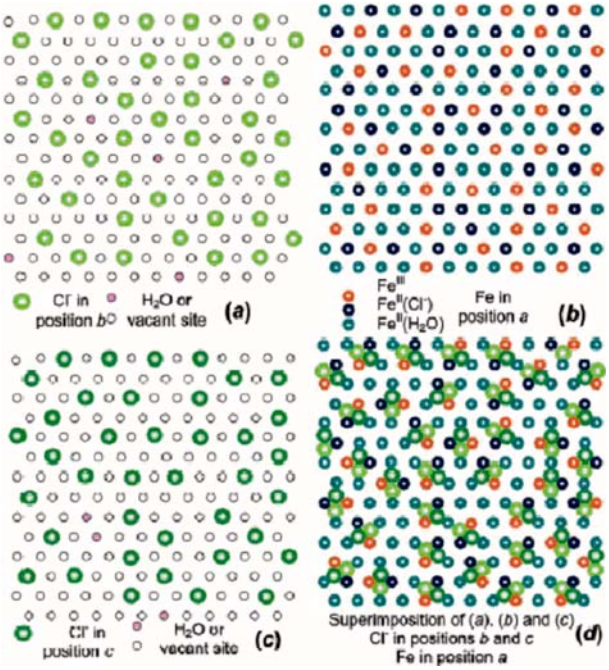

Fig. 30 (001) projections of the pavements of anions in green rust materials of the type $[Fe^{II}_{1-x}Fe^{III}_{x}(OH)_2]Cl_x \cdot yH_2O$: **a** a first interlayer of Cl^- ions; **b** the adjacent Fe cation layer; **c** the next interlayer of Cl^- ions; **d** the superimposition of **(a)**, **(b)** and **(c)**. Reprinted with permission from [241]. Copyright Elsevier SAS

alysis of the arrangement of anions and cations in Fe^{II}/Fe^{III} green rust type LDHs containing interlayer carbonate and sulfate ions has been carried out and the results used in aiding the interpretation of their Mössbauer spectra [241].

There have been many studies of the nature of the interlayer water in LDHs using a variety of methods. The structure of bulk liquid water is dominated by distorted local tetrahedral arrangements similar to those in ice I_h, although the long range order in the latter is lost in liquid water and on average there are fewer than four nearest neighbor water molecules. Molecular dynamics calculations [242] have shown that water molecules confined in brucite galleries show significant deviations from bulk water.

In comparison with brucite, the presence of interlayer anions in the galleries of LDHs introduces an additional level of complexity [3]. Jones et al. [243] have shown that in $Mg/Al-CO_3$ LDHs, interlayer water is more strongly bound than physisorbed water by some $12\,kJmol^{-1}$. Quasi-elastic neutron scattering measurements [244, 245] on Mg/Al LDHs containing either interlayer carbonate anions or terephthalate anions have demonstrated that the water molecules are not fixed in one position, but rather exhibit translational diffusion as well as reorientational motions. There is rapid breaking and forming of hydrogen bonds as water molecules hop from one site to another. The diffusion coefficients of the interlayer water are lower than that for bulk water, with the value being higher for the terephthalate intercalate than for the carbonate analogue [244]. Thermodynamic measurements on $Mg/Al-CO_3$ LDHs and mixtures of $Mg(OH)_2$, $Al(OH)_3$, $MgCO_3$ and water or ice have indicated [27] that the entropy of formation of the LDH is negative when water is used but positive in the case of ice, suggesting that interlayer water in LDHs has a higher entropy than ice, but lower than that in bulk water; this is consistent with the above spectroscopic data.

Molecular dynamics simulations [183] have suggested that the diffusion coefficient increases with increasing M^{II}/M^{III} ratio in the layers, which can be interpreted in terms of decreasing anion content and charge density on the layers. Comparison of the dielectric properties of mica-type silicates and LDHs has indicated [246] that the latter show anomalous low frequency dispersion, which is associated with charge carriers of low mobility. This suggests that the water molecules in silicate clays have a greater variety of available reorientational motions than those in LDHs. Impedance measurements have also been used to calculate the spatial disorder of the host layers, expressed by the fractal dimension d_s. This decreases from 2.7 to ≈ 2 on replacing nitrate ions with polyoxometallate anions, with the latter value indicating a molecularly smooth surface, suggesting that the stacking disorder decreases with increasing charge on the interlayer anions [246].

Far IR spectroscopy and molecular dynamics calculations have demonstrated the structural and dynamic similarity of chloride anions in the interlayer galleries of LDHs to those in bulk aqueous solution [223], as discussed

in Sect. 3.2.6. Molecular mechanics calculations have also suggested that the hydration energy of LDHs involves two components: one is controlled primarily by the formation of a hydrogen bonding network in the interlayer and the other is related to the decreasing electrostatic attraction between layers and interlayers as the structure expands along the *c* axis [233]. As noted in Sect. 3.2.6, for $[Mg_2Al(OH)_6]Cl{\cdot}yH_2O$, the most stable interlayer arrangement is for $y = 2$, in which all the interlayer sites are occupied giving a well-developed, although disordered, hydrogen bonding network.

The key role of hydrogen bonding in the interlayer of an LDH containing *tert*-butoxide anions has been investigated by means of *ab initio* plane-wave density functional theory calculations [247]. It has been suggested that the active catalyst is in fact a hydroxide charge-balanced LDH with co-intercalation of neutral *tert*-butyl alcohol molecules giving a hydrophilic region adjacent to the layers and a hydrophobic region in the center of the interlayer galleries. This results in organic substrates with polar functional groups being intercalated in a particular orientation, facilitating reactions and promoting catalytic behavior.

The hydration dynamics of a series of LDHs of the type $[Zn_{0.61}Al_{0.39}(OH)_2](CO_3)_{0.195(1-y)}Cl_{0.39y}{\cdot}nH_2O$ $[0 \leq y \leq 1, 0 \leq n \leq (0.4 + 0.2y)]$ have been studied by thermogravimetric analysis and XRD [95, 248]. For the fully hydrated samples, the basal spacing difference (0.019 nm) between end member compounds ($y = 0, 1$) is less than the height difference between Cl^- and CO_3^{2-} (0.053 nm). Furthermore, in the dehydrated materials the basal spacing of the LDH-chloride ($y = 1$) is smaller than that of the LDH-carbonate, i.e. dehydration of the former species causes a collapse in basal spacing although the amount of the (larger) ion remains constant. It was proposed that the chloride ion is able to nest in the trigonal pockets formed by the hydroxyl groups of the layers, but that this is not possible for carbonate. It was also suggested that in the fully hydrated LDH-chloride, the chloride anion is surrounded hexagonally by six water molecules, which must tilt about their C_2 axes in order to be accommodated and leading to an increased interlayer spacing. Removal of a small amount of water gives a five member hydration shell around the chloride which can be accommodated without any tilting of the water molecules and is consistent with the almost immediate decrease in basal spacing from 0.774 to 0.760 nm when a sample of the fully hydrated material is purged with dry nitrogen. Extensive drying leads to a further decrease in basal spacing to 0.729 nm, associated with formation of the material containing nested chloride ions [95].

The vibrational modes of layered double hydroxides have been examined using a combination of IR and Raman spectroscopy and inelastic neutron scattering [249]. All three techniques highlight the existence of an extensive hydrogen bonding network between the lattice water and the layer hydroxyl groups, but show that the lattice hydroxyl modes are not significantly affected by altering the interlayer anion (carbonate, nitrate or hydroxide).

The dynamic disorder in the interlayers of LDHs is also confirmed by single crystal XRD, since the interlayer anions and water molecules generally have occupancy factors less than unity and elevated temperature/displacement factors [172].

3.3 Long-range Cation Order-disorder

The extent of long-range or short-range ordering of the cations within the layers of LDHs has been widely discussed in the literature and contradictory conclusions have been drawn. Although interesting in its own right as a theoretical problem, the arrangement of cations is also of practical significance since where LDHs are used as catalysts [250], or as precursors to catalysts [251, 252], ferrimagnetic spinels [253–255] or other materials it should be advantageous to have a homogeneous distribution of cations without segregation of "lakes" of separate cations.

3.3.1 Experimental Studies

Magnetic susceptibility measurements [256] on $Cu^{II}/Co^{II}/Zn/Al$ LDHs indicate that the Curie–Weiss law is obeyed with a Weiss temperature close to zero, indicating the lack of magnetic interactions between paramagnetic ions and thus a random distribution in the lattice. It has been proposed, however, that the catalytic activity of Mg_nAl LDHs ($n = 2, 3$) containing interlayer carbonate anions in the oxyethylation of 1-dodecanol with ethylene oxide can be correlated with the distance between Al^{3+} cations in ordered lattices [250].

In terms of local order about the cations, it is generally argued that according to Pauling's rules [257], M^{III} cations should not occupy adjacent sites (unless accompanied by vacant cation sites, i.e. a gibbsite "unit" within a brucite layer [56]): the corollaries of this are that the minimum possible M^{II}/M^{III} ratio is 2 and that when M^{II}/M^{III} is exactly equal to 2 there is also a long range order with a superlattice involving an ordered array with each M^{III} cation having six M^{II} nearest neighbors and each M^{II} cation having three M^{II} and three M^{III} nearest neighbors [40]. As shown in Fig. 31, the superlattice is characterized by a cell parameter $a\sqrt{3}$ and is rotated by 30° compared with the lattice of non-ordered brucite-like layers with parameter a and is denoted $(\sqrt{3} \times \sqrt{3})R30°$.

Some workers, notably Hofmeister and von Platen [92], have argued that most or all LDHs, including those with M^{II}/M^{III} ratio greater than 2, also actually have a completely ordered distribution of cations but that this is not easily demonstrated experimentally because of high pseudosymmetry, micro-crystallinity and stacking faults. They argued that the prevalence of M^{II}/M^{III} ratios close to integral values of 2 and 3 in natural and synthetic

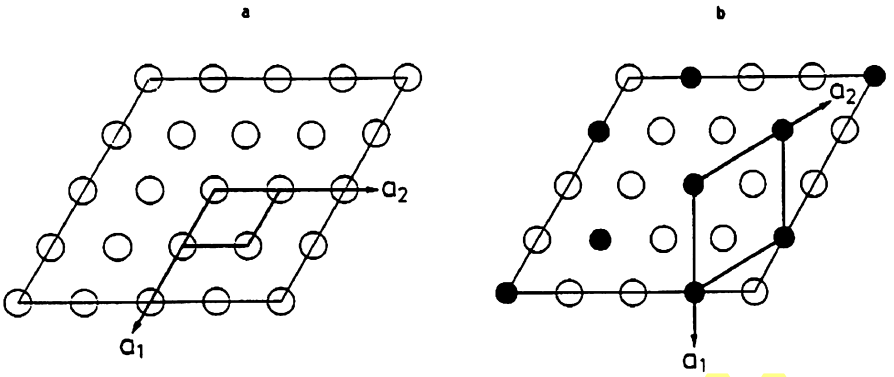

Fig. 31 **a** Unit cell and lattice for non-ordered brucite-like layers and **b** $(\sqrt{3} \times \sqrt{3})R30°$ superlattice of ordered layers with M^{II}/M^{III} ratio of 2. Reprinted with permission from [92]. Copyright Gordon and Breach Science Publishers

LDHs indicate a preference for ordered layers and that if the layers, as well as the interlayers, were disordered, long range ordered stacking of the layers in two- or three-layer polytypes would be unlikely to occur. Two possible ordered arrangements of cations with M^{II}/M^{III} ratios of 3 are shown in Fig. 32 [92, 206, 258]: one is based on a hexagonal supercell with $a = 2a_o$ and the other is based on an orthorhombic supercell with $a = a_o\sqrt{3}$ and $b = 2a_o$.

Hofmeister and von Platen [92] simulated the XRD powder patterns for a variety of LDHs with different metal ions, stoichiometries and stacking

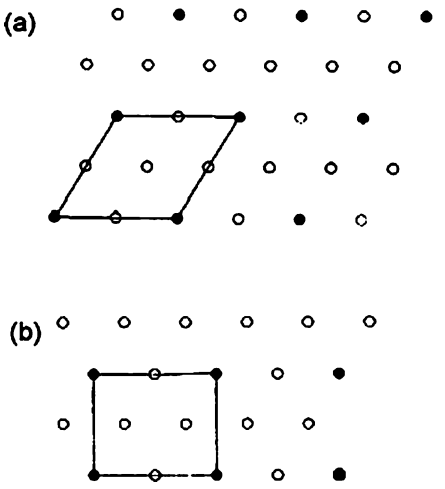

Fig. 32 Two possible ordered arrangements of cations with M^{II}/M^{III} ratios of 3: **a** a hexagonal supercell with $a = 2a_o$ and **b** an orthorhombic supercell with $a = a_o\sqrt{3}$ and $b = 2a_o$. Reprinted with permission from [206]. Copyright American Chemical Society

sequences in both ordered and disordered forms and found that the calculated intensity of superlattice reflections was always very much weaker than those from the subcell with dimension a_o, particularly when the scattering power of the M^{II} and M^{III} cations were similar (e.g. Mg and Al). Even where the scattering powers are quite different, simulations of XRD patterns show that a slight degree of either defective cation sequences or non-stoichiometry lead to a marked loss of intensity of the superlattice reflections [100]. For example in the case of Mg_2Fe layers, the cation sequence along (210), (120) and ($1\bar{1}0$) diagonal of the supercell of ordered cations is $\cdots$ Fe – Mg – Mg – Fe$\cdots$ (Fig. 33). Introduction of a small number of defective $\cdots$ Fe – Mg – Mg – Mg – Fe$\cdots$ and $\cdots$ Fe – Mg – Fe$\cdots$ sequences does not change the stoichiometry, but the superlattice reflections show a significant decrease in intensity. Note that even if the number of these defective sequences is large, there is still not complete disorder because no $\cdots$ Fe – Fe$\cdots$ or $\cdots$ Fe – Mg – Mg – Mg – Mg – Fe$\cdots$ sequences are present. Relatively small deviations in stoichiometry from Mg/Fe = 2 also lead to a dramatic decrease in the intensities of superlattice reflections.

Rebours et al. have investigated the structure of Mg/Al and Mg/Ga LDHs with interlayer carbonate anions [39]. The former did not reveal any evidence of cation ordering even for Mg_2Al, but a supercell of dimension $a\sqrt{3}$

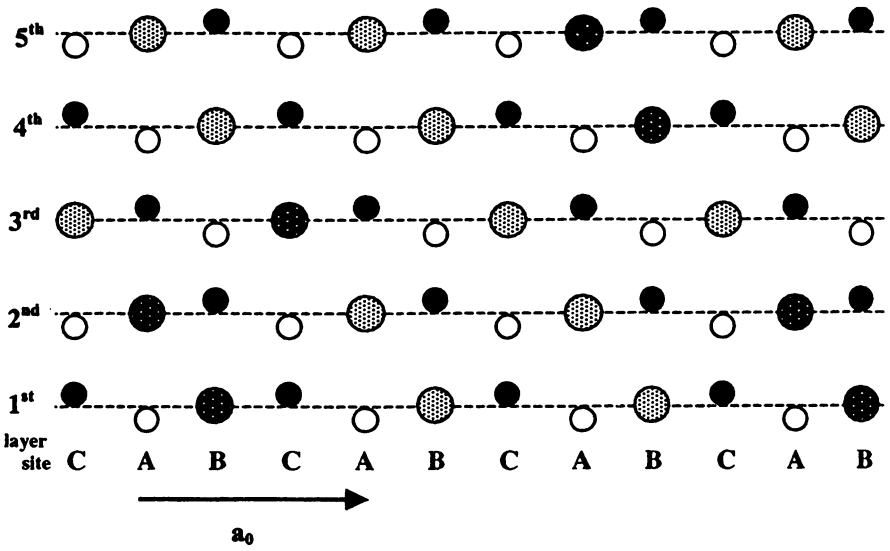

Fig. 33 Mg_2Fe LDH in the $3R_1$ polytype with ordered cation sequence $\cdots$ Fe – Mg – Mg – Fe$\cdots$ within the layers but no correlation of cation position between layers. *Light large circles* represent Mg^{2+}, *dark large circles* represent Fe^{3+}; *small circles* represent OH groups below (*open circles*) and above (*filled circles*) the metal ion plane. Reprinted with permission from [100]. Copyright Nova Science Publishers

was detected for the Mg_2Ga LDH as shown by the presence of a reasonably strong (100) reflection at 0.463 nm. The authors rationalized this by noting [39] that the brucite layers in LDHs and related structures are always compressed along the *c* axis and expanded along the plane as discussed in Sect. 2.1. The compression of the layer is limited by the close approach of oxygen atoms along shared octahedral edges – in brucite the O···O distance is 0.2785 nm whilst in gibbsite the O···O distance between shared edges of occupied and unoccupied octahedra is 0.2635 nm. In Mg/Al LDHs, the O···O distance was found to be close to the latter value and it was suggested that the structure cannot sustain the further shortening which would be associated with an ordering of cations. In contrast, since the ionic radii of Mg^{2+} and Ga^{3+} are similar, the ordering can take place without any significant distortions. An alternative explanation is that both Mg_2Al and Mg_2Ga systems are ordered, but the (100) reflection of the superlattice is not observed with the fomer because of the similar scattering powers of the isoelectronic Mg^{2+} and Al^{3+} ions. Refinement of the single crystal structure of the mineral shigaite discussed below has shown [259] that ordered Mn_2Al layers are accompanied by the presence of shared octahedral edges (0.2586–0.2610 nm) considerably shorter than those in gibbsite, suggesting that layer flattening is not a significant factor in determining whether or not cation ordering occurs. The presence of weak broad reflection ($d = 0.457$ nm) in the XRD pattern of an Mg_2Al LDH prepared by placing initial flocculated precipitates in cellulose dialysis bags immersed in water (changed daily) at 60 °C has been attributed [260] to the (100) reflection of a superlattice with $a = a_o\sqrt{3} = 0.528$ nm.

Although other values have also been claimed [38, 261], it has generally been asserted [25] that Zn_nCr-Cl LDHs can only be prepared for the case of $n = 2$, strongly suggesting the existence of ordered layers. This has been rationalized [262] by proposing that the synthesis proceeds via direct condensation of two hexaaquozinc(II) complexes with a deprotonated monomeric chromium species to give a trimeric species which subsequently condenses to give the $[Zn_2Cr(OH)_6]^+$ layers. The scattering powers of zinc and chromium are similar and no superlattice reflections are observed in the XRD: it has been calculated, however, that any such reflections would have an intensity of only $\approx 0.1\%$ of that of the most intense (003) reflection [25], so their absence cannot be taken as evidence of a lack of long-range order. Nickel-aluminum LDHs have been studied using a high intensity (rotating anode) X-ray generator [263]; long range ordering was indicated by the presence of a weak broad reflection which could be assigned to a superposition of three reflections from a $(\sqrt{3} \times \sqrt{3})R30°$ superlattice in the case of $x = 0.33$, but is lost at other compositions.

In the case of a synthetic Mg_2Al-CO_3 LDH, selected area electron diffraction (SAED) [264] patterns of a few crystals with zone axis (00*l*) showed evidence of a superlattice with $a = a_o\sqrt{3} = 0.532$ nm [71], although this was

not the case for the majority of the sample. No superlattice reflections were observed in the XRD pattern and a Rietveld type analysis gave a unit cell with $a = 0.30502(4)$ and $c = 2.2925(3)$ nm. Partially ordered regions in pyroaurite and sjögrenite crystals have also been detected by SAED [92, 265]. Rietveld refinement of the XRD patterns of an Mg_2Al LDH with interlayer carbonate [266] and Zn_2Al LDHs containing interlayer chloride [106] or carbonate [267] anions also gave no indication of cation ordering.

It has been suggested that powder XRD patterns of some mineral samples of LDH minerals show evidence of superlattice reflections [7, 113] but there is no clear consensus [100]. It should also be borne is mind that, as discussed in Sect. 3.5, superlattice reflections may be due to anion, rather than cation, ordering although the latter may be an indication of the former.

In contrast to the situation for most LDHs, there is ample evidence from powder diffraction [115, 258] and synchroton X-ray and neutron powder diffraction [16] that those based on $[LiAl_2(OH)_6]^+$ units always have an ordered array of cations with a hexagonal supercell of dimensions $a = a_o\sqrt{3} = 0.532$ nm in which vacancies in the dioctahedral gibbsite lattice are filled by lithium cations, which naturally gives rise to ordering [268]. ^{27}Al MAS NMR spectra of $[LiAl_2(OH)_6]Cl{\cdot}nH_2O$ have one narrow symmetric peak indicating that the aluminum cations occupy highly ordered and symmetric positions [269], consistent with the refined X-ray and neutron diffraction structures. In contrast, gibbsite has two ^{27}Al resonances with different quadrupolar products, which arise from the two crystallographically distinct sites in gibbsite. It was proposed that introduction of Li^+ into site vacancies in gibbsite leads to a more uniform distribution of positive charge within the octahedral sheet, thereby reducing the differences between individual Al – O bond lengths and O – Al – O angles [269].

In view of the difficulties in detecting any long-range cation ordering by powder XRD, it would be useful to have single crystal diffraction data. Unfortunately the microcrystalline nature of most synthetic LDHs means that suitable single crystals are not generally available. Even when they are available, there is always a possibility that they may not be representative of the bulk sample [232]. Single crystals of a variety of $[Ca_2Al(OH)_6]^+$ LDHs containing anions such as carbonate [231, 232], nitrate [171, 172] and chloride [229, 270] have been prepared starting from mixtures of powdered $Ca(OH)_2$, $Al(OH)_3$ and the corresponding calcium salt of the anion and water in sealed silver capsules [231]. These materials show complete ordering of cations with each aluminum cation surrounded by six nearest neighbor calcium cations and no edge-sharing between AlO_6 octahedra. In these cases, as discussed in Sect. 4.1, the structure differs from that of most LDHs in that the calcium ions are seven coordinate, being coordinated to an anion and/or oxygen atom of an interlayer water molecule in addition to six layer hydroxyl groups. It has generally been assumed in the literature that the fact that Ca/Al LDH-like materials are only formed with Ca/Al = 2 and have an ordered array of cations

is associated with the large difference in ionic radii between Ca^{2+} and Al^{3+}. However, it has recently been shown that replacement of Al^{3+} by larger Ga^{3+}, Fe^{3+} or Sc^{3+} ions does not lead to a loss of cation ordering. This has been interpreted as indicating that the cation ordering is associated with large size and the pronounced anisotropy of the coordination sphere of the Ca^{2+} ion, rather than the difference in cation radii [271].

There have been some studies of single crystals of minerals [4] that have indicated ordering of cations [7, 92, 100]. In the case of mineral samples, however, there are often considerable problems with intergrowth and twinning of crystals [92, 272]. The single crystal structure of shigaite, $[M^{II}_6Al_3(OH)_{18}][(SO_4)_2\{Na(OH_2)_6\}(H_2O)_6]$ (M = Mn), shows an ordered array of layer cations in a $(\sqrt{3} \times \sqrt{3})R30°$ array with a three layer rhombohedral polytype (space group $R\bar{3}$) [259]. The interlayer is also ordered and contains an array of sulfate anions and cationic hexaaquosodium cations with a periodicity of $3a_o$; there are two distinct Al sites with mean Al – O bond lengths of 0.1914 and 0.1912 nm together with a single Mn^{II} site (mean Mn – O = 0.2192 nm) (Fig. 34). The mineral nikischerite (M = Ni) has recently been shown [273] to be isostructural with shigaite, and motukoreaite, $[Mg_{5.6}Al_{3.4}(OH)_{18}](SO_4)_{1.3}(CO_3)Na_{0.6}(H_2O)_{12}$ also has essentially the same structure [274].

A single crystal refinement of the mineral zaccagnite, $[Zn^{II}_4Al_2(OH)_{12}]CO_3 \cdot 3H_2O$, has been reported [275]. The material has a hexagonal two-layer

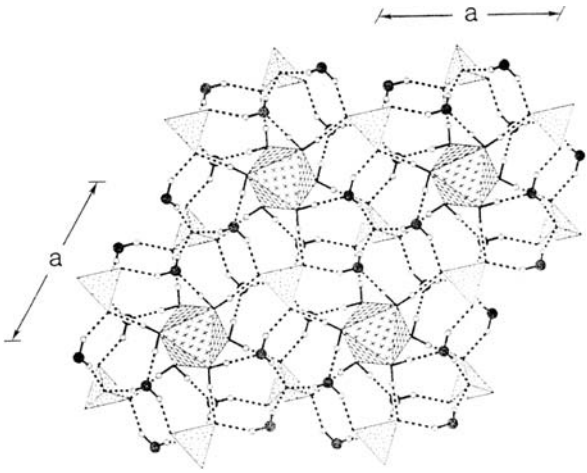

Fig. 34 Interlayer species in shigaite, $[Mn_6Al_3(OH)_{18}][(SO_4)_2\{Na(OH_2)_6\}(H_2O)_6]$, projected down (001): $\{Na(OH_2)_6\}$ octahedra are *cross-shaded*, SO_4 tetrahedra are *random-dot shaded*, oxygen atoms of water are shown as *black circles*, hydrogen atoms of water molecules as *small open circles* and *dotted lines* indicate hydrogen bonds. Reprinted with permission from [259]. Copyright Mineralogical Association of Canada

2H$_1$ polytype stacking (space group $P6_3/mmc$) and in addition to sharp reflections corresponding to cell parameters $a_o = 0.307$ and $c_o = 1.511$ nm, diffuse streaks parallel to c^* at positions defining a supercell with $a = a_o\sqrt{3}$ are observed. These can be indexed as (100) (0.462 nm), (200) (0.231 nm) and (210) (0.175 nm) (where the indices are referred to the supercell). The diffuseness of these reflections suggests that there is no correlation between the ordering in subsequent layers. Cation ordering has also been suggested [276] by the presence of superlattice reflections in single crystal X-ray photographs of other minerals of the type $[M^{II}{}_4Al_2(OH)_{12}]CO_3{\cdot}3H_2O$ known as charmarite (M = Mn), quintinite (M = Mg) and caresite (M = Fe). For charmarite and quintinite, both hexagonal two-layer and trigonal three-layer polytypes have been observed, whereas caresite has only been observed in the trigonal form. The reflections were indexed in a superlattice of the type $(2\sqrt{3} \times 2\sqrt{3})R30°$. It was subsequently shown [277] by means of a single crystal X-ray study on a mineral from the same source with the composition $[Mg_4Al_2(OH)_{12}]CO_3{\cdot}3H_2O$ that it had a two-layer hexagonal polytype (space group $P\bar{6}2m$) with an ordered cation distribution giving rise to a $(\sqrt{3} \times \sqrt{3})R30°$ superlattice with $a = a_o\sqrt{3} = 0.5283$ nm and $c = 1.5150$ nm.

In contrast to these results for LDHs with $M^{II}/M^{III} = 2$, determination of the single crystal structure of LDH minerals of the type $[M^{II}{}_6M^{III}{}_2(OH)_{16}]CO_3{\cdot}nH_2O$ such as pyroaurite [M^{II} = Mg, M^{III} = Fe, $n = 4.5$, **3R**$_1$ polytype], sjögrenite [M^{II} = Mg, M^{III} = Fe, $n = 4.5$, **2H**$_1$ polytype] and desautelite [M^{II} = Mg, M^{III} = Mn, $n = 4.0$, **3R**$_1$ polytype] show no evidence of cation ordering [100].

3.3.2 Theoretical Studies

There have been a small number of theoretical studies of cation ordering in LDHs. First principles molecular dynamics calculations [43] on $[Mg_3Al(OH)_8]Cl$ LDHs discussed in Sect. 3.2.6 suggested that structures with adjacent aluminum cations were energetically less favorable than one without, although the chosen arrangement for the latter lacked either hexagonal or rhombohedral supercell.

Calculations on a two-dimensional discrete Coulomb alloy $A_{1-x}B_x$, in which A and B have different charges and are free to move on the sites of a triangular lattice in order to achieve the lowest energy configuration have been reported [278]. It was suggested that this is a valid model of the Coulombic interactions between cations within the sheets of LDHs, since the screening of interactions between layers is sufficiently large. At certain values of the composition x it is possible to form regular superstructures. The most important class of these is when one set of ions, say B, lies on a triangular network where the separation between the nearest neighbor B ions is $a_o\sqrt{k}$, where $k = (n^2 + nm + m^2)$ and n, m are non-negative integers (i.e. $k = 3, 4, 7, 9, 12$, etc.). This gives rise to a set of compositions with $x = 1/k$, of which an ex-

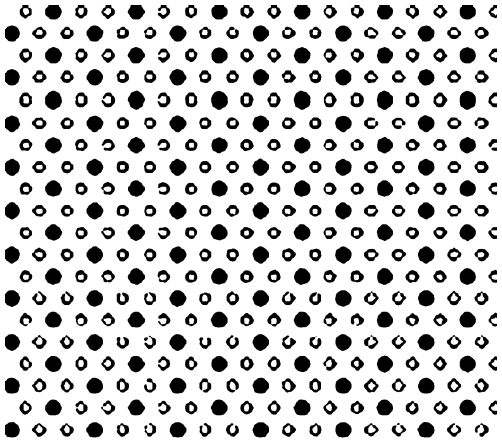

Fig. 35 Computer simulation of a regular triangular superlattice of a Coulomb alloy $A_{1-x}B_x$ with $x = 1/3$ as described in the text. Reprinted with permission from [278]. Copyright American Physical Society

ample with $k = 3$ is shown in Fig. 35. For some values of k, it was found that other superlattice structures may have an energy very close to the minimum energy of triangular lattice superstructures.

For example a piece of triangular superlattice with $k = 4$ (the *kagomé structure* [279]) is shown in Fig. 36 together with a piece of rectangular lattice with the domain boundaries marked (note that these two lattices have the unit cells shown in Fig. 32). For other values of $x < 1/3$, the B atoms form a triangular

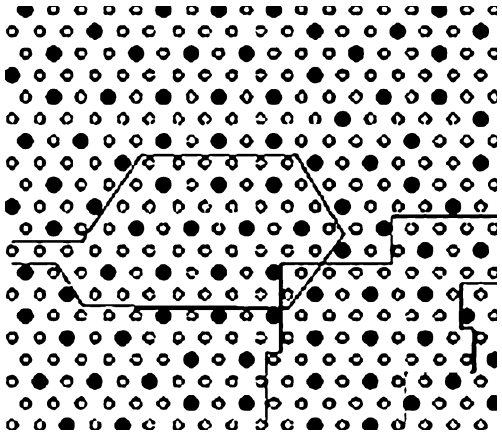

Fig. 36 Computer simulation of a regular triangular superlattice of a Coulomb alloy $A_{1-x}B_x$ with $x = 1/4$. A piece of triangular superlattice is shown together with a piece of rectangular lattice where the domain boundaries are marked. Reprinted with permission from [278]. Copyright American Physical Society

lattice at the commensurate points and otherwise a pseudotriangular lattice. For $1/3 < x < 1/2$, it was suggested that the lowest energy structures consist of chains of finite length arranged in a rectangular array. Commensurate configurations (those having rational ratios of subcell and supercell periodicities in the *ab* plane [263]) of this type are only possible for $x = n/2(n + 1)$ where n is any integer. For $x = 1/2$ it was found that the lowest energy structure has infinite straight chains of nearest neighbor ions. These results are consistent with those given in Sect. 3.3.1, where ordering of cations in a superlattice with $a = a_o\sqrt{3}$ is often observed for LDHs with $M^{II}/M^{III} = 2$ (i.e. $x = 1/3$). The presence of mixed domains of triangular and rectangular structure is a possible explanation for the lack of superlattice reflections generally observed in LDHs with $M^{II}/M^{III} = 3$ (i.e. $x = 1/4$).

3.4 Short-range Cation Order

Although the evidence for and against long-range cation ordering in LDHs is somewhat inconclusive, there is much stronger evidence for local ordering of cations. EXAFS is a powerful tool for studying local cation ordering. Analysis of the fine structure beyond the edge in XAS depends on the interference of the backscattered electron waves with the ejected photoelectron and as a consequence of the short mean free path of electrons in a solid, information can only be obtained to a distance of several tenths of nm from the absorbing atom. In the case of $Mg_nFe^{III} - CO_3$ LDHs with nominal values of $n = 2, 3$ and 4, it has been shown that Fe^{III} cations never (within the detection limits of EXAFS) occupy neighboring sites [40]. Powder XRD studies of the same samples showed no evidence of long-range cation ordering. It was noted that for $Mg/Fe^{III} = 2$ these two results can be consistent only if there are reasonably frequent defects to the ideal cation pattern, probably roughly every fifth to tenth cation in any direction – an example of one type of defect has been discussed in Sect. 3.3.1. This would result in coherent superlattice domains never exceeding a few nm and remaining X-ray silent, while only a few percent of sites would be affected and the average environment around Fe^{III} cations would remain effectively unchanged [40]. Other defects may involve cation vacancies or Mg^{2+} cations occupying sites that would be ideally occupied by Fe^{III}: indeed in the sample with a nominal Mg/Fe^{III} ratio of 2, the actual value is 2.17 indicating an excess of magnesium ions.

Ordering in Zn_2Cr systems with interlayer terephthalate anions has been reported on the basis of EXAFS measurements [280] with the Cr having 6 O at 0.198 nm and 6 Zn at 0.311 nm and the Zn having 6 O at 0.206–0.207 nm, 3 Zn at 0.309 nm and 3 Cr at 0.311 nm and 6 Zn at 0.536–0.537 nm. The local description of the arrangement around the cations in Zn_2Cr and Cu_2Cr LDHs with interlayer chloride anions has been studied by EXAFS at the cation K edges [25, 281]. The EXAFS Fourier transform in each case can be modeled

with a six shell model in which the first peak P_1 arises from the oxygen atoms coordinated to the metal whilst peaks P_2 to P_6 are mainly caused by metallic neighbors at a, $a\sqrt{3}$, $2a$, $a\sqrt{7}$ and $3a$ as shown in Fig. 37 [281].

The intensities of peaks P_4 and P_6 are characteristically enhanced by the so-called focusing and superfocusing effects, associated with multiple scattering phenomena from the large number of three and four atoms in a collinear arrangement with paths twice or three times that of the first metal-metal shell respectively [282]. Although the difference in scattering power is relatively small for Cu/Cr and Zn/Cr pairs, the marked difference in CuO_6 and CrO_6 coordination polyhedra associated with the Jahn-Teller distortion in the former allows it to be demonstrated unequivocally that the cations in the Cu_2Cr LDH are in an ordered distribution and that as a result the sheets show a pronounced corrugation, with two Cr – Cu distances observed for $P2$ at the Cr edge and one Cu – Cu distance for $P2$ at the Cu edge [281]. Strong evidence for local cation ordering in the Zn_2Cr LDH was also obtained [25, 262], but in this case the sheets preserve a relative flatness. It was noted that in this case, as in others [283], the interlamellar species do not make any contribution to the Fourier transform and it was suggested that this is possibly due to their thermal motion.

EXAFS studies at the Zn K edge of Zn_2Al – Cl LDHs have also demonstrated the ordered nature of the cation distribution [77]. The ordering is demonstrated by the presence of $P3$ and $P4$ peaks in the pseudo-radial distribution function, arising from multiple scattering by metal cation shells at $a\sqrt{3}$ and $2a$. Replacement of interlayer chloride ions by dodecylsulfate did not affect the intralayer cation arrangement. In contrast, however, delamination of the material followed reformation of the layered structure by evaporation of the solvent suggested that although the first (6 O) and second (3 Zn + 3 Al) coordination shells around Zn were retained, the intensity of the $P3$ and $P4$ bands was greatly reduced which suggests a loss of longer range order. Consistent with this interpretation, IR bands assigned to metal-oxygen lattice vibrations were broadened after the delamination-evaporation process.

EXAFS at the Co and Fe K edges has demonstrated [72] that the cations in LDHs of the type $[Co_2(Fe_yAl_{1-y})(OH)_6]Cl{\cdot}nH_2O$ $(0 \leq y \leq 1)$ are ordered. In particular, in an ordered $Co^{II}{}_2M^{III}$ lattice of the type shown in Fig. 37 each Co^{II} cation should have coordination shells with 3 Co^{II} and 3M^{III} ions at a, 6Co^{II} at $a\sqrt{3}$ and 3Co^{II} and 3M^{III} at $2a$. The data indicate that the contribution at the Co K edge from the shell at $a\sqrt{3}$ does not vary when aluminum is replaced by iron, but the contribution from the shell at $2a$ does vary with y over the range from 0 to 1, which is consistent with the ordered arrangement of cations shown in Fig. 37.

In related species of the type $[(Co_{1-y}Cu_y)_2Al(OH)_6]Cl{\cdot}nH_2O$ $(0 \leq y \leq 1)$ it was shown [284] by EXAFS that although the local order of M^{II} and Al cations was maintained as y increased, the layers consisted of mixtures of domains of $\{Co_2Al\}$ and $\{Cu_2Al\}$. The distortion in Cu^{II} coordination polyhedra associ-

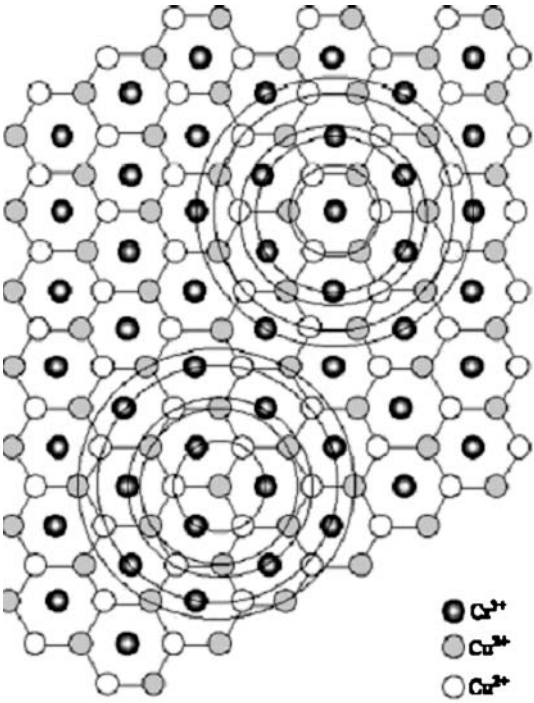

Fig. 37 Ordered Cu_2Cr layer showing shells P_2 to P_6 containing metallic neighbors at a, $a\sqrt{3}$, $2a$, $a\sqrt{7}$ and $3a$. Reprinted with permission from [281]. Copyright Elsevier BV

ated with the Jahn-Teller effect results in a non-linear arrangement of metal ions as shown by the disappearance of the focusing effect peaks in the case of the $\{Cu_2Al\}$ domains. A Zn /Al LDH with Zn/Al = 1.45 has been analyzed by Zn K edge EXAFS at 40 K [50]. The data were fitted to three Zn$\cdots$O and four Zn$\cdots$M (M = Zn, Al) shells and were also found to be consistent with an ordered distribution of cations. In the case of an LDH with Zn/Al $\approx$ 1.5, the cation avoidance rule can no longer be sustained and it was assumed that the trivalent cations were distributed as far apart as possible.

EXAFS data at the Co and Al K edges for Co_nAl-Cl LDHs were consistent with an ordered array of cations for $n = 2, 3$ and 4. In each case the Al has a second coordination shell of ≈ 6 Co^{II} ions and the Co^{II} has a second shell of $\approx 6/n$ Al and $(6–6/n)$ Co^{II} next nearest neighbors [46]. The peaks arising from the focusing effect are still observed in the Co K edge EXAFS of the material showing that the cobalt cations in the layers remain aligned.

The presence of local cation ordering in Mg_2Ga and Mg_5Ga-CO_3 LDHs noted in Sect. 3.3.1 has been confirmed by means of both EXAFS and by calculation of the electron radial distribution function from the Fourier transform of the diffracted X-ray intensity. In each case the gallium was found to have six magnesium ions and no gallium ions as next-nearest neighbors [39].

IR and Raman spectroscopy can give some insight into local cation order [77] and there have been a few other attempts to probe this aspect of the structure of LDHs using these techniques [285]. Each hydroxyl group is coordinated to three cations (and may also be hydrogen bonded to interlayer anions or water) and the number of distinct types of $M_3(OH)$ units will depend on the stoichometry of the LDH and the arrangement of cations in the lattice. For example, given hexagonally ordered lattices, for 2 : 1 LDHs $M^{II}{}_2M^{III}(OH)$ units should be present, whereas for 3 : 1 LDHs both $M^{II}{}_2M^{III}(OH)$ and $M^{II}{}_3(OH)$ units should be present with no $M^{II}M^{III}{}_2(OH)$ $M^{III}{}_3(OH)$ units in either case. It has been suggested [286] that the presence of five sharp lattice vibrations in the region 800–250 cm^{-1} of the IR spectra of Mg_2Al, Ni_2Al and Mg_2Fe LDHs containing interlayer carbonate anions is consistent with an ordered array of $M^{II}{}_2Al(OH)$ units, whereas the presence of five broader bands in the spectra of the analogous $M^{II}{}_3Al$ LDHs is indicative of a disordered array of cations. Deuteration studies later suggested the presence of six sharp lattice bands in the IR spectrum of $Ni_{2.5}Al$ analogue [287]. It should be noted that even for simpler species such as β-$Ni(OH)_2$, the interpretation of the vibrational spectrum has been the subject of controversy in the literature [288].

It has been suggested, however, [173] that in the Raman spectrum of an $Mg_{2.3}Al$ LDH with a mixture of interlayer carbonate and nitrate ions, separate hydroxyl stretching bands can be assigned to $Mg_3(OH)$, $Mg_2Al(OH)$ and $MgAl_2(OH)$ units; separate hydroxyl stretching bands have also been assigned to $Mg_3(OH)$, $Mg_2Cr(OH)$ and $Cr_3(OH)$ units in the Raman spectrum of stichtite ($[Mg_6Cr_2(OH)_{16}]CO_3{\cdot}4H_2O$) [289] and to Mg_3OH, Zn_3OH and Al_3OH moieties in the hydroxyl stretching region of the Raman spectrum of $[Mg_xZn_{6-x}Al_2(OH)_{16}](CO_3){\cdot}\ 4H_2O$ ($x = 0$–6) [290]. On the basis of the cation avoidance rule, however, some of these "units" would not be expected. *Ab initio* quantum mechanical modeling of the variation in vibrational frequencies of the OH group with the charge density and mass of the cations in dimers of the type $[(H_2O)_2(OH)_2M(\mu\text{-}OH)_2M'(OH)_2(OH_2)]^{n-}$ (M, M′ = Mg, Al, Fe^{II}, Fe^{III}) have been used in an attempt to understand the vibrational spectra of phyllosilicate clays [78, 291, 292] and these studies may also be useful in analyzing IR data for LDHs.

Raman studies on $[Cu_xZn_{6-x}Al_2(OH)_{16}]CO_3{\cdot}4H_2O$ have suggested that for $x < 2$, the cations are arranged in a regular array, but for larger values of x, separate OH stretching bands associated with "CuOH", "ZnOH" and "AlOH" were identified suggesting that the cations separate into "lakes" or "islands" of like cations [165]. As noted above, segregation of $\{Co_2Al\}$ and $\{Cu_2Al\}$ domains in other LDHs has been observed by EXAFS and attributed to the Jahn-Teller distortion associated with Cu^{II}, but segregation of Cu-only domains is inconsistent with the EXAFS results in this case [284].

Mössbauer spectroscopy is a potentially very useful way to study the cation ordering in LDHs containing iron [293–295], although care must be taken in order to avoid misinterpreting the results as has often happened

in publications in clay and soil science [296]. In pyroaurite type materials $[Mg_{1-x}Fe^{III}_x(OH)_2](CO_3)_{x/2}\cdot nH_2O$, a single Fe^{III} site is generally found to be present when $x \approx 0.25$ [238, 283]. (The quadrupole doublet is often asymmetric but this is usually ascribed to the effects of preferred orientation rather than the presence of a second doublet). At higher values of x, two quadrupole doublets can be observed, one corresponding to Fe^{III} with 6 Mg as next-nearest neighbors and another involving one or more Fe^{III} nearest neighbors (cluster-type arrangements). Results for so-called green rusts containing layers of the type $[Fe^{II}_{1-x}Fe^{III}_x(OH)_2]^{x+}$ indicate that they contain one type of Fe^{III} but generally (except in the case of sulfate [157, 297]) contain two types of Fe^{II} site as indicated by the presence of two quadrupole doublets in a ratio which depend on the anion [238, 241, 283, 297], as discussed in Sect. 3.2.7. It has been suggested that the observed range of stoichiometries (x) and extent of cation ordering in these materials is connected with the ordering of anions [241]. Related materials of the type $[Fe^{II}_{1-x-y}Mg_yFe^{III}_x(OH)_2]^{x+}$ have been shown to have two Fe^{II} quadrupole doublets as for the green rusts, and also two Fe^{III} quadrupole doublets [283]. The latter have been assigned to Fe^{III} ions with all Fe nearest neighbors and with Fe/Mg nearest neighbors and their intensity varies with magnesium content consistent with this interpretation. The spectral linewidths are relatively small and similar to what is observed at the same temperature for green rusts without magnesium cations. This is consistent with an ordered arrangement of cations in which each Fe^{III} cation is surrounded by six divalent cations. Mössbauer spectra of $[Fe^{II}_4Fe^{III}_{2-y}Al_y(OH)_{12}](SO_4)\cdot nH_2O$ show that there is only one Fe^{III} and one Fe^{II} doublet in the unsubstituted material ($y = 0$) but that for $y > 0$, it is necessary to have two Fe^{II} doublets in order to fit the data [298]. This was interpreted in terms of an ordered array of cations in which Al progressively replaces Fe^{III} in the next nearest neighbor shell at distance a_o around Fe^{II}.

UV-visible diffuse reflectance spectra of Zn/Cr – Cl LDHs have been reported [38, 261]. On the basis of the relatively narrow bands and the greater size of ligand field splitting compared with that in $Cr(OH)_3$, it was concluded that the $Cr^{III}O_6$ sites are surrounded by six Zn^{2+} ions as next nearest neighbors for Zn_2Cr and Zn_3Cr. The existence of Zn_xCr – Cl LDHs with $x < 2$ was ascribed to the formation of dimeric Cr – O – Cr links. As noted in Sect. 2.2.1, such links have been demonstrated [41] in $[Zn_7Cr_4(OH)_{22}]CO_3\cdot 5H_2O$, which has a ligand field splitting less than that of Zn_2Cr – Cl. It has been suggested [299] that the presence of similar Fe^{III} – O – Fe^{III} dimers in coalingite $[Mg_{10}Fe_2(OH)_{24}]CO_3\cdot 5H_2O$ can be demonstrated by UV-visible spectroscopy.

3.5 Anion Ordering

In addition to long-range ordering of the intralayer cations, there also exists the possibility of anion ordering within the interlayer galleries. This may be

a manifestation of an ordered arrangement of cations and/or a reflection of the hydrogen bonding network in the interlayers. It was suggested [44] that a peak at 0.454 nm in the powder XRD of an Mg_2Al-benzoate LDH resulted from the (100) reflection of a superlattice with dimensions $a_o\sqrt{3}$. In view of the similar scattering powers of Mg^{2+} and Al^{3+} cations, the reflection was attributed to an ordered arrangement of benzoate anions associated with an ordering of Al^{3+} cations, rather than directly from an ordered superlattice within the layers. A similar conclusion was drawn regarding a reflection at 0.46 nm observed [300] in the XRD pattern of an oxalate-intercalated LDH with Mg/Al = 2.2. On the basis of reflections observed at 0.465 and 0.369 nm, a superlattice (with $a = a_o\sqrt{3} = 0.5305$ nm) associated with the ordering of silicate anions in the interlayers of a Zn_3Al LDH has been proposed [301]. This is possibly associated with the hexagonal symmetry of the condensed silicate anions, which matches that of the layers. In the case of a silicate-intercalated Mg_3Al LDH, no superlattice reflections were observed in the XRD pattern but selected area electron diffraction demonstrated the presence of a superlattice with $a \approx 0.52$ nm [302]. It should be noted, however, that there is some evidence that LDHs decompose in the intense electron beam in SAED experiments [300] and this should be borne in mind when interpreting such data.

As discussed in Sect. 3.2.2 sulfate occurs in different types of interlayers in LDH minerals [99, 303]. When the basal spacing is ≈ 0.88 nm as in $[Mg_4Al_2(OH)_{12}]SO_4{\cdot}3H_2O$, there is no anion ordering and $a = a_o$. When the layer is expanded to ≈ 1.1 nm by inclusion of additional water and/or hydrated cations, the sulfate ions are generally ordered. The periodicity of the lattice may be $a_o\sqrt{3}$ (as expected for the cations in a 2 : 1 lattice) as in $[Mg_{3.96}(Al_{1.98}Fe^{III}_{0.06})(OH)_{12}][(SO_4)_{1.30}Na_{0.56}(H_2O)_{7.3}]$ [99, 303] or $3a_o$ as discussed in Sect. 3.3.1 for shigaite [259], $[Mn^{II}_6Al_3(OH)_{18}][(SO_4)_2\{Na(OH_2)_6\}(H_2O)_6]$. The same phenomenon occurs in synthetic LDHs [304, 305]. For example, the powder XRD patterns shown in Fig. 38 for $[Zn_{0.67}Cr_{0.33}(OH)_2][(SO_4)_{0.165}(H_2O)_{0.73}]$ and $[Zn_{0.67}Cr_{0.33}(OH)_2][(SO_4)_{0.22}Na_{0.11}(H_2O)_{1.25}]$ may be indexed in two-layer polytypes according to cells with ($a_o = 0.3120$, $c = 1.782$ nm) and ($a = a_o\sqrt{3} = 0.5411$, $c = 2.2116$ nm) respectively [305]. Note that in the case of the ordered cation distribution, the (01*l*) and (11*l*) indices determined for the disordered cation distribution are replaced by (11*l*) and (03*l*) respectively.

The structure of a green rust LDH-type material with the formula $[Fe^{II}_4Fe^{III}_2(OH)_{12}]SO_4{\cdot}ca.\ 8H_2O$ has been determined by Rietveld analysis [157]. The material exists as a one-layer polytype with the interlayers containing two planes of sulfate and water molecules giving a basal spacing of 1.1011 nm. The sulfate ions are oriented with their C_3 axes perpendicular to the layers and alternate anions point up and down (as shown earlier in Fig. 14) and form a superlattice with parameter $a = a_o\sqrt{3} = 0.5524$ nm (Fig. 39).

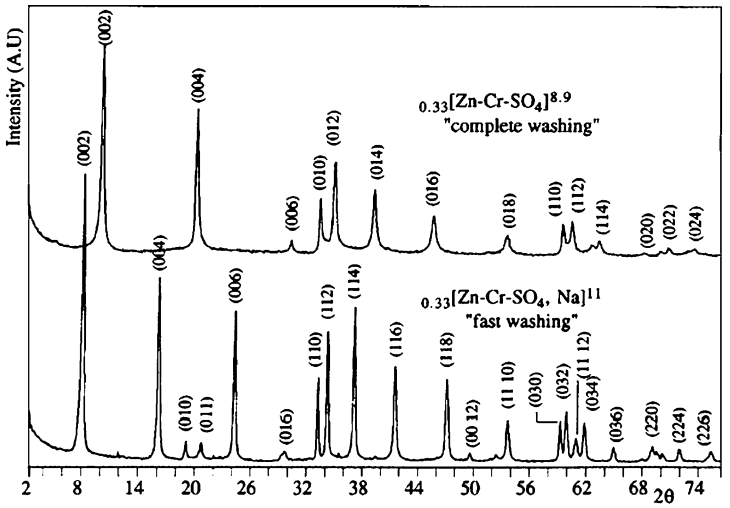

Fig. 38 XRD patterns of $[Zn_{0.67}Cr_{0.33}(OH)_2][(SO_4)_{0.165}(H_2O)_{0.73}]$ (*top*) and $[Zn_{0.67}Cr_{0.33}(OH)_2][(SO_4)_{0.22}Na_{0.11}(H_2O)_{1.25}]$ (*bottom*) which may be indexed in two-layer polytypes according to cells with ($a_o = 0.31204$, $c = 1.782$ nm) and ($a = a_o\sqrt{3} = 0.5411$, $c = 2.2116$ nm) respectively. Reprinted with permission from [305]. Copyright Academic Press

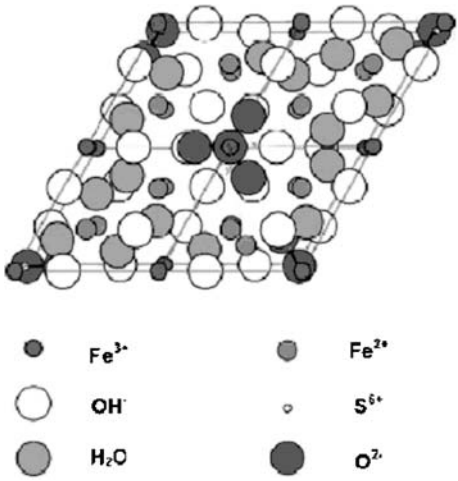

Fig. 39 Projection on the (001) plane of the ordered interlayer structure of the green rust with stoichiometry $[Fe^{II}_4Fe^{III}_2(OH)_{12}]SO_4 \cdot ca.8H_2O$. Reprinted with permission from [157]. Copyright Elsevier SAS

It was assumed that the sulfate oxygen atoms pointing towards the layers are oriented towards Fe^{III} cations. This does not necessarily imply long range ordering of the cations, however, because only half of the Fe^{III} sites are interacting with sulfate anions in this way and the other half of the sites could

be occupied by Fe^{II} cations (although this would also lead to the presence of adjacent Fe^{III} sites which would violate the cation avoidance rule). In the Mössbauer spectrum, there are two quadrupole doublets, one characteristic of Fe^{II} and one of Fe^{III}. It was suggested this is consistent with the ordered nature of the interlayers, since green rusts with disordered layers are characterized by two Fe^{II} signals [157].

LDHs of the type $[Ni_{1-x}Al_x(OH)_2](CO_3)_{x/2}\cdot yH_2O$ have been studied using a high intensity X-ray generator [263]. In addition to the ordering of cations noted in Sect. 3.3.1 for the case of $x = 0.33$, it was found that for $x = 0.30$, the carbonate anions form an ordered $(\sqrt{13} \times \sqrt{13})R13.90°$ superlattice as shown by the presence of four weak reflections which can be indexed as (10), (11), (21) and (30) in the superlattice (the reflections only require (hk) labels) as shown in Fig. 40 [263]. A possible arrangement of the carbonate anions is shown in the inset to the Figure. The anions are each centered over a triad of hydroxyl groups and oriented so that the hydroxyl oxygen atoms are on lines joining carbonate centers. For $x = 0.30$ and $a_o = 0.3032$ nm, the charge density of the layers can be calculated (as described in Sect. 3.2.4) to be 3.768 nm^{-2}, corresponding to a carbonate density of 1.88 ions nm^{-2}. This corresponds closely to the value calculated for the carbonate anion density in the supercell (1.93 nm^{-2}). The superlattice reflections have an asymmetric Warren lineshape and simulations of the diffraction patterns indicated that this is a result of uncorrelated stacking of the anions in the c direction, even though they are well-ordered in the ab plane. This was attributed to the high (26-fold) degeneracy of possible carbonate sites [306].

The effect of ordering of layer cations and/or ordering of interlayer carbonate anions on the crystal chemistry of LDHs has been analyzed [277]. The authors reported the single crystal structure of a mineral with the

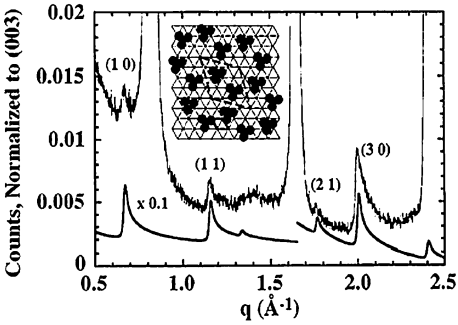

Fig. 40 Measured (*top*) and simulated (*bottom*) XRD patterns of $[Ni_{0.7}Al_{0.3}(OH)_2](CO_3)_{0.15}\cdot yH_2O$ showing ordered $(\sqrt{13} \times \sqrt{13})R13.90°$ superlattice of carbonate anions. [The data are given as a q plot, where $q = 4\pi \sin\theta/\lambda$]. Rhombohedral primitive cells of hydroxyl and carbonate ions are shown as *solid* and *dashed lines* respectively in the *inset figure*. Reprinted with permission from [263]. Copyright Elsevier Science Ltd

formula $[Mg_4Al_2(OH)_{12}]CO_3 \cdot 3H_2O$ which has an ordered distribution of layer cations. The stacking along the c axis is unprecedented in that alternate interlayers are composed of (i) carbonate anions with the three oxygen atoms displaced towards the carbon atom located on one of the three-fold axes and (ii) a net of water molecules whose oxygen atoms are arranged in a close-packed motif, i.e. the layer stacking is of the type – 1 – 2 – 1 – 3 – 1 – where layer 1 is the metal hydroxide, layer 2 the carbonate ions and layer 3 the water molecules. This gives a structure with space group $P\bar{6}2m$ with $a = a_o\sqrt{3} = 0.5283$ nm and $c = 1.5150$ nm. The usual disordered interlayer structure in carbonate-containing LDHs can be thought of as a superposition of nets 2 and 3 giving a statistical distribution of carbonate ions and water molecules projected onto a unit cell with parameter a_o.

A highly crystalline $Zn_{1.56}Al$ – Cl LDH has been prepared by displacing the carbonate anions in a precursor LDH synthesized using the urea method (see Chapter 2 by He et al. in this volume). The good crystallinity of the material combined with the use of a high intensity X-ray generator allowed the observation of three reflections (see Fig. 41) arising from a $(\sqrt{3} \times \sqrt{3})R30°$ superlattice of chloride anions in the dehydrated form [95]. The superlattice is not present in the hydrated form, however. As noted in Sect. 3.1, dehydration is accompanied by a change in stacking sequence from $\mathbf{3R}_1$ to $\mathbf{2H}_1$ and it was concluded that in the dehydrated form the chloride ions must occupy trigonal pockets of layer hydroxyl groups, if they are to form a commensurate superlattice arrangement.

The adsorption of anions on the surface of LDHs has been studied by scanning tunneling microscopy (STM) and atomic force microscopy (AFM) in the belief that the arrangement of anions adsorbed on the external (001) surface of the platelets may mimic the arrangement of the same anions in the interlayer galleries. The AFM image of the crystal surface of an LDH with

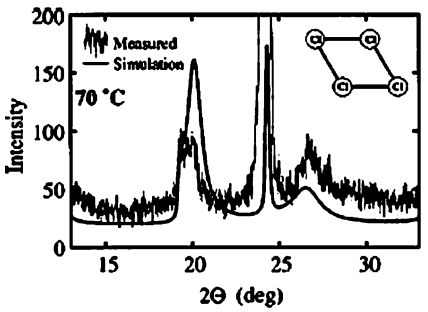

Fig. 41 Measured and simulated XRD patterns of a $Zn_{1.56}Al$ LDH consistent with the presence of a $(\sqrt{3} \times \sqrt{3})R30°$ superlattice of chloride anions. Reprinted with permission from [95]. Copyright American Physical Society

the formula $[Mg_6Al_2(OH)_{16}](CO_3)_{0.5}Cl{\cdot}2H_2O$ in contact with an aqueous solution of Na_2SO_4 shows two-dimensional periodicity with a unit lattice of $a = 0.31 \pm 0.02$ nm, $b = 0.31 \pm 0.02$ nm and $\alpha = 58 \pm 3°$, which was interpreted as being due to the hydroxyl anions of the basal plane, any adsorbed anions having been removed by the AFM tip [307]. (It should be noted, however, that in some cases anions preferentially adsorb on the lateral $(10\overline{1})$ faces rather than the basal surface e.g. HPO_4^{2-} on $[Fe^{II}_4Fe^{III}_2(OH)_{12}]CO_3{\cdot}nH_2O$ [308] and adsorption of catalytically active species on these faces of LDHs has also been proposed [309, 310]; the sulfate may therefore be adsorbed on these faces). STM of the same sample in air showed a two-dimensional lattice with $a = 0.75 \pm 0.04$ nm, $b = 1.10 \pm 0.03$ nm and $\alpha = 70 \pm 3°$. One bright spot, every 1.1 $[Mg_6Al_2(OH)_{16}]^{2+}$ unit was attributed to chloride anions adsorbed on the surface. STM of the same crystal at less negative bias voltage exhibited a two-dimensional lattice with $a = 0.62 \pm 0.03$ nm, $b = 0.62 \pm 0.03$ nm and $\alpha = 63 \pm 3°$, which was attributed to an ordered array of Al^{3+} cations with periodicity $2a_o$. The STM images of the crystal in contact with aqueous solutions of $[Fe(CN)_6]^{n-}$ $(n = 3, 4)$ showed two-dimensional lattices with $a = 1.43 \pm 0.06$ nm, $b = 1.86 \pm 0.06$ nm and $\alpha = 90 \pm 4°$ $(n = 3)$ and $a = 2.20 \pm 0.06$ nm, $b = 2.20 \pm 0.06$ nm and $\alpha = 75 \pm 3°$ $(n = 4)$ respectively, which were attributed to ordered arrays of the respective anions on the surface of the crystal. The calculated surface density of the anions is significantly less than that required in order to balance the positive charge on the layers, indicating that anion-anion repulsions are significant. The same workers reported similar results for $[Fe(CN)_6]^{n-}$ anions adsorbed on an LDH with the formula $[Mg_6Al_2(OH)_{16}](CO_3)_{0.75}(Cl)_{0.5}{\cdot}2H_2O$, although the lattice parameters of the anion arrays were significantly smaller in this case [311].

AFM studies suggested [180] that mono- and dianions of 5-benzoyl-4-hydroxy-2-methoxybenzenesulfonic acid (MBSA) form ordered arrays on the surface of an LDH and that the arrangement adopted is governed by an interplay between the Coulombic interactions between the MBSA anions and the positively charged surface, steric interactions between neighboring anions as well as the hydrogen bonding interactions between the sulfonate groups and hydroxyl triads groups discussed in Sect. 3.2.3.

A floating stearate monolayer has been used as a template for the formation of an LDH by means of spreading a chloroform solution of stearic acid on an aqueous Mg^{2+}/Al^{3+} (3 : 1) solution and followed by deposition onto mica as a Z-type film [312]. From the AFM images of the resulting films, it was concluded that the largest crystals were obtained when the stearate monolayer was compressed to give an area of 0.36 nm^2 per molecule, which is close to the area occupied by one negative charge for an Mg_3Al LDH (0.34 nm^2).

These studies all suggest that ordering of some organic anions is relatively common, in contrast to the generally disordered nature of interlayers containing inorganic anions.

4
Unusual Structural Features of Certain LDHs

4.1
Non-octahedral Coordination of Layer Cations

Although the structure of LDHs generally involves six coordinate M^{II} and M^{III} cations, as discussed previously there are exceptions in the case of M^{II} = Ca with a number of examples confirmed by single crystal XRD [7, 111, 112, 171, 172, 231, 270, 313] and reasons for this have been analyzed [271]. Molecular dynamics calculations on $[Mg_2Al(OH)_6]Cl{\cdot}2H_2O$ have suggested that the Mg^{2+} ion is seven coordinate, being coordinated to water or chloride in addition to the six layer hydroxyl groups and it has been speculated that this coordination geometry may be more common in LDHs than previously thought [233, 314], although to date, there is no direct experimental evidence to support this. Intriguingly, however, whilst the basal spacing in $Mg/Al-CO_3$ LDHs (≈ 0.76 nm) is generally said [7] to be incompatible with carbonate anions tilted at an angle to the layers, in two polymorphs of $[Ca_4Al_2(OH)_{12}]CO_3{\cdot}5H_2O$ where the carbonate ions are tilted at an angle of 21.8° [231] and 20.5° [232] to the layers and bonded to the calcium ions, the basal spacings are only 0.755 nm in each case. The seven coordination of the calcium ion, however, results in a higher water content than in the magnesium analogue $[Mg_4Al_2(OH)_{12}]CO_3{\cdot}3H_2O$.

It has also been argued that the high affinity of sulfonate compounds for LDHs (to the extent that, unlike most anions, they are not displaced by carbonate) indicates a coordinate bond between sulfonate oxygen and aluminum ions. It has been claimed that FT-IR and ^{13}C CP/NMR data support this hypothesis [139].

With the exception of calcium-containing LDHs, there is scant experimental evidence in support of anion coordination in addition to that by six hydroxyl groups but there is ample evidence that on heating LDHs, the interlayer anions can become grafted to the layers. In these cases, the anion replaces one of the hydroxyl groups, however, so that the cation retains octahedral six-coordination. Grafting has been widely observed for organic anions containing carboxylate, sulfonate, and phosphonate groups [199], oxometallate [146] and polyoxometallate anions [118, 131, 144] as well as simple oxoanions such as carbonate [110].

4.2
Staging of Interlayer Anions

The majority of LDH structures have all interlayers identical, but an increasing number of materials with more than one type of interlayer, giving rise to so-called staged structures [315] are being identified. Some min-

erals having this type of structure are known, as has been described in Sect. 3.5 for the material with composition $[Mg_4Al_2(OH)_{12}]CO_3{\cdot}3H_2O$ having alternate interlayers of carbonate anions and water molecules [277]. The mineral coalingite $[Mg_{10}Fe_2(OH)_{24}]CO_3{\cdot}3H_2O$ has interlayers containing carbonate and water which alternate with vacant interlayers (as found in brucite) giving a basal spacing of 1.25 nm [316]. There is a tendency to random interstratification, however, and the mineral contains intergrown regions of brucite and sjögrenite or pyroaurite. The mineral motukoreaite $[Mg_{5.6}Al_{3.4}(OH)_{18}](SO_4)_{1.3}(CO_3)Na_{0.6}{\cdot}12H_2O$ which has a basal spacing of 1.11 nm, readily changes to a dehydrated phase with reduced basal spacing of 0.87 nm. An intermediate staged phase with basal spacing of 1.98 nm (corresponding to 1.11 + 0.87 nm) with alternate hydrated and dehydrated interlayers can also be obtained [317]. A mineral with the stoichiometry $[Mg_4Al_2(OH)_{12}](SO_4)_{0.5}(CO_3)_{0.5}{\cdot}nH_2O$ has cell parameters $a = 0.304$ and $c = 5.562$ nm [303] and has been shown to have alternate interlayers of carbonate (0.756 nm) and sulfate (1.098 nm) anions, so that the basal spacing c_o is the sum of these two values (1.854 nm) and $c = 3c_o$. It has been proposed that the material has the $\mathbf{6R_4}$ polytype in which alternate O- and P-type interlayers are occupied by sulfate and carbonate ions respectively [303]. In the case of synthetic materials, staging has been observed in the case of Mg/Al LDHs with intercalated terephthalate anions. At low temperatures, the terephthalate anions are oriented vertically in the interlayer galleries, whilst on heating dehydration is accompanied by a reorientation of the anions to become parallel to the layers as noted in Sect. 3.2.4 [44]. At intermediate temperatures an interstratified intermediate containing alternate layers of vertical and horizontal anions can be isolated which has a six-layer rhombohedral repeat unit **AbC=CaB-CaB=BcA-BcA=AbC-AbC**. Staging has also been reported during reaction of these materials with inorganic anions giving partial exchange of terephthalate anions [318]. Staging in LDHs containing alternate interlayers of inorganic anions and organic anions such as (4-phenylazophenyl)acetate [153] or succinate or tartrate [281, 319] anions has also been reported. A series of experiments by O'Hare et al. [320, 321] described in Chapter 4 of this volume, demonstrate that staged intermediates can be observed in a variety of exchange reactions of LDHs.

To date, all examples of staging observed with LDH have involved second stage materials (i.e. the interlayers are filled according to an ABAB pattern and no examples of interconversion of third stage (AABAAB)) and second stage materials have been observed. This suggests that the staging phenomena can be explained by the Rüdorff model [322], rather than the Daumas and Hérold model involving buckling of the layers usually invoked for graphite [315]. From the observed change in the magnitude of the red shift in the photoluminescence of $[SmW_{10}O_{36}]^{9-}$ on its intercalation in LDHs, it has been suggested that LDHs do give rise to staging phe-

nomena involving buckled layers at low temperature, however [96, 97]. As discussed in Sect. 2.4 the layers in LDHs are more rigid than graphite but much less rigid than silicate clays, so buckling of the layers would seem to be plausible.

4.3 Double Layers of Anions or Cations/Anions

Although the interlayer galleries of most LDHs contain a single layer of anions and water molecules, more complex interlayer structures are also possible. In the case of sulfate anions, expansion of the interlayer to give a double layer of anions and water molecules is often observed as has been described in Sect. 3.5 for the green rust $[Fe^{II}_4Fe^{III}_2(OH)_{12}]SO_4 \cdot ca.8H_2O$ [157]. In the case of $Mg/Al-SO_4$ LDHs with interlayer sulfate anions, a material with a basal spacing of 1.115 nm is observed at high relative humidity corresponding to a similar double layer, which collapses on drying to a material with a basal spacing of 0.865 nm, corresponding to a single layer of anions and remaining water molecules [323]. There are also examples of expanded phases containing sulfate anions and hydrated alkali or alkaline earth metal cations. Some of these have been discussed in Sect. 3.5, including examples of synthetic materials such as Zn/Cr^{III} LDHs [305] and natural minerals [303] such as shigaite [259] and motukoreaite [317]. The mineral mountkeithite [324] contains interlayer Mg^{2+} cations and sulfate anions. Although it is generally assumed that anions such as chloride or nitrate are replaced by organic anions, this is not always the case and neutral organic molecules such as 4-nitrohippuric acid [196] or sodium salts of surfactants [204] may be incorporated in the interlayer galleries of LDH materials.

4.4 Absence of M^{III} Ions

A growing number of materials that have structures related to those of LDHs but contain only divalent, rather than a mixture of divalent and trivalent, cations in the layers have been reported. These include α-hydroxides of nickel and cobalt [129, 325], and layered hydroxy double salts such as $Zn_5(OH)_8(NO_3)_2 \cdot 2H_2O$ [326] and $Ni_{1-x}Zn_{2x}(OH)_2(CH_3CO_2)_{2x} \cdot nH_2O$ [327, 328]. In this latter class of materials, there are vacancies in the brucite-like layers with cations coordinated in tetrahedral sites above and below the vacancies. Some minerals also have this type of structure, e.g. lawsonbauerite $[(Mn, Mg)_9Zn_4(OH)_{22}](SO_4)_2 \cdot 8H_2O$ which has been characterized by single crystal XRD, has vacancies in two-ninths of the cation sites in a brucite-like lattice with oxygen atoms of the vacant sites coordinated to tetrahedral zinc ions [329]. Although the anions are generally coordinated to the tetrahedral metal anions, there are also examples of this type of material where

the anion is intercalated in the interlayer galleries as for LDHs. One such example, which has been recently characterized [330] by single crystal XRD is $[Co_7(OH)_{12}](O_3SC_2H_4SO_3)\cdot 2H_2O$.

5 Summary and Outlook

This review has covered experimental and theoretical studies of the structure of LDHs and highlighted areas where our undertstanding of the detailed structure is still incomplete. Although LDHs are easy to prepare, they are not necessarily easy to prepare as a pure single phase and there is still no clear consensus of opinion on a number of aspects of their structural chemistry, such as (i) the range of possible cations and the relative amounts of each which may be incorporated in the layers of a pure LDH phase, (ii) the different stacking arrangements which may be adopted and (iii) the extent of long-range of order of cations within the layers. Attention needs to be focused on the types of synthetic procedures (see Chapter 2 by He et al. in this volume) which give highly crystalline materials having powder patterns with a high information contents [116, 117, 131, 193, 266, 267] or even single crystals [231] in order to obtain the most accurate structural information. Technical advances such the ready availability of high intensity X-ray generators [95, 263], area detectors [331] and image plate technology [151] as well as improved methods of modeling static and dynamic disorder [332] may also facilitate detailed studies of the structure of LDHs. Possible avenues of approach include using the intensities of several (00*l*) reflections to calculate one-dimensional electron projections along the c axis and hence derive a model for the orientation of a guest anion in the interlayer galleries [150–153], comparing accurately measured intensities of reflections in order to determine polytype structure [98–100, 108] and observing weak superlattice reflections associated with long-range cation and/or anion ordering [95, 263]. A few examples of these have been discussed above, but others will surely follow. Some theoretical studies on LDHs and related simple models have been discussed above [43, 78, 247, 291, 292], and improvements in both hardware and software should also allow such studies to make future contributions to our understanding of the structure of LDHs. Further spectroscopic, thermodynamic and molecular dynamics studies as well as investigation of *in situ* reactions aimed at probing the way in which the arrangement of the guest anions in LDHs is determined by the interplay between layer-guest and guest-guest (including hydration) interactions as discussed in Sect. 3.2 would also be welcome.

References

1. Cavani F, Trifirò F, Vaccari A (1991) Catal Today 11:173
2. Rives V (ed) (2001) Layered Double Hydroxides: Present and Future. Nova Science Publishers, New York
3. Khan AI, O'Hare D (2002) J Mater Chem 12:3191
4. Gaines RV, Skinner HCW, Foord EE, Mason B, Rosenzweig A (1997) Dana's New Mineralogy, 8th edn. Wiley, New York
5. Allmann R (1968) Acta Cryst B 24:972
6. Taylor HFW (1969) Miner Mag 37:338
7. Taylor HFW (1973) Miner Mag 39:377
8. Catti M, Ferraris G, Hull S, Pavese A (1995) Phys Chem Miner 22:200
9. Greaves C, Thomas MA (1986) Acta Cryst B 42:51
10. Peterson RC, Hill RJ, Gibbs GV (1979) Canad Mineral 17:703
11. Brindley GW, Kao CC (1984) Phys Chem Miner 10:187
12. Parise JB, Leinenweber K, Weidner DJ, Tan K, von Dreele RB (1994) Amer Mineral 79:193
13. Nagai T, Hattori T, Yamanaka T (2000) Amer Mineral 85:760
14. Shinoda K, Aikawa N (1998) Phys Chem Miner 25:197
15. Marchi AJ, Apesteguía CR (1998) Appl Clay Sci 13:35
16. Besserguenev AV, Fogg AM, Francis RJ, Price SJ, O'Hare D, Isupov VP, Tolochko BP (1997) Chem Mater 9:241
17. Alberti G, Costantino U (1996) In: Alberti G, Bein T (eds) Solid State Supramolecular Chemistry: Two- and Three-Dimensional Inorganic Networks. Comprehensive Supramolecular Chemistry, vol 7, Chapter 1. Pergamon and Elsevier Science, Oxford UK
18. Takagi K, Saito N, Shichi T, Sawaki Y (1999) Chem Lett 275
19. Newman SP, Jones W (2001) In: Jones W, Rao CNR (eds) Supramolecular Organization and Materials Design. Cambridge University Press, Cambridge
20. Prakash AS, Kamath PV, Hegde MS (2000) Mater Res Bull 35:2189
21. de Roy A, Forano C, Besse JP (2001) Chapter 1 in [2]
22. Kloprogge JT, Wharton D, Hickey L, Frost RL (2002) Amer Mineral 87:623
23. Alejandre A, Medina F, Salagre P, Correig X, Sueiras JE (1999) Chem Mater 11:939
24. Iglesias AH, Ferreira OP, Gouveia DX, Souza Filho AG, de Paiva JAC, Filho JM, Alves OL (2005) J Solid State Chem 178:142
25. Roussel H, Briois V, Elkaïm E, de Roy A, Besse JP (2000) J Phys Chem B 104:5915
26. Bigey L, Depège C, de Roy A, Besse JP (1997) J Physique IV 7:C2-949
27. Allada RK, Navrotsky A, Boerio-Goates J (2005) Amer Mineral 90:329
28. Allada RK, Navrotsky A, Berbeco HT, Casey WH (2002) Science 296:721
29. Johnson CA, Glasser FP (2003) Clays Clay Miner 51:1
30. Johnson CA, Glasser FP (2003) Clays Clay Miner 51:357
31. Bravo-Suárez JJ, Páez-Mozo EA, Oyama ST (2004) Quim Nova 27:574
32. Bravo-Suárez JJ, Páez-Mozo EA, Oyama ST (2004) Quim Nova 27:601
33. Hansen HCB (2001) Chapter 13 in [2]
34. Bourrié G, Trolard F, Génin JMR, Jaffrezic A, Maître V, Abdelmoula M (1999) Geochim Cosmochim Acta 63:3417
35. Génin JMR, Bourrié G, Trolard F, Abdelmoula M, Jaffrezic A, Refait P, Maître V, Humbert B, Herbillon A (1998) Environ Sci Technol 32:1058
36. Bourrié G, Trolard F, Refait P, Feder F (2004) Clays Clay Miner 52:382
37. Boclair JW, Braterman PS (1999) Chem Mater 11:298

38. Boclair JW, Braterman PS, Jiang J, Lou S, Yarberry F (1999) Chem Mater 11:303
39. Bellotto M, Rebours B, Clause O, Lynch J, Bazin D, Elkaïm E (1996) J Phys Chem 100:8527
40. Vucelic M, Jones W, Moggridge GD (1997) Clays Clay Miner 45:803
41. Gutmann N, Müller B (1996) J Solid State Chem 122:214
42. Fogg AM, Williams GR, Chester R, O'Hare D (2004) J Mater Chem 14:2369
43. Trave A, Selloni A, Goursot A, Tichit D, Weber J (2002) J Phys Chem B, 106:12291
44. Vucelic M, Moggridge GD, Jones W (1995) J Phys Chem 99:8328
45. del Arco M, Malet P, Trujillano R, Rives V (1999) Chem Mater 11:624
46. Leroux F, Moujahid EM, Taviot-Guého C, Besse JP (2001) Solid State Sci 3:81
47. López-Salinas E, García-Sánchez M, Montoya JA, Acosta DR, Abasolo JA, Schifter I (1997) Langmuir 13:4748
48. Tsuji M, Mao G, Yoshida T, Tamaura Y (1993) J Mater Res 8:1137
49. Thevenot F, Szymanski R, Chaumette P (1989) Clays Clay Miner 37:396
50. Gago S, Pillinger M, Valente AA, Santos TM, Rocha J, Gonçalves IS (2004) Inorg Chem 43:5422
51. Pausch I, Lohse HH, Schürmann K, Allmann R (1986) Clays Clay Miner 34:507
52. Labajos FM, Sánchez-Montero, Holgado MJ, Rives V (2001) Thermochim Acta 370:99
53. Legrand L, Abdelmoula M, Géhin A, Chausé A, Génin JMR (2001) Electrochim Acta 46:1815
54. Inacio J, Taviot-Guého C, Morlat-Thérias S, de Roy ME, Besse JP (2001) J Mater Chem 11:640
55. Xu ZP, Zeng HC (2001) J Phys Chem B 105:1743
56. Brindley GW, Kikkawa S (1979) Amer Mineral 64:836
57. Turco M, Bagnasco G, Costantino U, Marmottini F, Montanari T, Ramis G, Busca G (2004) J Catal 228:43
58. Kaneyoshi M, Jones W (1999) J Mater Chem 9:905
59. Kooli F, Chisem IC, Vucelic M, Jones W (1996) Chem Mater 8:1969
60. Gardner EA, Yun SK, Kwon TH, Pinnavaia TJ (1998) Appl Clay Sci 13:479
61. Zeng HC, Xu ZP, Qian M (1998) Chem Mater 10:2277
62. Sanchez-Valente J, Millet JMM, Figueras F, Fournes L (2000) Hyperfine Interact 131:43
63. Kumbhar PS, Sanchez-Valente J, Millet JMM, Figueras F (2000) J Catal 191:467
64. Kanezaki E (1995) J Mater Sci 30:4926
65. Basile F, Fornasari G, Gazzano M, Kiennemann A, Vaccari A (2003) J Catal 217:245
66. Hibino T, Yamashita Y, Kosuge K, Tsunashima A (1995) Clays Clay Miner 43:427
67. Rives V (1999) Inorg Chem 38:406
68. Gutmann NH, Spiccia L, Turney TW (2000) J Mater Chem 10:1219
69. Intissar M, Jumas JC, Besse JP, Leroux F (2003) Chem Mater 15:4625
70. Shannon RD (1976) Acta Cryst A 32:751
71. de la Calle C, Pons CH, Roux J, Rives V (2003) Clays Clay Miner 51:121
72. Intissar M, Segni R, Payen C, Besse JP, Leroux F (2002) J Solid State Chem 167:508
73. Pérez-Ramírez J, Mul G, Kapreijn F, Moulijn JA (2001) J Mater Chem 11:2529
74. Ribet S, Tichit D, Coq B, Ducourant B, Morato F (1999) J Solid State Chem 142:382
75. Kukkadapu RK, Witkowski MS, Amonette JE (1997) Chem Mater 9:417
76. Mao G, Tsuji M, Tamaura Y (1993) Clays Clay Miner 41:731
77. Leroux F, Adachi-Pagano M, Intissar M, Chauvière S, Forano C, Besse JP (2001) J Mater Chem 11:105
78. Sainz-Diaz CI, Timon V, Botella V, Hernandez-Laguna A (2000) Amer Mineral 85:1038

79. Xu ZP, Zeng HC (2001) Chem Mater 13:4555
80. Frost RL, Erickson KL (2004) J Thermal Anal Calorim 76:217
81. Velu S, Ramaswamy V, Ramani A, Chanda BM, Sivasanker S (1997) Chem Commun 2107
82. Velu S, Sabde DP, Shah N, Sivasanker S (1998) Chem Mater 10:3451
83. Velu S, Suzuki K, Osaki T, Ohashi F, Tomura S (1999) Mater Res Bull 34:1707
84. Das NN, Konar J, Mohanta MK, Srivastava SC (2004) J Colloid Interface Sci 270:1
85. Velu S, Suzuki K, Okazaki M, Osaki T, Tomura S, Ohashi F (1999) Chem Mater 11:2163
86. Velu S, Suzuki K, Kapoor MP, Tomura S, Ohashi F, Osaki T (2000) Chem Mater 12:719
87. Tichit D, Das N, Coq B, Durand R (2002) Chem Mater 14:1530
88. Das N, Samal A (2004) Micropor Mesopor Mater 72:219
89. Ren QL, Luo Q, Liu DZ, Chen ST (2003) Mater Sci Forum (Funct Graded Mater VII) 423-425:157
90. Saber O, Tagaya H (2003) J Incl Phenom Macrocyclic Chem 45:109
91. Intissar M, Holler S, Malherbe F, Besse JP, Leroux F (2004) J Phys Chem Solids 65:453
92. Hofmeister W, von Platen H (1992) Cryst Rev 3:3
93. Solin SA, Hines D, Yun SK, Pinnavaia TJ, Thorpe MF (1995) J Non-Cryst Solids 182:212
94. Hines DR, Solin SA, Costantino U, Nocchetti M (2000) Mol Cryst Liq Cryst 341:1181
95. Hines DR, Solin SA, Costantino U, Nocchetti M (2000) Phys Rev B 61:11348
96. Park TR, Park TY, Kim H, Min P (2002) J Phys: Condens Matter 14:11687
97. Park TR (2004) J Korean Phys Soc 44:398
98. Bookin AS, Drits VA (1993) Clays Clay Miner 41:551
99. Bookin AS, Cherkashin VI, Drits VA (1993) Clays Clay Miner 41:558
100. Drits VA, Bookin AS (2001) Chapter 2 in [2]
101. Vaysse C, Guerlou-Demourgues L, Demourgues A, Lazartigues F, Fertier D, Delmas C (2002) J Mater Chem 12:1035
102. Guerlou-Demourgues L, Denage C, Delmas C (1994) J Power Sources 52:269
103. Thomas GS, Rajamathi M, Kamath PV (2004) Clays Clay Miner 52:693
104. Moggridge GD, Parent P, Tourillon G (1994) Clays Clay Miner 42:462
105. Stanimirova T (2001) Ann Univ Sofia Geol 94:73
106. Ennadi A, Legrouri A, de Roy A, Besse JP (2000) J Solid State Chem 152:568
107. Stanimirova TS, Kirov G, Dinolova E (2001) Mat Sci Lett 20:453
108. Newman SP, Jones W, O'Connor P, Stamires DN (2002) J Mater Chem 12:153
109. Parthasarathy G, Kantam ML, Choudary BM, Reddy CV (2002) Micropor Mesopor Mater 56:147
110. Vaysse C, Guerlou-Demourgues L, Delmas C (2002) Inorg Chem 41:6905
111. Renaudin G, Rapin JP, Elkaïm E, François M (2004) Cement Concrete Res 34:1845
112. Rapin JP, Renaudin G, Elkaïm E, François M (2002) Cement Concrete Res 32:513
113. Bookin AS, Cherkashin VI, Drits VA (1993) Clays Clay Miner 41:631
114. Fogg AM, Freij AJ, Parkinson GM (2002) Chem Mater 14:232
115. Thiel JP, Chiang CK, Poeppelmeier KR (1993) Chem Mater 5:297
116. Hansen HCB, Koch CB, Taylor RM (1994) J Solid State Chem 113:46
117. Hansen HCB, Taylor RM (1991) Clay Miner 26:507
118. Ménétrier M, Han KS, Guerlo-Demourgues L, Delmas C (1997) Chem Mater 36:2441
119. Zhao Y, Li F, Zhang R, Evans DG, Duan X (2002) Chem Mater 14:4286
120. Gago S, Pillinger M, Santos TM, Rocha J, Gonçalves IS (2004) Eur J Inorg Chem 1389
121. Drits V, Środoń J, Eberl DD (1997) Clays Clay Miner 45:461

122. Jaboyedoff M, Kübler B, Thélin P (1999) Clay Miner 34:601
123. Ennadi A, Legrouri A, de Roy A, Besse JP (2000) J Mater Chem 10:2337
124. Guggenheim S, Bain DC, Bergaya F, Brigatti MF, Drits VA, Eberl DD, Formoso MLL, Galan E, Merriman RJ, Peacor DR, Stanjek H, Watanabe T (2002) Clays Clay Miner 50:406
125. Radha AV, Kamath PV, Subbanna GN (2003) Mater Res Bull 38:731
126. Delmas C, Tessier C (1997) J Mater Chem 7:1439
127. Rajamathi M, Kamath PV, Seshadri R (2000) J Mater Chem 10:503
128. Ramesh TN, Jayashree RS, Kamath PV (2003) Clays Clay Miner 51:570
129. Xu ZP, Zeng HC (2000) Int J Inorg Mater 2:187
130. Prévot V, Forano C, Besse JP (1998) Inorg Chem 37:4293
131. Han KS, Guerlou-Demourgues L, Delmas C (1996) Solid State Ionics 84:227
132. Rey S, Mérida-Robles J, Han KS, Guerlou-Demourgues L, Delmas C, Duguet E (1999) Polymer Int 48:277
133. Aloisi GG, Costantino U, Elisei F, Latterini L, Natali C, Nocchetti M (2002) J Mater Chem 12:3316
134. Boclair JW, Braterman PS, Brister BD, Yarberry F (1999) Chem Mater 11:2199
135. Beaudot P, de Roy ME, Besse JP (2004) Chem Mater 16:935
136. Kanezaki E, Maeda K (2002) Nippon Kagaku Kaishi 393
137. Beaudot P, de Roy ME, Besse JP (2004) J Solid State Chem 177:2691
138. Beaudot P, de Roy ME, Besse JP (2001) J Solid State Chem 161:332
139. Kanezaki E (2003) J Incl Phenom Macrocyclic Chem 46:89
140. Kanezaki E, Sugiyama S, Ishikawa Y (1995) J Mater Chem 5:1969
141. Weir MR, Kydd RA (1998) Inorg Chem 37:5619
142. Kooli F, Rives V, Ulibarri MA (1995) Inorg Chem 34:5122
143. Hibino T, Tsunashima A (1997) Chem Mater 9:2082
144. Malherbe F, Bigey L, Forano C, de Roy A, Besse JP (1999) J Chem Soc Dalton Trans 3831
145. Malherbe F, Besse JP (2000) J Solid State Chem 155:332
146. Rives V, Ulibarri MA (1999) Coord Chem Rev 181:61
147. Liu YJ, Schindler JL, DeGroot DC, Kannewurf CR, Hirpo W, Kanatzidis MG (1996) Chem Mater 8:525
148. Zhang X, Lerner MM (1999) Chem Mater 11:1100
149. de La Calle C, Tejedor MI, Pons CH (1996) Clays Clay Miner 44:68
150. Bauer J, Behrens P, Speckbacher M, Langhals H (2003) Adv Funct Mater 13:241
151. Itoh T, Ohta N, Shichi T, Yui T, Tagaki K (2003) Langmuir 19:9120
152. Kanoh T, Shichi T, Takagi K (1999) Chem Lett 117
153. Iyi N, Kurashima K, Fujita T (2002) Chem Mater 14:583
154. McMurdie MF, Morris MC, Evans EH, Paretzkin B, Wong-Ng W, Hubbard CR (1986) Powder Diffraction 1:40
155. Refait PH, Abdelmoula M, Génin JMR (1998) Corrosion Sci 40:1547
156. Braithwaite RSW, Dunn PJ, Pritchard RG, Paar WH (1994) Miner Mag 58:79
157. Simon L, François M, Refait P, Renaudin G, Lelaurin M, Génin JMR (2003) Solid State Sci 5:327
158. Rives R (2002) Mater Chem Phys 75:19
159. Barriga C, Jones W, Malet P, Rives V, Ulibarri MA (1998) Inorg Chem 37:1812
160. Holgado MJ, Rives V, Sanroman MS, Malet P (1996) Solid State Ionics 92:273
161. Kloprogge JT, Frost RL (2001) Chapter 5 in [2]
162. Kloprogge JT (ed)(2005) The Application of Vibrational Spectroscopy to Clay Minerals and Layered Double Hydroxides. Clay Minerals Society, Aurora
163. Kloprogge JT, Frost RL (1999) J Solid State Chem 146:506

164. Frost RL, Martens W, Ding Z, Kloprogge JT, Johnson TE (2003) Spectrochim Acta A 59:291
165. Frost RL, Ding Z, Martens W, Johnson TE, Kloprogge JT (2003) Spectrochim Acta A 59:321
166. Kloprogge JT, Hickey L, Frost RL (2004) J Raman Spec 35:967
167. Marcelin G, Stockhausen NJ, Post JFM, Schutz A (1989) J Phys Chem 93:4646
168. Xu R, Zeng HC (2003) Chem Mater 15:2040
169. Hou XQ, Kirkpatrick RJ, Yu P, Moore D, Kim Y (2000) Amer Mineral 85:173
170. Xu ZP, Zeng HC (2001) Chem Mater 13:4564
171. Renaudin G, Rapin JP, Humbert B, François M (2000) Cement Concrete Res 30:307
172. Renaudin G, François M (1999) Acta Cryst C 55:835
173. Kloprogge JT, Hickey L, Frost RL (2001) Appl Clay Sci 18:37
174. Boclair JW, Braterman PS, Brister BD, Wang Z, Yarberry F (2001) J Solid State Chem 161:249
175. Kloprogge JT, Weier M, Crespo I, Ulibarri MA, Barriga C, Rives V, Martens WN, Frost RL (2004) J Solid State Chem 177:1382
176. Hansen HCB, Koch CB (1994) Clays Clay Miner 42:170
177. Braterman PS, Tan CQ, Zhao JX (1994) Mater Res Bull 29:1217
178. Raki L, Rancourt DG, Detellier C (1995) Chem Mater 7:221
179. del Arco M, Gutierrez S, Martin C, Rives V, Rocha J (2004) J Solid State Chem 177:3954
180. Franklin KR, Lee E, Nunn CC (1995) J Mater Chem 5:565
181. Cai H, Hillier AC, Franklin KR, Nunn CC, Ward MD (1994) Science 266:1551
182. Maxwell RS, Kukkadapu RK, Amonette JE, Cho H (1999) J Phys Chem B 103:5197
183. Newman SP, Williams SJ, Coveney PV, Jones W (1998) J Phys Chem B 102:6710
184. Hou XQ, Kirkpatrick RJ (2002) Chem Mater 14:1195
185. Hou XQ, Kirkpatrick RJ (2000) Chem Mater 12:1890
186. Kirkpatrick RJ, Yu P, Hou XQ, Kim Y (1999) Amer Mineral 84:1186
187. Kozlova SG, Gabuda SP, Isupov VP, Chupakhina LE (2003) J Struc Chem 44:198
188. van der Pol A, Mojet BL, van de Ven E, de Boer E (1994) J Phys Chem 98:4050
189. Morlat-Thérias S, Mousty C, Palvadeau P, Molinié P, Léone P, Rouxel J, Taviot-Guého C, Ennaqui A, de Roy A, Besse JP (1999) J Solid State Chem 144:143
190. Moggridge GD, Parent P, Tourillon G (1995) Physica B 209:269
191. Meyn M, Beneke K, Lagaly G (1990) Inorg Chem 29:5201
192. Costantino U, Coletti N, Nocchetti M, Aloisi GG, Elisei F, Latterini L (2000) Langmuir 16:10351
193. Costantino U, Coletti N, Nocchetti, Aloisi GG, Elisei F (1999) Langmuir 15:4454
194. Xing Y, Li D, Ren L, Evans DG, Duan X (2003) Acta Chim Sinica 61:267
195. Latterini L, Elisei F, Aloisi GG, Costantino U, Nocchetti M (2002) Phys Chem Chem Phys 4:2792
196. Cooper S, Dutta PK (1990) J Phys Chem 94:114
197. Sasai R, Shin'ya N, Shichi T, Takagi K, Gekko K (1999) Langmuir 15:413
198. Carlino S, Hudson MJ (1995) J Mater Chem 5:1433
199. Prévot V, Forano C, Besse JP (2001) Appl Clay Sci 18:3
200. Bravo-Suárez JJ, Páez-Mozo EA, Oyama ST (2004) Micropor Mesopor Mater 67:1
201. Bravo-Suárez JJ, Páez-Mozo EA, Oyama ST (2004) Chem Mater 16:1214
202. Choy JH, Jung EY, Son YH, Park M (2004) J Phys Chem Solids 65:509
203. Xu ZP, Braterman PS (2003) J Mater Chem 13:268
204. Crepaldi EL, Pavan PC, Tronto J, Valim JB (2002) J Colloid Interface Sci 248:429
205. Zhao H, Nagy KL (2004) J Colloid Interface Sci 274:613

206. Borja M, Dutta PK (1992) J Phys Chem 96:5434
207. Corma A, Fornés V, Rey F, Cervilla A, Llopis E, Ribera A (1995) J Catal 152:237
208. Raki L, Beaudoin JJ, Mitchell L (2004) Cement Concrete Res 34:1717
209. Kuk WK, Huh YD (1997) J Mater Chem 7:1933
210. Fogg AM, Green VM, Harvey HG, O'Hare D (1999) Adv Mater 11:1466
211. Fogg AM, Dunn JS, Shyu SG, Cary DR, O'Hare D (1998) Chem Mater 10:351
212. Weir MR, Morre J, Kydd RA (1997) Chem Mater 9:1686
213. Lee JH, Rhee SW, Jung DY (2004) Chem Mater 16:3774
214. Ocko BM, Wu XZ, Sirota EB, Sinha SK, Gang O, Deutsch M (1997) Phys Rev E 55:3164
215. Newman SP, Jones W (1998) New J Chem 105
216. Xu ZP, Braterman PS, Yu K, Xu H, Wang Y, Brinker CJ (2004) Chem Mater 16:2750
217. Greenwell HC, Jones W, Newman SP, Coveney PV (2003) J Mol Struct 647:75
218. Valim J, Kariuki BM, King J, Jones W (1992) Mol Cryst Liq Cryst 211:271
219. Shichi T, Takagi K, Sawaki Y (1996) Chem Commun 2027
220. Rhee SW, Jung DY (2002) Bull Korean Chem Soc 23:35
221. Takagi K, Harata E, Shichi T, Kanoh T, Sawaki Y (1997) J Photochem Photobiol A: Chem 105:47
222. Morel-Desrosiers N, Pisson J, Israëli Y, Taviot-Guého C, Besse JP, Morel JP (2003) J Mater Chem 132:2582
223. Wang JW, Kalinichev AG, Amonette JE, Kirkpatrick RJ (2003) Amer Mineral 88:398
224. Newman SP, Greenwell HC, Coveney PV, Jones W (2001) Chapter 3 in [2]
225. Newman SP, Di Cristina T, Coveney PV, Jones W (2002) Langmuir 18:2933
226. Hou XQ, Kalinichev AG, Kirkpatrick RJ (2002) Chem Mater 14:2078
227. Kalinichev AG, Kirkpatrick RJ, Cygan RT (2000) Amer Mineral 85:1046
228. Kalinichev AG, Kirkpatrick RJ (2002) Chem Mater 14:3539
229. Renaudin G, Kubel F, Rivera JP, Francois M (1999) Cement Concrete Research 29:1937
230. Andersen MD, Jakobsen HJ, Skibsted J (2002) J Phys Chem A 106:6676
231. François M, Renaudin G, Evrard O (1998) Acta Cryst C54:1214
232. Renaudin G, François M, Evrard O (1999) Cement Concrete Research 29:63
233. Wang JW, Kalinichev AG, Kirkpatrick RJ, Hou XQ (2001) Chem Mater 13:145
234. Kalinichev AG, Wang J, Kirkpatrick RJ, Cygan RT (2001) AIChE Symp Ser 325:251
235. Fogg AM, Rohl AL, Parkinson GM, O'Hare D (1999) Chem Mater 11:1194
236. Toraishi T, Nagasaki S, Tanaka S (2002) Radiochim Acta 90:671
237. Toraishi T, Nagasaki S, Tanaka S (2002) Appl Clay Sci 22:17
238. Drissi, SH, Refait P, Abdelmoula M, Génin JMR (1995) Corrosion Sci 37:2025
239. Yun SK, Pinnavaia TJ (1995) Chem Mater 7:348
240. Hou XQ, Bish DL, Wang SL, Johnston CT, Kirkpatrick RJ (2003) Amer Mineral 88:167
241. Génin JMR, Ruby C (2004) Solid State Sci 6:705
242. Wang J, Kalinichev AG, Kirkpatrick RJ (2004) Geochim Cosmochim Acta 68:3351
243. Pesic L, Salipurovic S, Markovic V, Vucelic D, Kagunya W, Jones W (1992) J Mater Chem 2:1069
244. Kagunya W, Dutta PK, Lei Z (1997) Physica B 234:910
245. Mitra S, Pramanik A, Chakrabaty D, Mukhopadhyay R (2004) Pramana – J Phys 63:437
246. Mehrotra V, Giannelis EP (1992) J Appl Phys 72:1039
247. Greenwell HC, Stackhouse S, Coveney PV, Jones W (2003) J Phys Chem B 107:3476
248. Hines DR, Solin SA, Costantino U, Nocchetti M (1998) Solid State Comm 12:971
249. Kagunya W, Baddour-Hadjean R, Kooli F, Jones W (1998) Chem Phys 236:225

250. Kim D, Huang C, Lee H, Han I, Kang S, Kwon S, Lee J, Han Y, Kim H (2003) Appl Catal A: Gen 249:229
251. Basile F, Vaccari A (2001) Chapter 10 in [2]
252. Monzón A, Romeo E, Marchi AJ (2001) Chapter 11 in [2]
253. Chellam U, Xu ZP, Zeng HC (2000) Chem Mater 12:650
254. Liu JJ, Li F, Evans DG, Duan X (2003) Chem Commun 542
255. Li F, Liu JJ, Evans DG, Duan X (2004) Chem Mater 16:1597
256. Porta P, Morpurgo S, Pettiti I (1996) J Solid State Chem 121:372
257. Pauling L (1929) J Am Chem Soc 51:1010
258. Serna CJ, Rendon JL, Iglesias JE (1982) Clays Clay Miner 30:180
259. Cooper MA, Hawthorne FC (1996) Canad Mineral 34:91
260. Gastuche MC, Brown G, Mortland M (1967) Clay Miner 7:177
261. Boclair JW, Braterman PS (1998) Chem Mater 10:2050
262. Roussel H, Briois V, Elkaïm E, de Roy A, Besse JP, Jolivet JP (2001) Chem Mater 13:329
263. Solin SA, Hines DR, Seidler GT, Treacey MMJ (1996) J Phys Chem Solids 57:1043
264. Steeds JW, Morniroli JP (1992) Rev Miner Geochem 27:37
265. Ingram L, Taylor HFW (1967) Miner Mag 36:465
266. Costantino U, Marmottini F, Nocchetti M, Vivani R (1998) Eur J Inorg Chem 1439
267. Costantino U, Casciola M, Massinelli L, Nocchetti M, Vivani R (1997) Solid State Ionics 97:203
268. Sissoko I, Iyagba ET, Sahai R, Biloen P (1985) J Solid State Chem 60:283
269. Hou X, Kirkpatrick RJ (2001) Inorg Chem 40:6397
270. Terzis A, Filippakis S, Kuzel HJ, Burzlaff H (1987) Z Kristallogr 181:29
271. Rousselot I, Taviot-Guého C, Leroux F, Léone P, Palvadeau P, Besse JP (2002) J Solid State Chem 167:137
272. Dunn PJ, Peacor DR, Palmer TD (1979) Amer Mineral 64:127
273. Huminicki DMC, Hawthorne FC (2003) Canad Mineral 41:79
274. Rius J, Plana F (1986) Neues Jahrb Miner Monatsh 263
275. Merlino S, Orlandi P (2001) Amer Mineral 86:1293
276. Chao GY, Gault RA (1997) Canad Mineral 35:1541
277. Arakcheeeva AV, Pushcharovskii DY, Rastsvetaeva RK, Atencio D, Lubman GU (1996) Krystallografiya 41:1024; Crystallog Rep 41:972
278. Xiao YQ, Thorpe MF, Parkinson JB (1999) Phys Rev 59:277
279. Chen J, Thorpe MF, Davis LC (1995) J Appl Phys 77:4349
280. Evans J, Pillinger M, Zhang J (1996) J Chem Soc Dalton Trans 2963
281. Taviot-Guého C, Leroux F, Payen C, Besse JP (2005) Appl Clay Sci 28:111
282. Scheinost AC, Sparks DL (2000) J Colloid Interface Sci 223:167
283. Refait P, Abdelmoula M, Trolard F, Génin JMR, Ehrhardt JJ, Bourrié G (2001) Amer Mineral 86:731
284. Leroux F, Moujahid EM, Roussel H, Flank AM, Briois V, Besse JP (2002) Clays Clay Miner 50:254
285. Frost RL, Weier ML, Clissold ME, Williams PA (2003) Spectrochim Acta A – Molec Biomolec Spec 59:3313
286. Hernandez-Moreno MJ, Ulibarri MA, Rendon JL, Serna CJ (1985) Phys Chem Miner 12:34
287. d'Espinose de la Caillerie JB, Kermarec M, Clause O (1995) J Am Chem Soc 117:11471
288. Mockenhaupt C, Zeiske T, Lutz HD (1998) J Mol Struct 443:191
289. Frost RL, Erickson KL (2004) Spectrochim Acta A 60:3001

290. Johnson TE, Martens W, Frost RL, Ding Z, Kloprogge JT (2002) J Raman Spec 33:604
291. Martínez-Alonso S, Rustad JR, Goetz AFH (2002) Amer Mineral 87:1224
292. Martínez-Alonso S, Rustad JR, Goetz AFH (2002) Amer Mineral 87:1215
293. Koch CB (2001) Chapter 7 in [2]
294. Hansen HCB, Guldberg S, Erbs M, Koch CB (2001) Appl Clay Sci 18:81
295. Génin JMR (2004) Hyperfine Interact 156/7:471
296. Rancourt DG (1998) Hyperfine Interact 117:3
297. Refait P, Génin JMR (1997) Corrosion Sci 39:539
298. Aissa R, Ruby C, Gehin A, Abdelmoula M, Génin JMR (2004) Hyperfine Interact 156/7:445
299. Mattson SM, Rossman GR (1984) Phys Chem Miner 11:225
300. Roelofs JCAA, van Bokhoven JA, van Dillen AJ, Geus JW, de Jong KP (2002) Chem Eur J 8:5571
301. Depège C, El Metoui FZ, Forano C, de Roy A, Dupuis J, Besse JP (1996) Chem Mater 8:952
302. Schutz A, Biloen P (1987) J Solid State Chem 68:360
303. Drits VA, Sokolova TN, Sokolova GV, Cherkashin VI (1987) Clays Clay Miner 35:401
304. Bish DL (1980) Bull Minéral 103:170
305. Khaldi M, de Roy A, Chaouch M, Besse JP (1997) J Solid State Chem 130:66
306. Hines DR, Seidler GT, Treacy MMJ, Solin SJ (1997) Solid State Sci 101:835
307. Yao K, Taniguchi M, Nakata M, Takahashi M, Yamagishi A (1998) Langmuir 14:2410
308. Bocher F, Géhin A, Ruby C, Ghanbaja J, Abdelmoula M, Génin JMR (2004) Solid State Sci 6:117
309. Sels B, de Vos D, Buntinx M, Pierard F, Kirsch-de Mesmaeker A, Jacobs P (1999) Nature 400:855
310. Choudary BM, Madhi S, Chowdari NS, Kantam ML, Sreedhar B (2002) J Amer Chem Soc 124:14127
311. Yao K, Taniguchi M, Nakata M, Yamagishi A (1998) J Electroanal Chem 458:249
312. He JX, Yamashita S, Jones W, Yamagishi A (2002) Langmuir 18:1580
313. Allmann R (1977) Neues Jahrb Miner Monatsh 136
314. Cygan RT, Liang JJ, Kalinichev AG (2004) J Phys Chem B 108:1255
315. Fogg AM, Dunn JS, O'Hare D (1998) Chem Mater 10:356
316. Pastor-Rodriguez J, Taylor HFW (1971) Miner Mag 38:286
317. Brindley GW (1979) Miner Mag 43:337
318. Kaneyoshi M, Jones W (1998) Chem Phys Lett 296:183
319. Pisson J, Taviot-Guého C, Israëli Y, Leroux F, Munsch P, Itié JP, Briois V, Morel-Desrosiers N, Besse JP (2003) J Phys Chem B 107:9243
320. Williams GR, Norquist AJ, O'Hare D (2004) Chem Mater 16:975
321. Williams GR, Norquist AJ, O'Hare D (2003) Chem Commun 1816
322. Timp G, Dresselhaus MS (1984) J Phys C: Solid State Phys 17:2641
323. Brindley GW, Kikkawa S (1980) Clays Clay Miner 28:87
324. Hudson DR, Bussell M (1981) Miner Mag 44:345
325. Kamath PV, Therese GHA, Gopalakrishnan J (1997) J Solid State Chem 128:38
326. Stählin W, Oswald HR (1970) Acta Cryst B26:860
327. Choy JH, Kwon YM, Han KS, Song SW, Chang SH (1998) Mater Lett 34:356
328. Choy JH, Kwon YM, Song SW, Chang SH (1997) Bull Korean Chem Soc 18:450
329. Treiman AH, Peacor DR (1982) Amer Mineral 67:1029
330. Forster PM, Tafoya MM, Cheetham AK (2004) J Phys Chem Solids 65:11
331. Bhuvanesh NSP, Reibenspies JH (2003) J Appl Cryst 36:1480
332. Izumi F (2004) Solid State Ionics 172:1